OPTICAL SPECTROSCOPY BASED URINE ANALYSIS FOR DISEASE DIAGNOSIS

Ph.D. Thesis

By

SURJENDU BIKASH DUTTA

DISCIPLINE OF PHYSICS

INDIAN INSTITUTE OF TECHNOLOGY INDORE

OCTOBER 2019

OPTICAL SPECTROSCOPY BASED URINE ANALYSIS FOR DISEASE DIAGNOSIS

A THESIS

Submitted in partial fulfillment of the requirements for the award of the degree

of

DOCTOR OF PHILOSOPHY

by

SURJENDU BIKASH DUTTA

DISCIPLINE OF PHYSICS

INDIAN INSTITUTE OF TECHNOLOGY INDORE

OCTOBER 2019

INDIAN INSTITUTE OF TECHNOLOGY INDORE

CANDIDATE'S DECLARATION

I hereby certify that the work which is being presented in the thesis entitled **OPTICAL SPECTROSCOPY BASED URINE ANALYSIS FOR DISEASE DIAGNOSIS** in the partial fulfillment of the requirements for the award of the degree of **DOCTOR OF PHILOSOPHY** and submitted in the **DISCIPLINE OF PHYSICS, Indian Institute of Technology Indore**, is an authentic record of my own work carried out during the time period from January 2014 to October 2019 under the supervision of Dr. Sharad Gupta, Associate Professor, Indian Institute of Technology Indore, and Dr. Shovan Kumar Majumder, Professor, Raja Ramanna Centre for Advanced Technology, Indore & Homi Bhabha National Institute , Mumbai.

The matter presented in this thesis has not been submitted by me for the award of any other degree of this or any other institute.

S. B. Dutta 30/06/2020

Signature of the student with date
(SURJENDU BIKASH DUTTA)

This is to certify that the above statement made by the candidate is correct to the best of my/our knowledge.

Signature of Thesis Supervisor #1 with date
(DR. SHARAD GUPTA)

Signature of Thesis Supervisor #2 with date
(PROF. SHOVAN KUMAR MAJUMDER)

SURJENDU BIKASH DUTTA has successfully given his/her Ph.D. Oral Examination held on **June 30, 2020.**

Signature of Chairperson (OEB)
Date:

Signature of External Examiner
Date: June 30, 2020

Signature(s) of Thesis Supervisor(s)
Date:

Signature of PSPC Member #1
Date: 30th June 2020

Signature of PSPC Member #2
Date:

Signature of Convener, DPGC
Date: 30th June 2020

Signature of Head of Discipline
Date: 30th June 2020

ACKNOWLEDGEMENTS

I owe special gratitude to all of them who providing me all types of academic, research, teaching, and moral supports to the execution of most important and exciting scientific achievement of my life. It has been a true privilege to spend near about the past six years (from January 2014 to October 2019) as a PhD student at Indian Institute of Technology Indore. I am also fortunate be a part of the Laser Biomedical Applications Division, Raja Ramanna Centre for Advanced Technology (RRCAT) Indore.

I would like to express my most sincere gratitude and gratefulness to my supervisors, Dr. Sharad Gupta and Prof. Dr. Shovan Kumar Majumder, for providing me the opportunity to perform this research work under their guidance. I am also thankful to them for their erudite guidance, generous support and encouragement at every step of this work. I am deeply indebted and grateful to them for sharing their knowledge, views and ideas in the field of optical spectroscopy. The various conceptual and logical discussions with them during the entire thesis work have helped me strengthen in the understanding of fundamentals of optical spectroscopy and its biomedical applications. They have made important and valuable suggestions to improve this thesis.

I wish to convey my depth felt gratitude to my research progress committee members Dr. Preeti Anand Bhobe and Dr. Debasis Nayak. Their evaluation, worthful comments and valuable suggestions help me a lot to improve and complete the research work.

I would also like to take this opportunity to give my special thanks to the Head and DPGC convener of Discipline of Physics, IIT Indore for their support during the whole PhD journey.

I would like to take this opportunity to thank all my colleagues at IIT Indore and RRCAT Indore for their constant supports and guidance during the

entire period of this work. They patiently handled all my queries and made valuable suggestions towards updating my knowledge in this research field. My sincere thanks to all of them for their interests, encouragements and advices.

I wish to express my heartiest thanks to Dr. Sudeep Ghosh for being with me in the entire PhD journey. Without his help this journey would not have been completed. I also wish to thank all my friends for their supports.

Last but not the least, I would like to express my deep gratitude to my family members for their constant mental and moral supports. I want to express my deepest appreciation to them for their silent supports and all the sacrifices to the completion of this journey. It's my pleasure to take the opportunity to thank all of them.

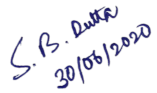

Surjendu Bikash Dutta

DEDICATION

This thesis is dedicated to my family

SYNOPSIS

Urine is a clinically important and easily accessible body-fluid having extensive diagnostic information about the health status of an individual. Human urine specimen has been subjected to analysis for different disease diagnosis since ancient times. In general, urine consists of more than 95% water, several non-protein nitrogenous compounds (NPNs) such as urea, creatinine, uric acid *etc*., trace amounts of proteins, hormones, enzymes, bacteria, metabolites, and some inorganic ions such as chloride, sodium, potassium *etc*. The varying concentration of different constituents or metabolites present in urine identify a wide range of disorders in their early stages such as kidney disorders, urinary tract infections (UTI), liver diseases, diabetes, cancers *etc*. In current medical practice, different analytical methods such as high-performance liquid chromatography, liquid chromatography-mass spectrometry/mass spectroscopy, gas chromatography, capillary zone electrophoresis *etc*. have been widely used to estimate the concentration changes of metabolites present in urine. However, all these methods follow sequences of sample preparation steps, need multiple reagents, and specialized training. Further, these methods require sophisticated, bulky and expensive instruments for urine analysis. Therefore, there is a need for an alternate approach which is rapid, reliable, inexpensive, and does not require any special sample preparation.

Recently, optical techniques such as Raman and fluorescence spectroscopy have shown immense potential for rapid urine analysis or

urinalysis by overcoming the aforementioned limitations. These techniques are able to correlate specific biochemical changes of the analytes present in urine with their normal and disease conditions. The simple instrumentation, cost-effectiveness, and molecular sensitivity of these techniques make them as suitable analytical tools for human health monitoring. Despite the promising development, the clinical applications of optical techniques are limited due to the poor signal collection and lack of reproducibility in the measured signal intensities from the analytes present in body fluids including urine. These limitations could be addressed by incorporating the nanotechnology and improved optical signal detection strategies.

The goal of the present thesis is to investigate the use of optical spectroscopy in urine analysis for rapid and reliable disease diagnosis. In this regard, an attempt has been made for the quantitative determination of trace amounts of analytes present in urine using drop-coating deposition Raman spectroscopy (DCDRS) and nano-trap enhanced Raman spectroscopy (NTERS). DCDRS is a comparatively new variant of Raman spectroscopy in which analytes or molecules get deposited in ring shape pattern on an appropriate substrate due to the coffee ring effect and improves the sensitivity of Raman signal measurement from analytes. NTERS is a new Raman signal enhancement technique in which nanoclusters of metallic nanoparticles are formed at the focus of the excitation laser beam due to optical trapping. The analytes get trapped within these nanoclusters at the peripheral region (laser beam focus) of the dried drop of solution where maximum deposition of the

solute has been occurred. The Raman signals measured from these analytes trapped within the nanoclusters get highly enhanced due to the both surface plasmon and coffee ring effects. In the subsequence of these studies the fluorescence photobleaching dynamics of urine samples has been studied and used for the oral cancer diagnosis.

This thesis is divided in six chapters and the chapter wise organization is summarized below.

Chapter 1 provides the general overview of urine analysis including the currently used analytical techniques in clinical settings and their major drawbacks. This is followed by the comprehensive review of the applications of optical spectroscopy, with a special focus on Raman and fluorescence spectroscopy, for urine analysis. Further, the motivation and specific aims of the thesis are introduced. This chapter is concluded with the organization of the present thesis work.

Chapter 2 describes the materials and methods used to carry out this research work. The details of sample preparations, experimental arrangements, and data processing are explained in this chapter.

Chapter 3 demonstrates the applicability of drop-coating deposition Raman spectroscopy (DCDRS) for quantitative determination of creatinine present in urine. The elevated level of urinary creatinine is the indicator of kidney diseases and other muscle diseases like muscular poliomyelitis, muscular dystrophy, hyperthyroidism *etc*. In order to find the potentiality of

DCDRS technique over other commonly used Raman techniques, first normal Raman spectra were measured from the aqueous solutions of creatinine as well as the artificial urine samples prepared with the varying concentration of creatinine. Then the normal Raman spectra were compared with the corresponding DCDRS spectra measured from the dried-up drops of these samples. It was observed that the measured DCDRS signal of creatinine has significantly higher intensity as compare to the Raman signal measured from its aqueous solution. Further, the possibility of the use of surface-enhanced Raman spectroscopy (SERS) was evaluated for the detection of trace quantity of creatinine present in artificial urine samples and described in detail in this chapter. SERS is a frequently used Raman signal enhancement technique based on the surface plasmon resonance of metallic nanoparticles. Although the measured SERS signal intensity of creatinine was higher as compared to the measured DCDRS signal, the repeatability of DCDRS measurement was considerably greater than the corresponding SERS measurement. Following, the varying concentrations of creatinine present in artificial urine samples were quantified using a multivariate chemometric algorithm based on partial least square in the recorded DCDRS spectra and the results are presented. Finally, the ability of DCDRS technique has been evaluated to detect the analytes present in human urine samples.

In spite of the promising potential of DCDRS technique, the detection of Raman signal of analytes presents in body fluids in millimolar (mM) to nanomolar (nM) concentration range is limited. Therefore, the sensitive and

accurate detection of disease-specific analytes present in body fluids including urine is highly desired. **Chapter 4** elaborates the design and development of nano-trap enhanced Raman spectroscopy (NTERS) technique. NTERS is a new Raman signal enhancement technique in which two phenomena are happening simultaneously (i) the maximum deposition of the solute at the periphery due to coffee ring effect during drying up of the solution drop, and (ii) the formation of nanoparticles clusters at the laser beam focus due to optical trapping. Thus, in NTERS, when the laser beam is focused at the peripheral region, it leads to the formation of nanoparticle aggregates at the region of the maximum deposition of the solute thereby causing maximum enhancement of the backscattered Raman signal. The performance of this technique for both qualitative and quantitative determination of analytes present in urine sample has been assessed and discussed in this chapter.

Photo stability of urine is important for the optical spectroscopy-based diagnosis of any disease where urine is used as a sample of choice. It has been observed that urine samples go through photobleaching process upon optical irradiation. In this chapter (**Chapter 5)** fluorescence photobleaching dynamics of urine samples has been used for disease diagnosis. This chapter evaluates the applicability of photobleaching characteristics of urine to discriminate the oral cancer patients from healthy volunteers. A classification algorithm based on nearest mean classifier (NMC) has been developed and applied on the photobleaching decay constants obtained from the fluorescence spectra of urine samples to discriminate the two categories. NMC is a classification

model which considers the least Euclidean distance of the test data from the means of the prototype data of the corresponding classes in the training set as the classification criterion.

This thesis is concluded with C**hapter 6** by summarizing the major findings followed by the possible future directions of this work in clinical applications.

LIST OF PUBLICATIONS

(A) Publications from Ph. D. thesis work:

In international refereed journals:

(Published / Accepted): Three (3)

1. **Dutta, S. B.**, Shrivastava, R., Krishna, H., Khan, Md. K., Gupta, S. and Majumder, S. K., "*Nano-Trap Enhanced Raman Spectroscopy: An Efficient Technique for Trace Detection of Bioanalytes*", ***Analytical Chemistry,*** (2019), 91, 5, 3555-3560, **I. F.: 6.35**

2. **Dutta, S. B.**, Krishna, H., Gupta, S. and Majumder, S. K., "*Fluorescence Photo-bleaching of Urine and Its Applicability in Oral Cancer Diagnosis*", ***Photodiagnosis and Photodynamic Therapy***, (2019), 28, 18-24, **I. F.: 2.589**

3. **Dutta, S. B.**, Krishna, H., Khan, Md. K., Shrivastava, R., Sahu, K., Gupta, S., and Majumder, S. K., "*Drop-Coating Deposition Raman Spectroscopy (DCDRS) for Quantitative Detection of Urinary Creatinine: A feasibility study*", ***Laser Physics***, **I. F.: 1.231 (**Accepted for publication 27 May 2020**, In Press)**

Under revision: One (1)

1. **Dutta, S. B.**, Krishna, H., Khan, Md. Khan., Gupta, S., and Majumder, S. K., "*Fluorescence photobleaching of urine for improved signal to noise ratio of the Raman signal-An exploratory study*", ***Spectrochimica Acta Part A: Molecular and Biomolecular Spectroscopy,*** **I. F.: 2.931,** (Revision received)

Manuscript under preparation: One (1)

1. **Dutta, S. B.**, Krishna, H., Khan, Md. Khan., Gupta, S., and Majumder, S. K., "*Quantitative determination of uric acid using Nano-Trap Enhanced Raman Spectroscopy*".

Conference proceedings: Three (3)

1. **S. B. Dutta**, R. Srivastava, Khan Md. Khan, S. Gupta, S. K. Majumder, "*Improving the Performance of SERS For Detecting Analytes of Biomedical Importance*", Proceedings of DAE-BRNS National Laser Symposium (NLS-26), December 20 -23, 2017, BARC – Mumbai.

2. **S. B. Dutta**, R. Srivastava, Khan Md. Khan, H. Krishna, S. Gupta, S. K. Majumder "*Reagent free creatinine measurement in urine – A novel Raman spectroscopic approach*", International symposium on Emerging Areas in Biosciences and Biomedical Technologies (eBBT), January 5 - 6, 2018, IIT Indore.

3. **S. B. Dutta**, H. Krishna, S. Gupta, S. K. Majumder, "*Studies on photo-bleaching of urine for improved signal-to-noise ratio of the Raman signal*", Proceedings of DAE-BRNS National Laser Symposium (NLS-27), December 3 -6, 2018, RRCAT – Indore.
(Best Poster award in NLS -27, December 3 -6, 2018)

(B) Other publications during PhD:

International journals: Nine (9)

1. P. Kharey, **S. B. Dutta**, A. Gorey, A. Kumari, S. Vasudevan, S. K. Majumder, S. Gupta, "Pimenta dioica-mediated Biosynthesis of Gold Nanoparticles and Evaluation of its Potential for Theranostic Applications", ***ChemistrySelect***, **I. F.: 1.716 (**Accepted for publication June 2020**, In Press)**

2. P. Kharey, **S. B. Dutta**, S. K. Majumder, S. Gupta, "Green synthesis of copper nanoparticles and their applications for plasmonic sensing", ***Asian Journal of Physics,*** Vol.29 Nos1 & 2, 2020

3. Majumder, S. K, Shrivastava, R, and **S. B. Dutta,** "Sensitive Detection of Analytes in Body-fluids for Biomedical Diagnosis: The Potential of Raman Spectroscopy", **ISRAPS Bulletin**, 32, 1, January 2020

4. Kharey, P., **S. B**. **Dutta,** Manikandan, M.; I. A, Palani; Majumder, S.; Gupta, S., "*Green synthesis of near-infrared absorbing eugenate capped iron oxide nanoparticles for photothermal application*", ***Nanotechnology***, (2019), Just Accepted, **I. F: 3.399**

5. Khan Md. Khan, **S. B. Dutta**, N. Kumar, A. Dalal, A. Srivastava, H. Krishna, S. K. Majumder, "*Inverse spatially-offset Raman spectroscopy using optical fibers – An axicon lens free approach*", ***Journal of Biophotonics*** (2019): e201900140, **I. F: 3.768**

6. A. Mathur, **S. B. Dutta**, D. Pal, J. Singhal, A. Singh, S. Chattopadhyay, "*High Efficiency Epitaxial-Graphene/Silicon-Carbide Photocatalyst with Tunable Photocatalytic Activity and Bandgap Narrowing*", ***Adv. Mater. Interfaces***, 2016, 1600413, **I. F: 4.834**

7. D. Pal, A. Mathur, A. Singh, J. Singhal, A. Sengupta, **S. Dutta**, S. Zollner, S. Chattopadhyay, "*Tunable Optical Properties in Atomic Layer Deposition grown ZnO Thin Films*", ***Journal of Vacuum Science & Technology,*** A35, 01B108 (2017), **I. F: 1.761**

8. D. Pal, J. Singhal, A. Mathur, A. Singh, **S. Dutta**, S. Zollner, S. Chattopadhyay, "*Effect of Substrates and Thickness on Optical Properties in Atomic Layer Deposition Grown ZnO Thin Films*", ***Applied Surface Science***, 421, 341-348, (2017), **I. F: 4.439**

9. Khan Md. Khan, **S. B. Dutta**, H. Krishna, and S. K. Majumder, "*Inverse SORS for detecting a low Raman-active turbid sample placed inside a highly Raman-active diffusely scattering matrix – A feasibility study*", ***Journal of Biophotonics***, 9, 879–887, (2016), **I. F: 3.768**

Conference proceedings: Six (6)

1. K. Sahu, **S. B. Dutta**, Khan Md. Khan and S. K. Majumder, "*Characterization of wound healing in mice using Raman spectroscopy and optical coherence tomography*", Proceedings of DAE-BRNS National Laser Symposium (NLS-27) 3 -6 Dec. 2018, RRCAT – Indore

2. A. Srivastava, Khan Md. Khan, **S. B. Dutta,** A. Dalal, N. Kumar, S. K. Majumder, "*Reverse confocal Raman spectroscopy (RCRS) for analysis of layered biological tissue*", Proceedings of DAE-BRNS National Laser Symposium (NLS-27) 3 -6 Dec., 2018, RRCAT – Indore

3. Khan Md. Khan, H. Krishna, **S. B. Dutta**, N. Kumar and S. K. Majumder, "*Off-confocal fluorescence spectroscopy (OCFS) – A novel approach for depth-sensitive fluorescence measurement in layered biological tissue*", International symposium on Emerging Areas in Biosciences and Biomedical Technologies, eBBT 2018, January 5 - 6, 2018, IIT Indore

4. V. Kumar, **S. B. Dutta**, H. Krishna, P. Saini and S. K. Majumder, "*Raman Spectroscopy of Radiochromic Films: An Approach to Low Energy Radiation Dosimetry*", Proceedings of DAE-BRNS National Laser Symposium (NLS-26) 20 -23 Dec., 2017, BARC – Mumbai

5. R. B. Nair, **S. B. Dutta**, Khan Md. Khan, H. Krishna, K. D. Rao, S. K. Majumder, "*Studies on Raman Spectroscopy and Optical Coherence Tomography of Formalin Fixed And Paraffin-Embedded (FFPE) Breast Tissues*", Proceedings of DAE-BRNS National Laser Symposium (NLS-26) 20 -23 Dec., 2017, BARC – Mumbai

6. A. Srivastava, Khan Md. Khan, N. Kumar, H. Krishna, **S. B. Dutta**, S. K. Majumder, "*Polarized Micrometer Scale Spatially-Offset Raman Spectroscopy (μ-SORS) For Layered Biological Media*", Proceedings of DAE-BRNS National Laser Symposium (NLS-26) 20 -23 Dec., 2017, BARC – Mumbai

TABLE OF CONTENTS

LIST OF FIGURES

LIST OF TABLES

NOMENCLATURE

E	Energy (eV)
h	Plank's constant (6.626176×10^{-34} J S)
v	Frequency (HZ)
c	Speed of light (3×10^{8} m/s)
λ	Wavelength (m)
P	Induced dipole moment (coulomb × m)
α	Polarizability ($A^2s^4 \cdot kg^{-1}$)
E	Amplitude of electric field (V/m)
t	time (Sec)
dQ	Physical displacement of atoms
Q_0	Maximum displacement
v_{vib}	Vibrational frequency (Hz)
A	Absorbance
ε	Molar extinction constant (M^{-1} cm^{-1})
l	Path length (cm)
C	Concentration of solution (M, or mol/L)
θ_R	Angular resolution (radians)
D	Diameter (m)
v	Velocity (mS^{-1})
p	Momentum (Kg mS^{-1})
m_0	Rest mass of an electron (9.1×10^{-31} Kg)
τ	Time constant (Sec)

ABBREVIATIONS

Ribonucleic acid	RNA
Deoxyribonucleic acid	DNA
Urine analysis or urinalysis	UA
Mass spectrometry	MS
High-performance liquid chromatography	HPLC
Nuclear magnetic resonance spectroscopy	NMR
Gas chromatography/mass spectrometry	GC/MS
Liquid chromatography-mass spectrometry	LC/MS
Reduced nicotinamide adenine dinucleotide	NADH
Flavin adenine dinucleotide	FAD
Surface-enhanced Raman spectroscopy	SERS
Liquid-core optical fiber	LCOF
Electrochemical-SERS	E-SERS
Drop coating deposition Raman spectroscopy	DCDRS
Nano-trap enhanced Raman spectroscopy	NTERS
Chloroauric acid	$HAuCl_4$
Sodium borohydride	$NaBH_4$
Trisodium citrate dehydrate	TSC;$Na_3C_6H_5O_7$
Silver nitrate	$AgNO_3$
Sodium hydroxide	NaOH
Rhodamine 6G	R6G
Protoporphyrin IX	PpIX
Gold nanoparticles	AuNPs
Silver nanoparticles	AgNPs
Ultraviolet visible	UV-Vis
Transmission electron microscopy	TEM
Lanthanum hexaboride	LaB_6
Collimating lens	CL
Band Pass Filter	BPF

Dichroic mirror	DM
Mirror	M
Microscope objective lens 1	MO1
Microscope objective lens 2	MO2
Laser collimator	LC
Laser clean up filter	LCF
Objective lens 1	OL1
Objective lens 2	OL2
Achromatic doublet lens	ADL
Objective lens	OL
Notch filter	NF
Focusing lens	F
Wave plate	WP
Polarizer	PL
Signal to noise ratio	SNR
Range independent algorithm	RIA
Partial least square	PLS
Root mean square error	RMSE
Percentage absolute error	PAE
Standard error	SE
Degrees of freedom	DOF
Relative standard deviations	RSD
Microalbuminuria	MAU
Signal to background ratio	SBR
Nearest mean classifier	NMC

Chapter 1

Introduction

Accurate and rapid disease diagnosis plays crucial role in disease management, proper treatment, and successful therapy [1-7]. A periodic screening of several chronic diseases like cancers, diabetes, cardiovascular disease, tuberculosis, Alzheimer's, dementia, etc., improves the patient survival rate [3, 8-12]. Therefore, nowadays the focus on the detection of disease-specific biomolecules has significantly increased before the diseases become more fatal and complicated [13-17]. Deoxyribonucleic acid (DNA), ribonucleic acid (RNA), proteins, lipids, carbohydrates, metabolites, etc., present in biological samples are considered as the important biomarkers in clinical practice for disease diagnosis and prognosis [18-26].

In clinical settings, different kinds of biological samples are regularly used for monitoring the health status of an individual. The clinical samples can be solid or liquid in nature. Solid samples are mostly pieces of tissues, stool, mucus from the genital area, throat, nose, etc. [18, 19], whereas, the liquid samples include several types of body fluids such as blood, sputum, urine etc. [20, 21]. Although in clinical practice, different types of solid and liquid samples are used for different purposes, liquid samples are preferred for large scale health screening because these can be collected in more rapid and easy manner. Additionally, the changes in the system biology, human physiology and cellular networks due to different disease conditions could directly be identified by monitoring the quantitative change of proteins in body fluids [20, 21, 27, 28].

1.1 Body Fluids:

The analysis of body fluids plays significant role in disease diagnosis. The change in concentration of a specific constituent or biomolecule present in body fluids is used to identify the disease condition [11, 29, 30]. Early-stage detection and quantification of such biomolecules can improve the patient's survival rate [31, 32]. In clinical examinations, blood and its components, saliva, urine, lymph, cerebrospinal fluid, synovial fluid, etc., are the major body fluids routinely used for disease diagnosis [33-43].

1.1.1 Blood:

In current medical practice, the chemical assays of blood get special attention for disease diagnosis than other body fluids [33, 34, 44]. It is one of the most abundant body fluids and flows through the arteries and veins. Blood mainly carries O_2 and CO_2 from the lungs to tissues and tissues to lungs. It also carries the nutrients and waste products from the digestive system to tissues and tissues to excretory organs respectively [45]. Whole blood is a complex sample and is the mixture of several types of cells and liquid. The cellular elements (~ 40 – 50% of blood volume) are mainly erythrocytes, leukocytes, and platelets. The non-cellular liquid portion is called plasma (~ 50 – 60 % of whole blood); many substances are dissolved in it. In plasma, near about 92% is water and the remaining are the dissolved solids out of which ~ 7% are proteins. The remaining 1% includes glucose, enzymes, lipids, hormones, vitamins, and several waste products such as urea, creatinine, etc. When plasma clots, a clear liquid is squeezed from this clot known as blood serum, which contains all the components of plasma except fibrinogen. In clinical examinations, the dissolved components are tested during the blood analysis to identify the physiological and biochemical states of the human body [44]. A schematic representation of the principal components of blood is shown in **Figure 1.1**.

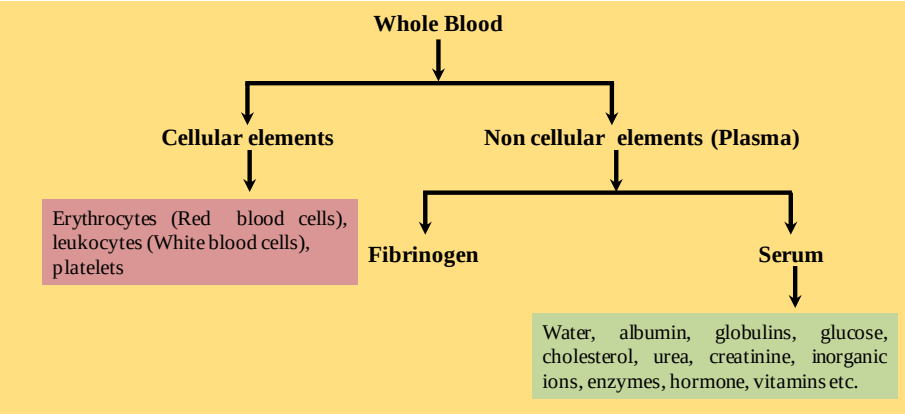

Figure 1.1: *Schematic representation of the principal components of blood*

1.1.2 Saliva:

Saliva is one of the important extracellular fluids secreted by the salivary glands and plays crucial role in oral health maintenance [46, 47]. It is an exocrine solution containing more than 90% of water and the remaining are electrolytes, proteins, mucus, epithelial cells, enzymes, etc. [48-50]. Different oral and systematic diseases such as dental caries, oral infection, etc. can be diagnosed by the compositional analysis of saliva [36, 50, 51].

1.1.3 Tears:

Tears contain the molecular information about the health status of human eyes and body [52, 53]. Tear fluid is a complex clear liquid composed of water and different proteins, electrolytes, antibodies, metabolites, etc. [52, 54]. The qualitative and quantitative analysis of tear fluid composition leads to the diagnosis of different ocular surface diseases [55, 56].

1.1.4 Urine:

Urine is a liquid by-product of metabolic wastes excreted by the kidneys from the human body and is used as a potential clinical sample for diagnosing various diseases since ancient times [37, 38]. Normally, urine contains more than 95% of water and the rest is the dissolved waste products.

The daily amount of urine excretion is ~ 1.5 – 2 L and varies greatly from person to person [57]. A thorough study of the constituents or metabolites present in urine provides crucial information about the human health status and helps to diagnose several diseases including kidney disorders, liver diseases, diabetes, etc. in their earlier stages [58-60].

1.1.5 Other Body Fluids:

Lymph, cerebrospinal fluid, synovial fluid, semen, etc. are the other body fluids present in the human body [61-64]. Chemical assays of these body fluids have been also carried out occasionally for monitoring the health status [39, 63, 65, 66].

In clinical practice, different body fluids are analyzed to detect and diagnose a wide range of disorders and all of these have their pros and cons. Analysis of blood and its derivatives are the most abundantly used disease screening method in clinical practice. Similarly, the urine analysis is the other most frequently screening procedure used in the laboratory for disease diagnosis.

1.2 Importance of Urine Analysis:

Urine has many advantages to be used as a clinical specimen than other body fluids. For example, it can be obtained in a large quantity and more readily without the involvement of any trained personal [37, 38]. Additionally, it is a less complex sample than blood plasma due to less protein content and can be collected in a non-invasive, pain-free and unrestricted manner [67, 68].

1.2.1 Brief History of Urine Analysis:

The analysis of human urine in laboratory medicine began more than 6000 years ago and until the seventeenth century, it was known as uroscopy [69, 70], today which is called the urine analysis or urinalysis. From ancient times urine was used as the primary diagnostic sample, whereas in today's

medicine it is used for the selective disease diagnosis. The art of the uroscopy began by the Babylonian and Egyptian physicians [71]. The term uroscopy is inferred from the word ‘uroscopia’. It means the ‘scientific examination of urine’. It is derived from the Greek words ‘ouron’, means ‘urine’ and ‘skopeo’, means ‘examine, inspect’ [71]. In 4000 BC, the Sumerian and Babylonian physicians assessed their urine on clay tablets [72]. In Hindu cultures, it was identified that in case of some individuals the urine tasted sweet and black ants were attracted to the sweet urine, a disease characteristic now is widely known as diabetes mellitus [72]. In recent scenario, the word uroscopy is not prolonged, but urinalysis stays as a successful diagnostic technique with a long and vibrant history.

1.2.2 Composition of Urine:

In modern clinical practice the term, urine analysis or urinalysis refers to a group of physical, chemical and microscopic tests of urine [73]. In urinalysis screening of different disease conditions including kidney disorders, liver problems, diabetes, urinary tract infections, or other metabolic dysfunctions, etc. are carried out [74-79]. In general, urine consists of more than 95% water, several nitrogenous compounds such as urea, creatinine, uric acid, etc. trace amounts of proteins, hormones, enzymes, bacteria, metabolites, and some inorganic ions such as chloride, sodium, potassium, etc. [80, 81]. The detail of the chemical composition of urine is presented in **Figure 1.2**. As a clinically important and easily accessible body fluid, the analysis of urinary metabolites is being used as an effective diagnostic method to identify specific pathological conditions.

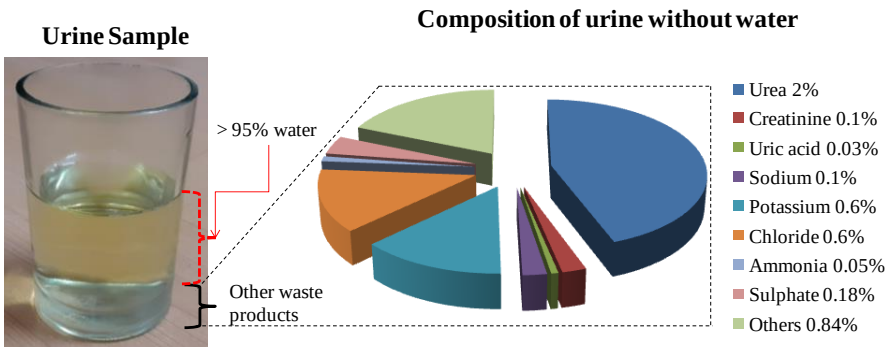

Figure 1.2: *A representation about the chemical composition of urine*

1.3 Conventional Techniques Used for Urine Analysis:

An array of analytical techniques is being used routinely for the compositional and quantitative analysis of urinary metabolites in clinics. These include different types of mass spectrometry (MS), high-performance liquid chromatography (HPLC), nuclear magnetic resonance spectroscopy (NMR), etc. [57, 82-87]. In clinics, the initial screening of urine samples is carried out by the techniques where MS is coupled with different chromatographic methods. The gas chromatography/mass spectrometry (GC/MS) is a choice for biomedical diagnosis due to its sensitivity, specificity and widespread availability [84]. The coupling of MS with liquid chromatography known as liquid chromatography-mass spectrometry (LC/MS) is also an alternate approach for clinical applications [88]. In clinics, HPLC is also used for the simultaneous quantification of urinary metabolites [87]. Additionally, the ability to identify an analyte molecule in a complex mixture of sample makes NMR as a potential diagnostic tool for metabolomics [89].

Despite the several advantages, these analytical techniques still have limitations like all these methods follow a sequence of sample preparation steps, need multiple reagents, and require specialized training of sample preparation [84]. Moreover, these techniques require sophisticated, bulky and expensive instruments for urine analysis [85]. Therefore, there is a need for an

alternative approach that would provide the label-free, inexpensive, rapid and reliable assays of urine analysis. Recent research has demonstrated that optical spectroscopy-based urine analysis might be an efficient alternative of conventional urine analysis techniques as it does not require any specialized training of sample handling or instrumentations.

1.4 Optical Spectroscopy Based Urine Analysis:

Recently, optical spectroscopy based techniques have shown immense potential for urinalysis [90, 91]. These techniques can correlate specific biochemical changes of the analytes present in urine with their normal and disease conditions [92]. The simple instrumentation, cost-effectiveness, and molecular sensitivity of these techniques make them a suitable analytical tool for human health monitoring [93].

1.4.1 Basic Principle of Optical Spectroscopy:

When light interacts with matter (or any sample) different basic phenomena such as reflection, absorption, emission, and scattering occur as shown in **Figure 1.3.** The radiation intensity of the interactions is measured as a function of wavelength and known as spectroscopy [94].

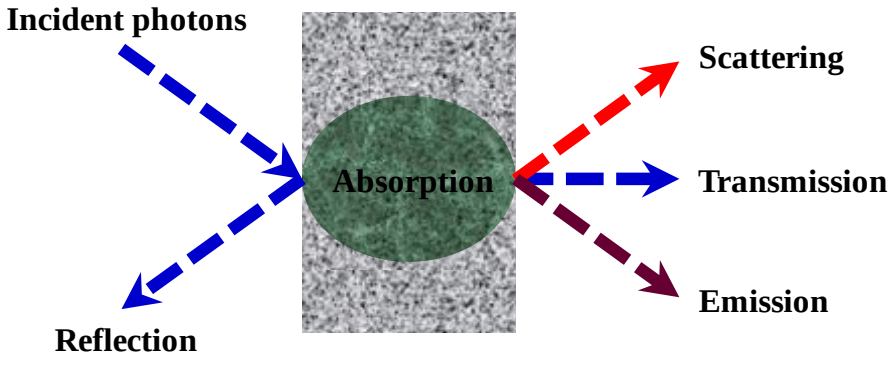

Figure 1.3: *A representation of the interaction of light with matter*

1.4.2 Absorption:

Electrons, protons, and neutrons are the fundamental particles of any atoms. The neutral neutrons and positively charged protons reside inside the nucleus. Electrons are the negatively charged particles revolving around the nucleus. Electrons have different energy levels [95]. The electrons which are revolving near the nucleus have the lowest energy level and revolving at the farthest distance from the nucleus have the highest energy level. The electrons are in the lower energy level need extra energy to jump to the higher energy level and this energy can be provided in the form of light. When the lower energy level electrons get sufficient energy, they are excited and move to the higher excited energy level. This process is known as absorption and the energy difference between the two energy levels is equal to the absorption energy as expressed in **equation 1** [94, 96].

$$\Delta E = h\nu = E_2 - E_1 \quad \text{..... (1)}$$

where, E is the energy of the incident photon, h is the Plank's constant, ν is the frequency of the photon, and E_2 and E_1 are the energy of the first excited and ground electronic states, respectively. The electronic structure of an atom and the operation of absorption are described in the energy level diagram shown in **Figure 1.4**.

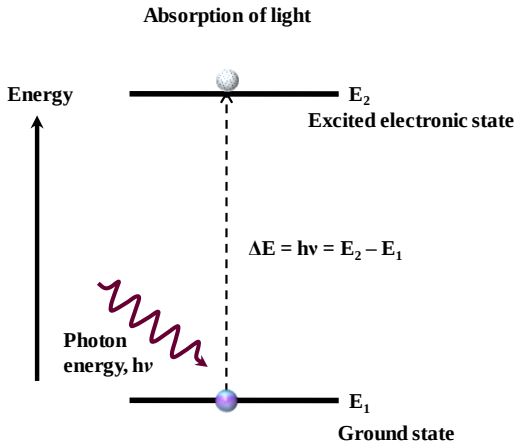

Figure 1.4: *Absorption of a photon by an atom or a molecule*

Absorption occurs only if the energy of the incident photons is equal or greater than the energy difference between the two energy levels [95]. The spectroscopic technique which measures the absorption of the radiation in forms of the transmittance or reflectance as a function of frequency or wavelength is called the absorption spectroscopy.

1.4.3 Fluorescence Emission:

During absorption, the electrons absorb the energy of the incident photons and get excited to the higher energy levels [97]. The electrons in the higher energy level are unstable, so after a short span of time, the electrons return to the lower energy level by losing their energy in the form of either light (radiative relaxation) or heat (non-radiative) [97]. The radiative relaxation phenomenon is known as fluorescence emission [97]. Fluorescence spectroscopy utilizes on the emission phenomenon of light. In fluorescence, the molecules present in the lowest vibrational energy level of ground electronic state absorb the incident photons and get excited to the various vibrational states of higher electronic state. Then the excited molecules start to lose the vibrational energy. The energy loss is continue until the molecules reach to the lowest vibrational energy level of the excited electronic state due to the collisions with other molecules [97]. Finally, the molecules return to the various vibrational energy levels of the ground electronic state by emitting photons in the form of fluorescence with different energies. This is described by the Jablonski diagram presented in **Figure 1.5** [97, 98].

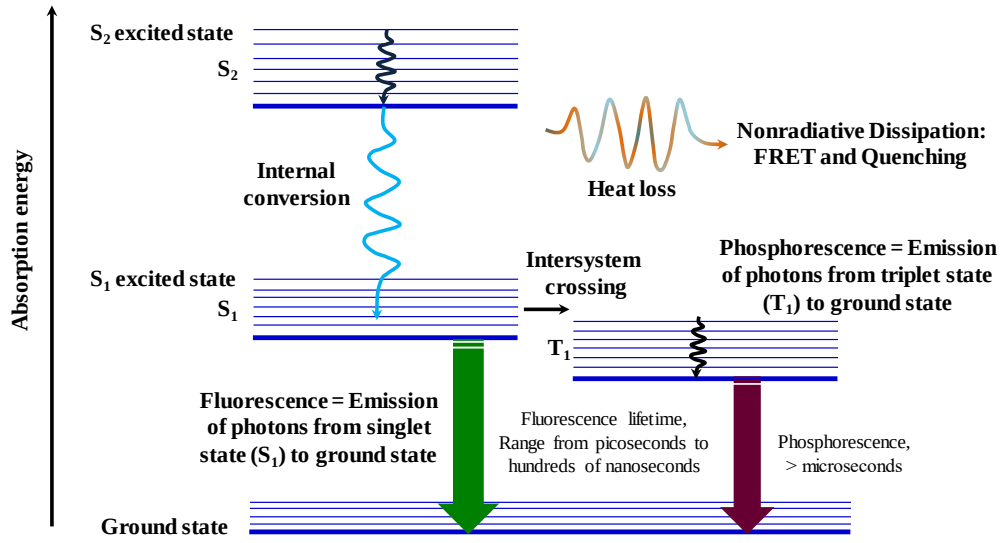

Figure 1.5: *Fluorescence emission described by the Jablonski diagram [refs. 97 & 98]. S_1 and S_2 are the singlet and doublet excited electronic states, respectively*

1.4.4 Scattering:

Scattering occurs, when the incident photons are deflected from the direction of incident ones after interacting with the molecules of the sample. There are two types of scattering; (a) elastic scattering and (b) inelastic scattering. In elastic scattering, the frequency (or energy) of the incident photon does not change after getting scattered from the molecules. This is known as Rayleigh scattering [99, 100]. In inelastic scattering, the frequency of the incident photon changes after scattering, commonly known as Raman scattering [101]. Raman scattering is a very weak process, ~1 in 10^7 photons scattered inelastically. Based on the decrease or increase of the frequency of scattered photons, Raman scattering is called Stokes or anti-Stokes [102]. The scattering process can be illustrated using the energy level diagram as shown in **Figure 1.6.**

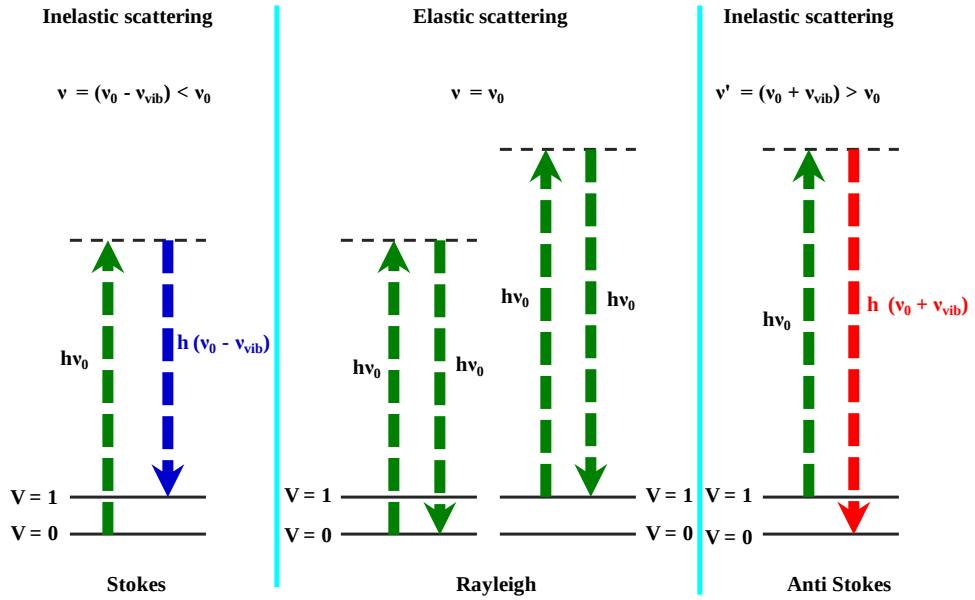

Figure 1.6: *Energy level diagram corresponding to scattering processes. h is the Plank's constant, ν_0 is the frequency (in Hz) of the incident electromagnetic wave ($\nu_0 = c/\lambda$), c is the speed of light, λ is the wavelength, and ν_{vib} is the vibrational frequency*

1.4.4.1 Raman Scattering:

When an electromagnetic wave is incident on a sample, the oscillation of the electron cloud within the constituent molecules occurs in presence of this applied electric field. It results in the periodic separation of charges within the molecules known as induced dipole moment [102]. The oscillating induced dipole moment thereby results in scattering. The energy of the scattered light is shifted from the incident light due to the molecular vibrations. The vibrational mode changes the polarizability and results in the change in energy of the incident photons, which is described mathematically. The strength of the induced dipole moment (***P***) is expressed as

$$\boldsymbol{P} = \alpha \mathbf{E} \quad \text{..... (2)}$$

where α is the polarizability and **E** is the amplitude of the incident electric field. The polarizability is the material property and depends on the

molecular structure and nature of the bonds. The electric field of the incident electromagnetic wave is expressed as

$$\mathbf{E} = \mathbf{E_0} \cos\ (2\pi\nu_0 t) \quad \text{..... (3)}$$

Where $\mathbf{E_0}$ is the amplitude of the incident wave and ν_0 ($\nu_0 = c/\lambda$) is the frequency of the incident wave. By considering the applied electric field, the induced dipole moment can be re-written as,

$$\boldsymbol{P} = \alpha\mathbf{E_0} \cos\ (2\pi\nu_0 t) \quad \text{..... (4)}$$

In addition, due to the applied electric field, some distortions occur, i.e., the molecular structure is perturbed. Hence, the atoms within the molecule are displaced physically depending on the vibrational and rotational energy. The physical displacement (*dQ*) of the atoms from their equilibrium position for the vibrational mode is expressed as

$$dQ = Q_0 \cos\ (2\pi\nu_0 t) \quad \text{..... (5)}$$

Here Q_0 is the maximum displacement from the equilibrium position. This small displacement changes the polarizability and is approximated by a Taylor series expansion [103] such as,

$$\alpha = \alpha_0 + \left(\frac{\delta\alpha}{\delta Q}\right) dQ \quad \text{..... (6)}$$

By considering the vibrational displacement the polarizability can be expressed as

$$\alpha = \alpha_0 + \left(\frac{\delta\alpha}{\delta Q}\right) Q_0 \cos\ (2\pi\nu_0 t) \quad \text{..... (7)}$$

After substituting the equation (7) into equation (4), the induced dipole moment, $\boldsymbol{P}$ can be expressed as

$$\boldsymbol{P} = \alpha_0\mathbf{E_0} \cos\ (2\pi\nu_0 t) + \left(\frac{\delta\alpha}{\delta Q}\right) Q_0\mathbf{E_0} \cos\ (2\pi\nu_0 t)\ \cos\ (2\pi\nu_0 t) \quad \text{... (8)}$$

Finally, by using the trigonometric identity, equation (8) can be rewritten as

$$\boldsymbol{P} = \alpha_0 \mathbf{E_0} \cos\,(2\pi\nu_0 t) + \frac{\left(\frac{\delta\alpha}{\delta Q}\right) Q_0 \mathbf{E_0}}{2} \{\cos[2\pi(\nu_0 - \nu_{vib})t] + \cos[2\pi(\nu_0 + \nu_{vib})t]\} \quad \text{..... (9)}$$

The above equation reveals that the induced dipole moment results in three distinct frequencies such as ν_0, ($\nu_0 - \nu_{vib}$), and ($\nu_0 + \nu_{vib}$) due to the scattering. The first one, known as elastic scattering (e.g. Rayleigh scattering), corresponds to the incident frequency. The second and third are referred as inelastic scattering (Raman scattering), correspond to the shifting of frequency (energy) to the lower or higher frequencies (energies) from incident frequency. When the frequency is down-shifted or lower it is known as Stokes scattering and up-shifted or higher it is referred to as anti-Stokes scattering.

However, for Raman scattering, the change in polarizability ($\delta\alpha/\delta Q$) must be non-zero [104]. This can be explained physically that the vibrational displacement of atoms for a particular vibrational mode results in a change in the polarizability [105]. It is evident that the value of ($\delta\alpha/\delta Q$) is non-zero at the equilibrium position (i.e., at $dQ = 0$), which further suggests that the fundamental vibrational mode of the diatomic molecule would generate inelastically scattered light and the molecule would be the Raman active. Therefore, the change in polarizability with the vibrational displacement is the necessary condition and may be thought as the Raman selection rule [105]. This is the description of Raman scattering in terms of classical mechanics. The Raman scattering can also be described by the discrete vibrational energy levels of each molecular vibrational mode.

The above discussion suggests that, polarization plays an important role in determining the Raman scattering intensity of a molecule [105]. Raman

scattering intensity is linearly proportional to the change in polarizability of the molecule or functional group [105]. Therefore, Raman spectroscopy has the inherent ability to identify the constituting molecules of a given sample [105]. However, its direct use in diluted samples is limited due to weak Raman signatures observed from the constituents. For low concentration samples, the detection becomes further difficult [93, 106]. The researchers, therefore, modified either the instrumentation or the method of the sample preparation to improve the detection sensitivity for the low concentration samples.

1.5 Current Status of Fluorescence and Raman Spectroscopy for Urine Analysis:

1.5.1 Fluorescence Spectroscopy Based Urine Analysis:

Fluorescence spectroscopy is a simple, fast, inexpensive and routinely used spectroscopic technique to analyze the sample based on its fluorescence properties [107, 108]. Urine contains several native fluorophores such as urinary albumin, reduced nicotinamide adenine dinucleotide (NADH), collagen, elastin, flavin adenine dinucleotide (FAD), porphyrins, and aromatic amino acids like tryptophan, tyrosine, etc.[109] . Most of the fluorophores display a blue-green fluorescence when excited in the wavelength from ~ 280 to ~ 450 nm [109]. The fluorescence spectra of urine samples are the combination of the characteristics emission peaks of various fluorophores present within it and the relative concentrations of these fluorophores. Hence, the fluorescence emission spectra of urine have been used to diagnose different pathological conditions in clinical settings, such as cancers, proteinuria, renal disorder, etc. [110]. Leiner et al., in their work, first measured the total fluorescence emission spectra of human urine for different excitation and emission wavelengths and found that the measured spectrum was the combination of multiple fluorescent urinary metabolites [109]. J. Kusnır et al. also provided the synchronous fluorescence spectrum concentration matrices of urinary metabolites which further improved the fluorescence analysis of

urine [110]. Rabinwitz et al. reported that the intensities of the different fluorescence emission peaks of urine samples of benign and malignant patients differed significantly from the urine samples of normal individuals. The importance of porphyrin for cancer diagnosis was also highlighted in this work [23]. Anwer et al. in their work discriminated the bacteriuria individuals from the normal subjects by measuring urine autofluorescence [111]. Perinchery et al. diagnosed urinary tract infection by measuring the autofluorescence of urine samples [112]. Recently, Yi-Qun et al. reported the variation of isoxantopterin levels in the urine of stomach cancer patients with healthy subjects by measuring the synchronous fluorescence spectra of urine samples [113]. Rajasekaran et al. characterized and diagnosed cancer by analyzing the fluorescence emission spectra and excitation-emission matrices of urine samples [114]. Lang et al., screened the attacks of acute porphyria by the spectrophotometric quantification of urinary porphyrins and porphobilinogen [115]. Masilamani et al., in their work, showed that the release of flavoproteins and porphyrins into urine can be used as biomarkers for the identification of cancers [116]. In another work, Masilamani et al. used the fluorescence emission spectra of urine for detection of cervical cancer [91]. These results suggest that urine fluorescence can be used to identify different diseases.

1.5.2 Raman Spectroscopy Based Urine Analysis:

Similar to fluorescence spectroscopy, Raman spectroscopy has also been used for urine analysis in recent years [117, 118]. Normally, the nitrogenous compounds such as urea, creatinine, uric acid, etc., have been identified and quantified using Raman spectroscopy [119]. Most commonly, near-infrared laser (785 or 830 nm) is used as the excitation source for the Raman measurement of biological samples such as tissues or body fluids to avoid the endogenous fluorescence [120, 121].

Depending on the molecular specificity and capacity for quantitative analysis without the requirements of chemicals and reagents, Raman

spectroscopy has been used for disease diagnosis by monitoring the urine samples. For the first time, Premasiri et al, showed the use of Raman spectroscopy for urine analysis [90]. In their work, they have investigated the use of both the conventional and surface-enhanced Raman spectroscopy (SERS) approaches for urine analysis. After that, several studies have been described the use of Raman spectroscopy for disease diagnosis where urine is used as a sample of choice [122-124]. Canetta et al., identified the presence of cellular components in the urine of neoplasia patients using Raman spectroscopy [125]. Shapiro et al. showed that the diagnosis of urothelial carcinoma is possible using Raman molecular imaging [123]. Goodacre et al., and Oliveira et al. used Raman spectroscopy to identify the bacteria responsible for urinary tract infection [126]. Kloss et al. identified the infectious agents in non-cultured urine samples using Raman micro-spectroscopy and chemometrics [127]. Park et al. determined the glucose concentration in urine using Raman spectroscopy [128]. McMurdy et al. first time measured the creatinine concentration in urine at clinical level by Raman spectroscopy with the near-infrared excitation source (785 nm) [122]. Qi and Berger were able to measure the urea and creatinine concentrations in clinical urine and blood samples using liquid-core optical fiber (LCOF) Raman spectroscopy by increasing the intensity of the collected signals [129]. Wang et al. applied SERS technique to detect the creatinine in urine samples of diabetic patients and diagnosed the kidney diseases [130]. Bispo et al. evaluated the potentiality of Raman spectroscopy for urine analysis to discriminate the diabetic and hypertensive patients by principal component analysis (PCA). In their work they identified urea, creatinine, and glucose from the mid-stream urine samples using a dispersive Raman spectroscopy [131]. Westley et al. quantified uric acid in human urine using SERS technique to identify the pregnancy related preeclampsia [132]. Barbara et al. used the electrochemical SERS (E-SERS) technique for the diagnosis of early preeclampsia by detecting the uric acid level in urine [133]. Huang et al. detected the tobacco related biomarkers (nicotine, cotinine, etc.) in urine by coupling SERS with

chromatography technique [134]. L.P. Moreira et al. in their work demonstrated that during the physical training (swimming) the concentrations of urinary metabolites (urea, creatinine, ketone bodies, etc.) varied significantly [135]. Y Zou et al. detected diabetes non-invasively using a portable Raman spectrometer by measuring the SERS spectra of urine samples [136]. Several other studies also demonstrated the potential of Raman spectroscopy based urine analysis for disease diagnosis [137-139]. These results suggested that Raman Spectroscopy could be utilized for the measurements of the concentrations of analytes present in urine for diagnostics of different diseases in clinics.

1.5.3 Challenges in Optical Techniques for Urine Analysis:

The simple instrumentation, cost-effectiveness, and molecular sensitivity of fluorescence and Raman spectroscopy techniques make these analytical tools suitable for human health monitoring. However, the clinical applications of these techniques for urine analysis are limited due to the low detection of trace quantity of analytes, poor signal collection and lack of reproducibility in the measured signal. These limitations could be addressed by incorporating nanotechnology and improved optical signal detection strategies.

1.6 Aim of the thesis:

The specific aim of the present thesis is to investigate the feasibility of optical spectroscopy in urine analysis for rapid and reliable disease diagnosis by overcoming the above-mentioned challenges.

The objectives of the thesis are divided into two parts.

1. One of the main objectives is to quantify the trace amounts of analytes present in urine. In this regard, attempts have been made for the use of drop coating deposition Raman spectroscopy (DCDRS) and nano-trap enhanced Raman spectroscopy (NTERS)

for the quantitative determination of the constituents present in urine.

- DCDRS is relatively a new variant of Raman spectroscopy in which analytes or molecules get deposited in ring shape pattern on an appropriate substrate due to the coffee-ring effect and improves the sensitivity of Raman signal measurement from analytes.
- NTERS is a new Raman signal enhancement technique in which nanoclusters of metallic nanoparticles are formed at the focus of the excitation laser beam due to optical trapping. The analytes get trapped within these nanoclusters at the peripheral region of the dried drop of solution where maximum deposition of the solute has occurred. The Raman signals measured from these analytes trapped within the nanoclusters get highly enhanced due to the surface plasmon and coffee ring effects.

2. The other major objective was to investigate the fluorescence photo-bleaching dynamics of urine samples for the diagnosis of different metabolic disorders including cancer. In this respect,

- The photo stability of urine samples has been studied for both Raman and fluorescence spectroscopic measurements and observed that this is an important parameter for the optical spectroscopy-based diagnosis of any disease where urine is used as a sample of choice.
- Analyzed the temporal characteristics of photo-bleaching of urine, which show promising potential to be used as an alternative tool for oral cancer diagnosis.

1.7 Thesis Organization:

This thesis is divided in six chapters. **Chapter 2** describes the materials and methods used to carry out this research work. **Chapter 3** demonstrates the applicability of DCDRS for the quantitative determination of creatinine present in urine. The design, development and the performance of NTERS technique for both qualitative and quantitative determination of analytes present in urine samples have been assessed and discussed in **Chapter 4**. In C**hapter 5,** the fluorescence photo-bleaching dynamics of urine samples have been described and the applicability of photo-bleaching characteristics of urine has been investigated to discriminate oral cancer patients from healthy volunteers. This thesis is concluded with **Chapter 6** by summarizing the major findings followed by the possible future scopes of this work in clinical applications.

Chapter 2

Materials and Methods

2.1 Introduction:

This chapter describes the materials and methods used to successfully carry out this thesis work. The details of sample preparations, experimental arrangements, and data processing are explained in this chapter. The synthesis of metallic gold and silver nanoparticles is also explained in this chapter.

2.2 Materials:

Pure urea, creatinine and uric acid powders (≥ 99% purity) were purchased from Fisher Scientific, Himedia and Sigma-Aldrich, respectively. Aqueous solutions of urea, creatinine and uric acid were prepared in Milli-Q water. In urine, the clinically relevant ranges of urea, creatinine and uric acid are 900 – 3000 mg/dl, 28 – 259 mg/dl and 16 – 100 mg/dl, respectively [140, 141]. Different sets of artificial urine samples were prepared by mixing three major constituents of urine, namely- urea, creatinine and uric acid in water, at varying concentrations in the physiological and clinically relevant ranges. The average physiological concentration of urea, creatinine and uric acid in the urine of a healthy human is ~1639 mg/dl, 104 mg/dl, and 34 mg/dl, respectively [90]. Aluminium foil (Fresh wrap) was brought from local market. Cover slip, quartz substrates and silicon wafers were procured from Blue Star, Sigma-Aldrich, and Siegert wafer GmbH respectively. Chloroauric acid ($HAuCl_4.3H_2O$), sodium borohydride ($NaBH_4$,> 99% pure), trisodium citrate dehydrate (TSC; $Na_3C_6H_5O_7.2H_2O$), Silver nitrate ($AgNO_3$, > 99% pure), sodium hydroxide (NaOH), Rhodamine 6G (R6G), and protoporphyrin IX (PpIX) were procured from Sigma-Aldrich.

2.3 Synthesis of Nanoparticles:

2.3.1 Gold Nanoparticles (AuNPs) Synthesis:

AuNPs were prepared using Citrate reduction method [142, 143]. In brief, the synthesis of AuNPs is as follows, 10 ml of 1 mM $HAuCl_4$ solution was brought to boil at 100°C temperature. At the same time this was stirred with a speed of 1000 rpm on a magnetic stirrer. Six ml of 39 mM sodium citrate was added with the solution drop wise when boiling began, and continuously stirred until the solution appears reddish. The solution was further stirred on magnetic stirrer until the heating being switched off and reaches at the room temperature.

2.3.2 Silver Nanoparticles (AgNPs) Synthesis:

AgNPs were synthesized using a co-reduction approach proposed by Agnihotri et al. [144]. In this method, two different reductants, sodium borohydride ($NaBH_4$) and trisodium citrate (TSC) were used for nucleation and growth of nanoparticles. $NaBH_4$ contributes for the fast reduction and results the formation of mono-dispersed silver nanoparticles. TSC contributes for reducing and acts as the stabilizing agent also. In brief, 20 ml of 0.5 mM $NaBH_4$ was added to 20 ml of 3.5 mM TSC and stirred for 30 min at 60°C in dark. Then, 10 ml of 2 mM $AgNO_3$ was added to the solution drop wise and subsequently the temperature was raised to 90°C. Simultaneously, added 0.1M NaOH drop wise to the solution and adjusted the pH of the solution to 10.5. Heating was continued for 20 min until the color change of the solution was observed from colorless to bright blue.

2.4 Instrumentation:

In the present work, various instrumentations were used for characterization. UV-Vis absorption spectroscopy and transmission electron microscopy were used to characterize the synthesized gold and silver

nanoparticles. Further, tabletop fluorescence and Raman spectroscopy setups were developed in house to investigate the applicability of optical spectroscopy techniques in urine analysis for rapid and reliable disease diagnosis. Details of the instrumentation are described as follows.

2.4.1 UV-Vis Absorption Spectroscopy:

The spectroscopic technique which measures the absorption of the radiation in forms of the transmittance or reflectance as a function of wavelength is called the absorption spectroscopy. Generally, a spectrophotometer is used for the absorbance measurement of any sample, in which, a lamp (UV-Visible) is used as a source of light. The schematic of absorption spectroscopy set-up is shown in **Figure 2.1.**

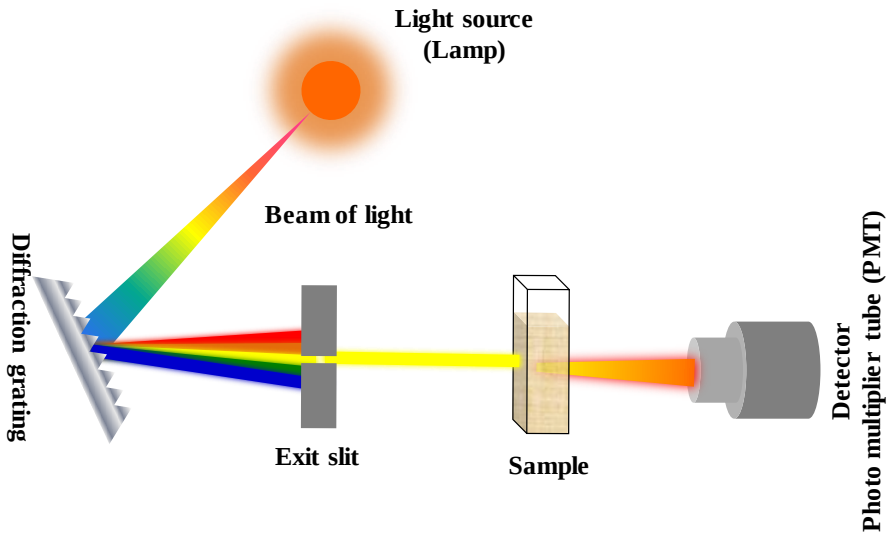

Figure 2.1: *Schematic of the absorption spectroscopy set-up*

The light strikes on the diffraction grating. Grating separates the different wavelength components of the incident light. Specific wavelength of the incident light is then passing through the exit slit by rotating the grating and interacts with the sample. Depending on the sample property the light transmits or reflects from the sample. Finally, the detector measures the transmitted or reflected light and provides the absorbance of the sample. The

light that completely passes through the sample i.e., transmitted light and/or the light that reflects from the sample i.e., reflected light finally reach the detector. In spectrophotometers generally photomultiplier tubes (PMTs) are used as detector.

Absorbance is the amount of light that is absorbed by the sample and can be calculated from the incident (I_0) and transmitted (I_T) or reflected (I_R) radiation by Beer-Lambert's law as mention in the following equation (**equation 1**) [145]. Absorbance,

$$A = \log\left(\frac{I_0}{I_T}\right) = \varepsilon l c \quad \text{..... (1)}$$

Where ε is the molar absorptive or molar extinction constant (in M^{-1} cm^{-1}), l is the path length of the solution in centimeter (cm), and c is the concentration of the solution in molarity (M, or mol/L).

2.4.2 Transmission Electron Microscopy (TEM):

TEM is an imaging technique which provides the high-resolution images where electrons are used to generate images rather than the light which is used in conventional microscopy or normal light microscopy [146]. In an electron microscope the electrons are generated from a filament by the thermionic emission [147]. Then the generated electrons are accelerated by the electric potential and focused onto the sample and get transmitted from the sample. Finally, the image formed by the information containing within the transmitted beam.

In general, the resolution of any imaging system is defined by the smallest distance between two nearest points that can be resolved. For human eye, this varies from ~ 50 µm to 150 µm with person to person under normal lightning condition [148, 149]. The instrument which could resolve the distance of less than 50 µm, is defined as a microscope [150-154]. In optical microscope, the resolution is limited by the Rayleigh criterion [155-157] as:

$$\theta_R = 1.22\,\lambda/D \text{ ..... (2)}$$

where λ is the wavelength of the light and *D* is the diameter of the lens. The resolution of the optical microscope mainly depends on the excitation wavelength. This comes out to be in the range of hundreds of nanometers for the excitation wavelength range of ~ 300 – 1000 nm. This is not enough in solid samples where the separation between two nearby atoms is ~ 0.2 nm [158, 159].

In this regard, electron microscopy gets more attention and shows significant advantage over optical microscopy. An electron possesses both the wave and particle properties. Hence, a beam of electron can be focused and diffracted like light due to its wave nature. The wavelength of electrons is defined by the de Broglie equation [160, 161] as:

$$\lambda = \frac{h}{p} = \frac{h}{mv} \text{ ..... (3)}$$

Where *h* is the Planck's constant, *m* is the mass of the electron moving at a velocity *v* and *p* is the momentum. If the energy of the accelerated electron is *E*, then the wavelength of the electron can be described by considering the relativistic effects, as the velocity of electron in TEM defined by the fraction of the speed of light c, hence

$$\lambda = \frac{h}{\sqrt{2\,m_0 E\left(1+\frac{E}{2m_0c^2}\right)}} \text{ ..... (4)}$$

where m_0 is the rest mass of an electron.

For the morphological characterization of the synthesized nanoparticles Philips CM200 TEM was used. The basic ray diagram of a typical TEM system is shown in **Figure 2.2** [146]. It consists of a Lanthanum Hexaboride (LaB_6) gun as the electron source operated with a maximum accelerating voltage of 200kV. The other components are condenser lens, sample specimen, objective lens, projector lens, and fluorescent screen. The lenses are used to focus or defocus the electron beam and changing the

magnification. The optimum image resolution for this microscope is ~ 0.25 nm.

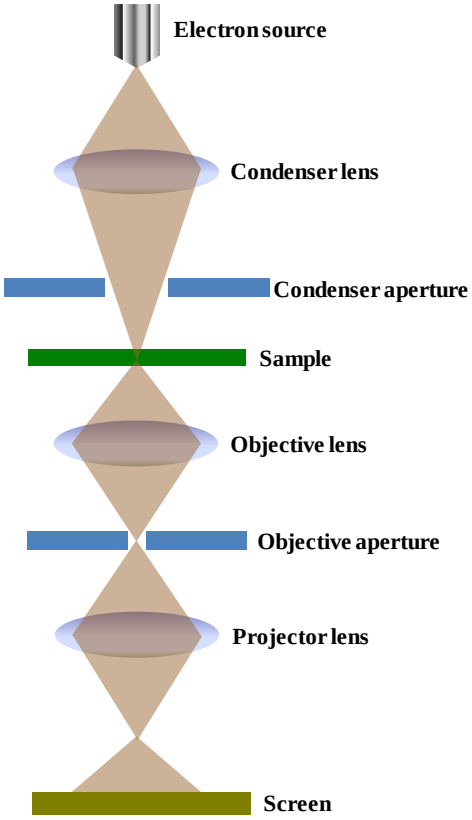

Figure 2.2: *Ray diagram of a typical TEM system [ref. 146]*

2.4.3 Fluorescence Spectroscopy:

The fluorescence spectra of urine samples were recorded using a home built tabletop fluorescence spectroscopy set-up. The schematic representation of the developed set-up is shown in **Figures 2.3.** It uses a 405 nm solid state diode laser for the illumination. At first, the output laser light is collimated using a collimating lens and then spectrally purified by a band pass filter (Full Width Half Maximum = 10 nm). The filtered beam is then reflected by a dichroic mirror and plane mirror towards the sample direction. Finally, the illumination light is focused on the sample surface using a 10 X microscope objective lens (Comar Optics Ltd.). The backscattered fluorescence signal of urine samples was transmitted through the same dichroic mirror and focused

on a fiber tip using a 20 X microscope objective lens (Comar Optics Ltd.). The other end of the fiber is connected to the spectrometer (Ocean optics), which detects the measured fluorescence intensity of the samples as a function of wavelength.

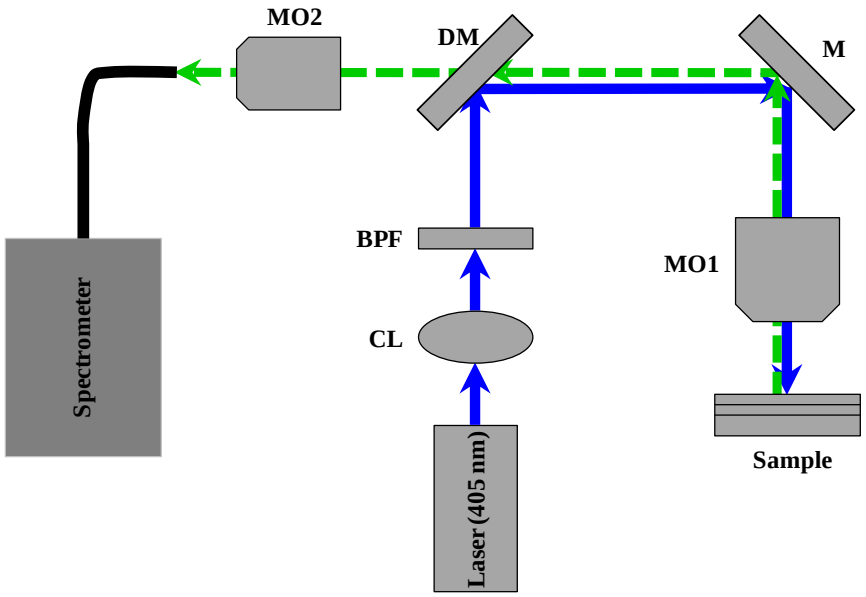

Figure 2.3: *Schematic representation of the fluorescence spectroscopy system*

The home built tabletop experimental set-up used for fluorescence spectroscopic measurements of urine samples is shown in **Figure 2.4**. This is showing that urine samples were kept in a quartz cuvette and the samples were excited using a diode laser of 405 nm. The measured fluorescence spectra were recorded with the spectrometer as shown in the following figure (**Figure 2.4**).

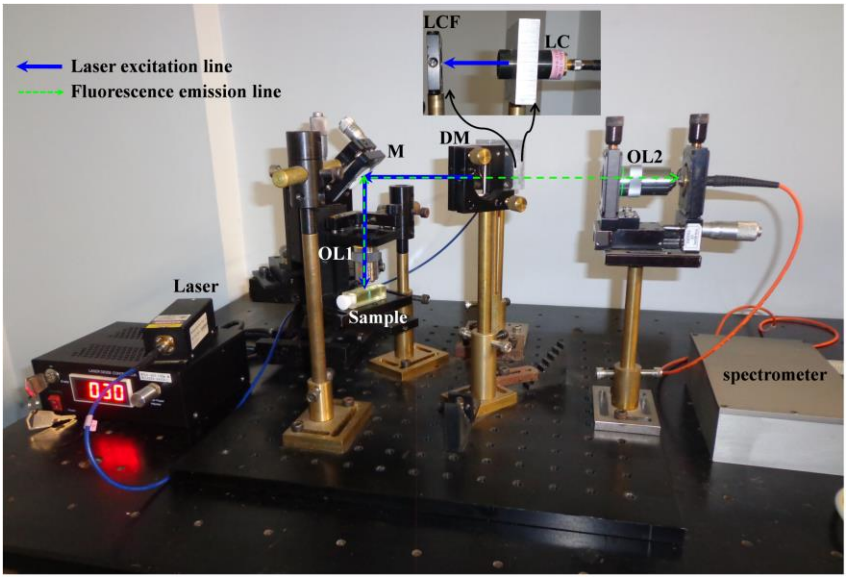

Figure 2.4: *The home-built tabletop experimental set-up of fluorescence spectroscopy system*

First morning urine samples were collected from healthy volunteers (n = 22). Prior to the sample collection the health status of each volunteer was recorded. The samples were collected from these volunteers who did not have any history of major illness in the past two months. Additionally, urine samples were collected from the oral cancer patients (n = 18) who were admitted at the Government cancer hospital, Indore. Before the sample collection the volunteers were advised to maintain proper water intake to avoid excretion of concentrated urine. The collected urine samples were stored at 4°C until spectroscopic measurements were performed.

The fluorescence emission spectra of urine samples of both healthy volunteers and the oral cancer patients were acquired in a spectral region covering from 410 to 760 nm. Each sample was excited using a 405 nm diode laser with a laser power of 1.5 mW at the focal plane and the backscattered fluorescence signals were detected using a spectrometer.

2.4.4 Raman Spectroscopy:

The Raman spectra of urine phantoms and urine samples were recorded using a home-built tabletop Raman spectroscopy set-up. The schematic of the home-built tabletop Raman spectroscopy system used for experiments is shown in **Figure 2.5**.

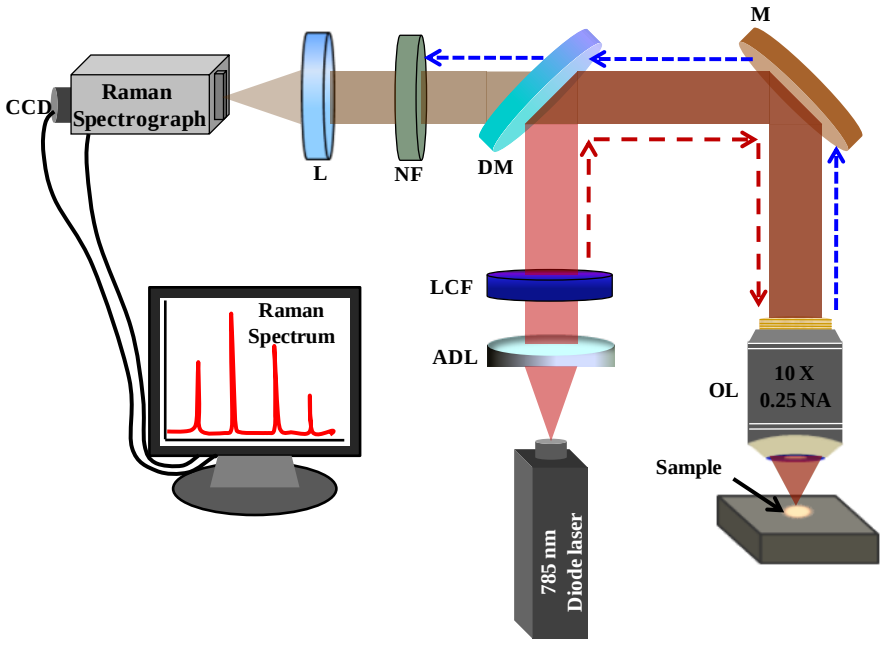

Figure 2.5: *Schematic representation of the home-built tabletop Raman Spectroscopy system*

A single-mode diode laser (785 nm) is used as the excitation source. The laser beam is first collimated using an achromatic doublet lens of focal length 50 mm. The collimated beam is then filtered using a laser clean up filter or band pass filter (HQ782/20X, 279142, Chroma tech Crop.) and reflected by a dichroic mirror, DM (LPD02-785RU-25, Semrock, Inc) placed at an angle of 45°. Another mirror (M) is placed at an angle of 45° to steer the beam towards the sample. The excitation laser beam is focused on the sample surface using a microscope objective lens (10 X, 0.25 NA). The backscattered Raman signal of the sample is collected through the same objective lens, reflected by M and transmitted through DM. The Raman signal is then passed through a notch

filter which removes the elastically scattered Rayleigh component. Further, a convex lens coupled the Raman signal at the entrance slit of an imaging spectrograph (SR-303iA, Andor Shamrock) equipped with a thermoelectrically cooled, back-illuminated, deep-depletion CCD camera (DU416A-LDC-DD, Andor). **Figure 2.6** shows the home-built tabletop Raman spectroscopy system.

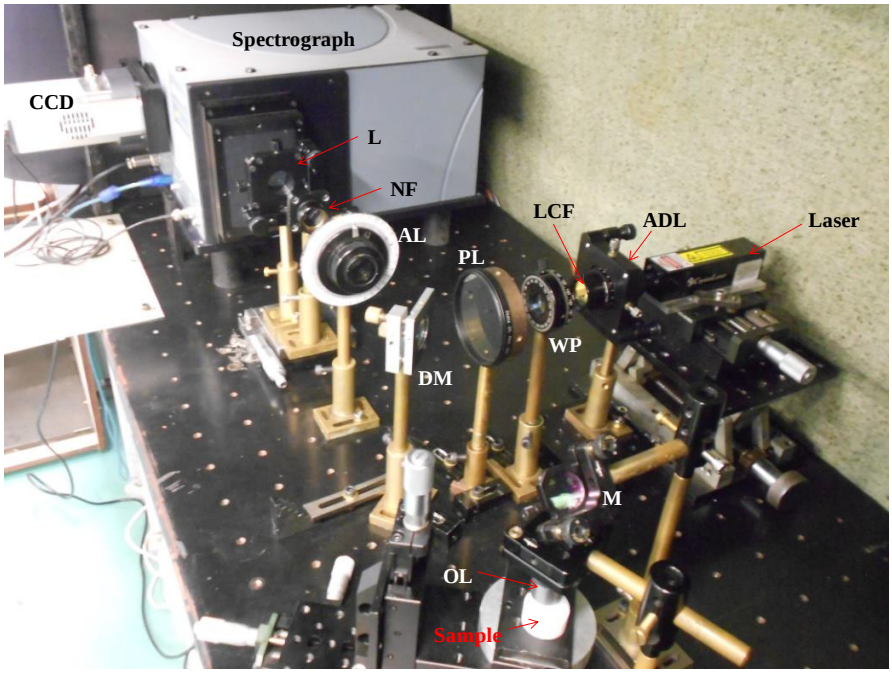

Figure 2.6: *Experimental set-up of the home-built tabletop Raman Spectroscopy system*

Before the Raman measurement, the wavenumber axis was calibrated with the illumination laser line and the most intense Raman peak of naphthalene and silicon wafer were centered at 1382 cm^{-1} and 520 cm^{-1}respectively. All the spectra were measured in the spectral range of 400 – 2100 cm^{-1} at a grating of linear dispersion 600 lines/mm. The signal to noise ratio (SNR) for 1382 cm^{-1} naphthalene Raman peak at an integration time of 0.2 s with 50 mW laser power at the sample surface was found to be ~ 350. Here, SNR is the ratio of the intensity of the maximum intense characteristic Raman peak of the targeted analyte to the standard deviation of the noise

present in the spectra. After optimizing the settings of the developed system, the Raman spectra of different samples were measured.

2.4.4.1 Drop-Coating Deposition Raman Spectroscopy (DCDRS):

In this work, the DCDRS technique was applied for the quantitative determination of creatinine in urine. DCDRS is based on the evaporation of a sessile droplet on a solid substrate. In DCDRS, the evaporation of a drop of non-volatile solutes occurred at the contact line of pinning by the formation of coffee ring patterns [162]. During evaporation, the fluid flux of the drop is driven by the surface tension towards the edge of the drop [163-167]. The movement of suspended particles to the edge leads the ring like deposition [162]. The detail mechanism of drop evaporation is presented in **Figure 2.7**.

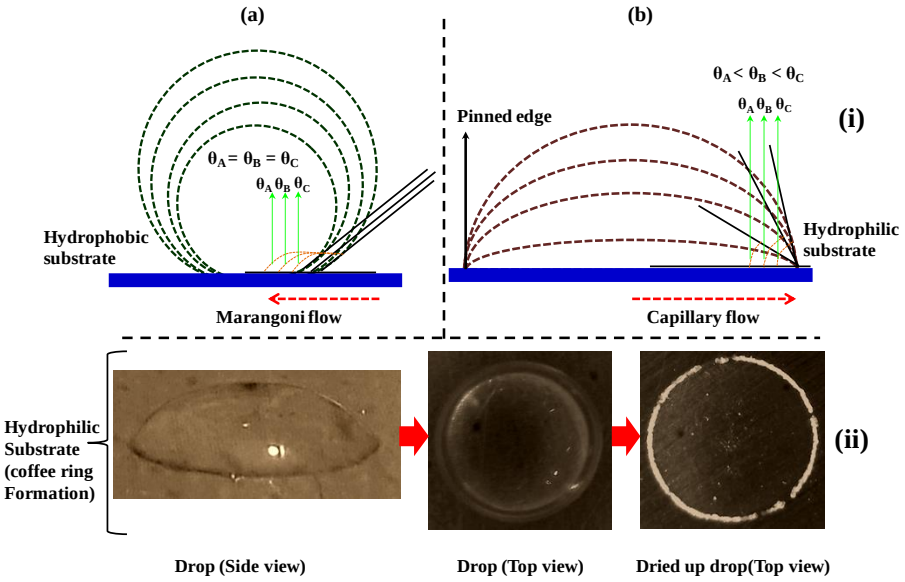

Figure 2.7: *Mechanism of the drop evaporation.* ***(i)*** *Basic principles of drop evaporation due to the (a) Marangoni flow and (b) capillary flow respectively.* ***(ii)*** *Drop evaporation and coffee ring formation of the aqueous solution of creatinine on aluminum foil.*

Figure describes that there are two types of flow exhibits depending on the substrates structure. One is Marangoni flow [168-170] when the substrate is hydrophobic in structure and the other is capillary flow [171] for hydrophilic

substrate. The contact pinning line and contact angle hysteresis play important role during the drop evaporation. In Marangoni flow the contact angles remain fixed whereas for capillary flow the contact radius (pinned edge) remains constant. Figure also presents the process of the drop evaporation and coffee ring formation of the aqueous solution of creatinine on aluminum foil. As aluminum foil is hydrophilic in nature the solute molecule (creatinine) get deposited in a ring like structure.

For the quantitative detection of urinary creatinine, the conventional Raman spectra were measured from the aqueous creatinine samples. The samples were kept in a quartz cuvette for spectral measurements. To obtain the DCDRS spectra, a 4 µl drop of the same aqueous solution of creatinine was dried on different DCDRS substrates including aluminum foil at room temperature and the laser light (λ = 785 nm) was focused at the circumference of each dried drop. DCDRS spectra were measured from five different points along the circumference of each dried drop. Such data were recorded in triplicate samples. For comparison sake, the SERS spectra of creatinine were also measured using silver nanoparticles as SERS substrate. To measure the SERS spectra, a 4 µl drop of the aqueous solution of creatinine was placed on the previously dried drop (4 µl in volume) of silver nanoparticles. The incident laser power and the data acquisition times were adjusted for all the measurements such that it allows full utilization of the dynamic range of the detector. Conventional Raman measurements from liquid samples of creatinine were carried out at the laser power of 20 and 50 mW with a data acquisition time of 60 and 25 s, respectively. SERS and DCDRS measurements were performed with the laser power of 20 mW and data acquisition time of 1 s.

2.4.4.2 Surface-Enhanced Raman Spectroscopy (SERS):

In this thesis work, we have also measured the SERS signals of the analytes such as R6G, creatinine, urea, and uric acid. SERS is an efficient analytical tool used for the trace detection of analytes present in liquid as well as gaseous samples in presence of the metallic nanoparticles or nanostructures

[172], in which the analyte molecules are adsorbed on the metal surface. SERS exploits the interaction of electromagnetic wave (light), metallic nanostructures, and the molecules to enhance the Raman signal of the molecules in several orders of magnitude (> 10^4 – 10^5). In some cases, the Raman signal enhancement is the order of magnitude greater than 10^{12} – 10^{14} [173, 174]. The chemical structure of the materials can be detected in single-molecule level using SERS. The Raman scattering intensity (I_R) of a molecule is directly proportional to the intensity of the incident electric field ($\mathbf{E_0}^2$) and Raman scattering cross section [$(\partial\alpha/\partial Q)^2$], as defined in the following equation [172, 175].

$$I_R \propto |\mathbf{E_0}|^2 \left(\frac{\partial \alpha}{\partial Q}\right)^2 \text{ …….. (5)}$$

Hence, the huge Raman signal enhancement of molecules on metallic surface of nanoparticle is the product of two types of enhancement, one is the electromagnetic enhancement depends on the incident electric field and another is the chemical or electronic enhancement depends on the Raman scattering cross section. The SERS enhancement factor (EF_{SERS}) of a molecule can be expressed as:

$$EF_{SERS} = EF_{EM} * EF_{CE} \text{ …….. (6)}$$

The first term (EF_{EM}) depends on the localization of the incident electric field on the metal surface and results in the enhancement of incident and Raman scattered electric fields. The second term (EF_{CE}) occurs due to the enhancement of Raman scattering cross section which depends on the electronic charge transfer between the molecule and metal when they are close together. The electromagnetic field enhancement (EF_{EM}) can be described in terms of localized surface plasmon resonance (LSPR), as shown in **Figure 2.8** [172, 175]. Plasmon occurs when the incident light interacts with a much smaller metallic nanoparticle than the incident wavelength and the valance electrons of metallic nanoparticles collectively oscillate locally around the

nanoparticles with a frequency in the resonant with the incident frequency, known as LSPR [172, 175].

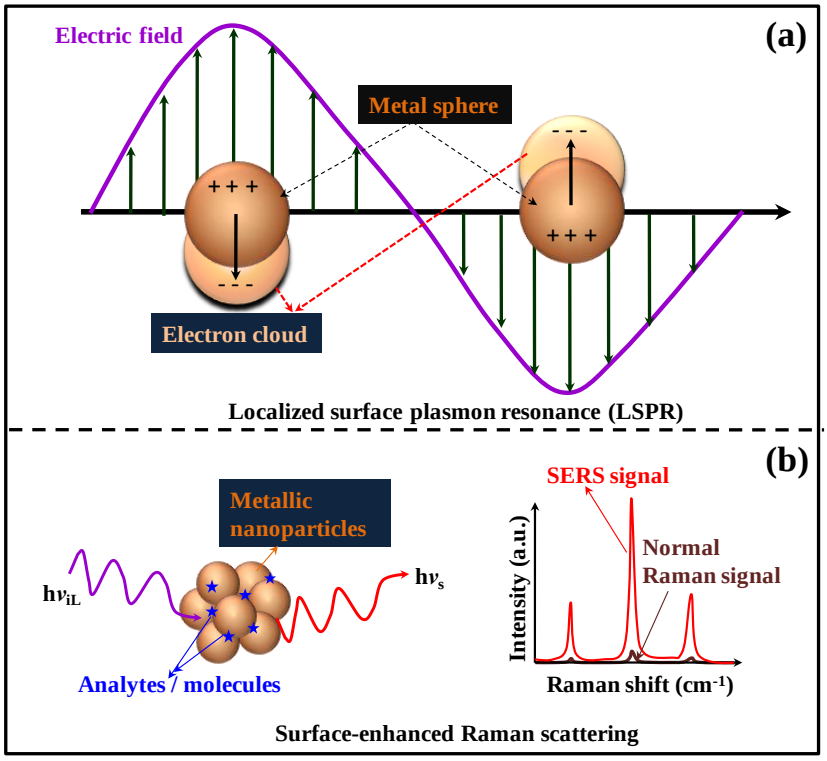

Figure 2.8: *Basic mechanism of SERS technique. (a) The localized surface plasmon resonance phenomenon of metallic nanoparticles [refs. 172 & 175]. (b) The Raman signal enhancement of the analytes adsorbed on the metal surface due to the SERS effect.*

The SERS enhancement factor largely depends on the LSPR and contribute ~10^4 - 10^5 times enhancement in the scattered Raman signal. The SERS effect is also depending on another factor called the chemical enhancement factor. In chemical enhancement, the Raman polarizability of a molecule adsorbed on a metal surface is enhanced. This contributes ~10^1 – 10^2 times enhancement in the scattered Raman signal. This is the theoretical aspect of the SERS enhancement factor for a given molecule adsorbed on the metal surface. The same can also be calculated in practical using the following equation

$$Enhancement\ factor\ (EF) = \left[{(I_{SERS}/I_{RS})}\Big/{(C_{SERS}/C_{RS})} \right] \quad \ldots\ldots\ldots\ldots (7)$$

where, I_{SERS} and I_{RS} are the intensities of SERS and Raman signals respectively and C_{SERS}, C_{RS} are the molecule concentrations for SERS and Raman measurements, respectively.

The other important parameter for the SERS measurement is the reproducibility in the measured SERS signal of an analyte. The reproducibility (*R*) is defined by the following equation as:

$$R = 1 - \left(\frac{Standard\ deviation\ in\ intensity\ for\ a\ given\ peak}{Mean\ intensity\ for\ the\ same\ peak}\right) \ldots\ldots (8)$$

In this thesis work, we have measured the SERS signals of the analytes such as R6G, creatinine, urea, and uric acid. The measured SERS signals were also compared with the Raman signals of analytes measured with the other variants of Raman spectroscopy like DCDRS and NTERS techniques.

2.4.4.3 Nano-Trap Enhanced Raman Spectroscopy (NTERS):

In the progress of this thesis work, a new Raman signal enhancement technique called NTERS was invented for the detection of trace amount of analytes present in body fluids including urine. The detail mechanism of NTERS is described in **Figure 2.9**. In NTERS, hotspots are formed by drying up a micro volume drop of a liquid, containing an aqueous mixture of nanoparticles and analytes in the presence of a focused laser beam. A focused laser beam on a nanoparticle creates two forces; gradient and scattering [176-179]. If the wavelength of the laser is chosen away from the absorption band of the nanoparticle, the gradient force dominates over the scattering force and the particle is pushed towards the focus of the beam i.e. it is trapped [180-182]. Due to trapping, nanoparticles form clusters around the focus of the laser beam. Then, detect the Raman signal from these spots containing the analytes localized within the nanoparticle aggregates.

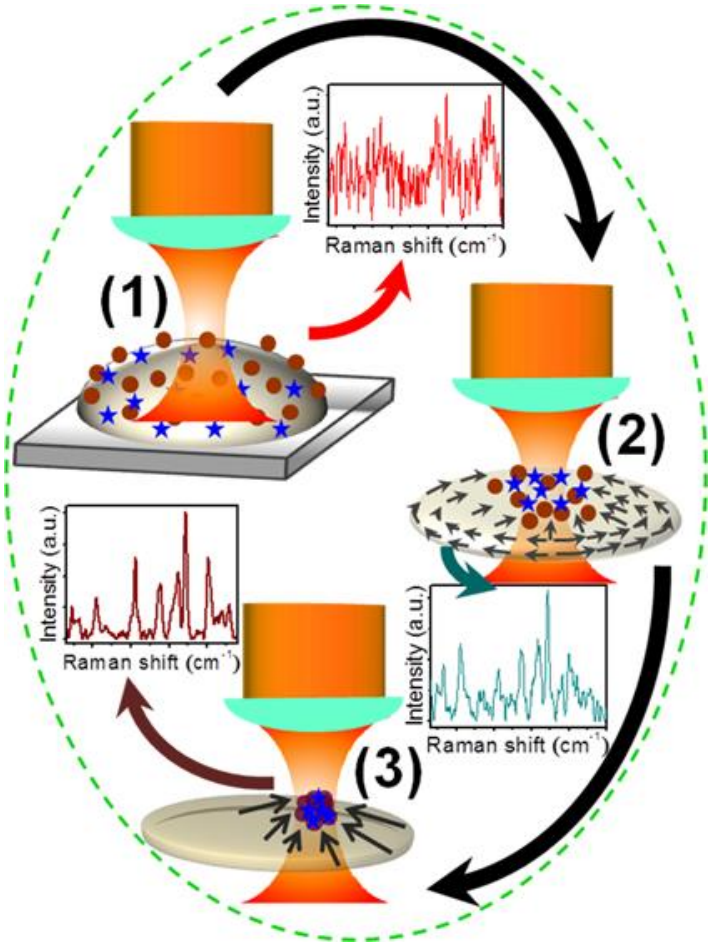

Figure 2.9: *Mechanism of NTERS technique: nano-aggregates formation and NTERS measurements*

In NTERS, this process is simultaneous with the evaporation of the liquid drop due to the coffee ring effect which results the formation of nanoparticle aggregates at the region of the maximum deposition of the solute (i.e. “hotspots”) thereby causing maximum enhancement of the backscattered Raman signal from the analytes. Further, the stability of laser power allows for maintaining the constant gradient force required for trapping of the nanoparticles. The high reproducibility in the laser mediated formation of the nanoparticle aggregates combined with simultaneous drying up of the aqueous drop leading to efficient embedding of the analyte molecules in the 3D aggregates (of nanoparticles) results in a very high reproducibility in the measured NTERS signal.

To evaluate the performance of NTERS, experiments were carried out using aqueous solutions of Rhodamine 6G (R6G) as samples. The concentrations of R6G in these solutions ranged from 50 nM to 2.5 µM. For evaluating the performance on a biologically relevant molecule, an aqueous solution of urea of 4 mM concentration, which is equivalent to its physiological concentration in human blood, was used. All these samples were prepared by mixing 5 µl of 2.5 nM spherical gold nanoparticles (GNPs) with 5 µl of aqueous solutions containing varying concentrations of the analyte molecules to be probed. For NTERS measurement, a 4 µl drop of the sample mixture (i.e. the mixture of nanoparticles and analytes) was placed on an aluminum foil, and the laser beam was shone onto a point lying along the contact line of the drop with the surface. The drop was allowed to dry in this condition. Once the 3D aggregates of GNPs were formed, the Raman signal was measured from the same point. The optical power delivered on to the sample was 50 mW and the spectra were acquired for an integration time of 1 s.

After evaluation of the performance of the NTERS technique, we have used this technique for the quantitative assessment of biomolecules. In this regard, the quantitative determination of uric acid has been done using NTERS. At first, stock solution (1 mM) of uric acid was prepared by mixing 16.8 mg of uric acid in 98 ml Milli-Q water. After that 2 ml of 1 M NaOH was added with the solution to dissolve the uric acid completely in water. Then different sets of samples were prepared using the stock solution. For NTERS measurement silver nanoparticles were mixed with sample solutions in a 1: 1 ratio. A 4 µl drop of the mixture (i.e. the mixture of uric acid solutions and nanoparticles) was placed on an aluminum foil, and the laser beam (20 mW at sample surface) was focused along the contact line of the drop and let it be in this condition to form the nanoclusters or aggregates. Finally, the Raman signals were acquired from these aggregates for 1 s integration time.

In addition to the Raman spectroscopic measurements, the fluorescence photobleaching phenomenon of urine sample was investigated during both the Raman and fluorescence spectral measurements. To generate a set of time-lapse fluorescence spectra of a given urine sample, spectra were acquired sequentially for 600 s at a time interval of 1 s and with an integration time of 10 ms. Each sample was continuously illuminated by the laser light of a central wavelength of 405 nm till all the spectral measurements were completed for that particular sample. Similarly, the time-lapse Raman spectra of urine samples were measured. Each sample was continuously illuminated by the laser light of a central wavelength of 785 nm till all the spectral measurements were completed for that particular sample. The time-lapse spectra were sequentially acquired for a total time of 600 s with the acquisition time of 1 s.

2.5 Data Processing:

After the Raman measurements, the measured Raman spectra were processed for further uses. In brief, for each measured Raman spectrum, the signal from the CCD was binned along the vertical axis to create a single spectrum per measurement. Before signal processing, the spectrum was truncated to include the fingerprint region from 400 to 2100 cm^{-1}. The spectrum was then noise smoothened using a second-order Savitzky–Golay filter [183] and background-subtracted using the range independent background subtraction algorithm (RIA) [184] for extracting the sample Raman signatures buried in the background. The RIA uses a model based on modified iterative smoothing of the measured Raman spectrum in such a manner that the high-frequency Raman peaks are gradually eliminated finally leaving the underlying broad baseline which can be subtracted from the raw spectrum to yield the Raman signal with zero baseline. The spectrum thus obtained was then used for further analysis.

2.6 Statistical Analysis:

2.6.1 Quantitative Estimation of Analytes using Partial Least Square (PLS) Analysis:

The processed Raman spectra were analyzed for the quantitative prediction using multivariate partial least square (PLS) analysis [185, 186]. PLS relates the spectral variation of the full range of data with the concentration of the constituents [187, 188]. The PLS model has the following form:

$$Y = XB + E \quad \text{..... (9)}$$

Here, X is an $N \times D$ matrix, which contains the N *number* of Raman spectra of the samples. D is the wavenumber dimension of each spectrum. Similarly, Y is an $N \times C$ matrix, where C is the number of constituents whose concentrations are to be determined. B matrix is the matrix of regression coefficients and the size of B is $D \times C$ and the residuals which are not fit by the model is E.

First, the calibration model was developed using a set of known concentration sample, then the developed model further used for the prediction of unknown concentrations (Y_{new}) from the measured set of Raman spectral data (X_{new}) according to:

$$Y_{new} = X_{new}B \quad \text{..... (10)}$$

To evaluate the accuracy of the PLS model, the root mean square error (RMSE) [189]was estimated which is defined as the square root of the average of the squares of the difference between reference and predicted concentration as given by the following equation:

$$RMSE = \sqrt{\frac{1}{N}\sum_{i=1}^{N}(C_{Ri} - C_{Pi})^2} \quad \text{..... (11)}$$

Where C_R and C_P represent the reference and predicted concentrations respectively.

Another statistical parameter, percentage absolute error (PAE) was calculated to estimate the prediction error at each of the constituents' concentrations [190]. PAE is defined as:

$$PAE\ (\%) = \frac{|C_R - C_P|}{C_R} \times 100 \text{ ..... (12)}$$

2.6.2 Identification of Statistically Different Spectral Regions:

In order to identify the region of statistically spectral differences between the fluorescence spectra of urine samples from healthy volunteers and patients with oral cancer, standard error (SE) confidence intervals were utilized [191, 192]. The SE was calculated at each wavelength as:

$$SE\ (\lambda) = \sqrt{\frac{\sigma^2_{Normal}(\lambda)}{n_{Normal}} + \frac{\sigma^2_{Cancer}\ (\lambda)}{n_{Cancer}}} \text{ ..... (13)}$$

Here, σ^2 is the variance of the intensities at each wavelength and *n* is the number of samples of a given category. The SE was then multiplied by appropriate *t*-values based on total degrees of freedom (DOF = n_{Normal} + n_{Cancer} - 2) and a predefined confidence level ($p < 0.05$) to produce a confidence interval. This helps to qualitatively identify the wavelength regions having statistically significant spectral differences. These are the wavelengths at which intensity differences between two sample types are larger than the confidence interval.

Chapter 3

Drop-Coating Deposition Raman Spectroscopy (DCDRS) for Quantitative Detection of Urinary Creatinine: A Feasibility Study[*]

This chapter evaluates the applicability of drop coating deposition Raman spectroscopy (DCDRS) technique for the quantitative measurement of creatinine present in urine. The comparison of the conventional Raman and the DCDRS spectra measured from artificial urine, as well as actual urine samples from human volunteers, showed significant improvement in signal-to-noise ratio for DCDRS. The quantification of creatinine in artificial urine samples was done by applying the partial least square (PLS) based chemometric algorithm on the measured DCDRS spectra. The result suggests that DCDRS could detect creatinine present in the artificial urine samples with an accuracy of over 94% in the physiological concentration range.

3.1 Introduction:

Urinary creatinine gives information about the functioning of the kidneys. The elevated levels of creatinine in urine signal towards the muscle diseases, like muscular poliomyelitis, muscular dystrophy, hyperthyroidism, etc. [193-197]. Therefore, the quantification of creatinine present in urine has significant importance for diagnosing these disease conditions [198-201]. In

[*] *This chapter is largely taken from the paper: S. B. Dutta et al, "Drop-Coating Deposition Raman Spectroscopy (DCDRS) for Quantitative Detection of Urinary Creatinine: A feasibility study", Laser Physics-IOP Science, (Accepted for publication 27 May 2020, In Press)*

recent years, there has been an increasing interest in the use of Raman spectroscopy as an alternative technique for the analysis of urinary creatinine [90, 140, 202, 203]. Raman spectroscopy could detect a small change of individual components with different concentration levels in a mixture sample by measuring the relative intensity changes of their corresponding Raman peaks. The other advantage provided by the Raman spectroscopy is that it is rapid and non-destructive do not require any sample preparation [120, 121, 204-206]. Several earlier studies, reported in the literature have showed the feasibility of this approach for urine analysis [90, 140, 196, 202]. However, the scope of the conventional Raman spectroscopy is limited due to the rather weak Raman signatures observed from the creatinine in the aqueous phase. Recently, researchers have proposed the use of surface-enhanced Raman spectroscopy (SERS) to improve the sensitivity of Raman in detecting the urinary creatinine [130, 136, 207-209]. However, the very poor reproducibility of the approach prevents its practical utility in the quantitative determination of urinary creatinine.

We report here the results of a study carried out to evaluate the applicability of DCDRS for the quantitative determination of creatinine present in urine. DCDRS technique already has been shown the immense potential for biofluids and protein analysis towards the disease diagnosis [210-220]. The technique relies on the formation of a "coffee ring" pattern [221-223]by drying up of a microliter volume drop of a liquid containing an aqueous solution of the analyte and then, detecting the Raman signal from the dried-up pattern of this drop. Aqueous creatinine solutions, as well as artificial urine samples, were prepared with varying concentrations of creatinine in ultra-pure water. The DCDRS spectra were measured from the dried-up spots of these samples and real urine samples formed on an aluminum foil. The results of our study showed that this technique could detect creatinine present in the artificial urine samples with an accuracy of over 94% in the physiological concentration range. Following the investigation of the ability of DCDRS in detecting

creatinine in artificial urine samples, the ability of this technique was evaluated in detecting the analytes in actual human urine samples.

3.2 Results and Discussions:

Figure 3.1 shows the measured Raman spectra of pure creatinine powder. The integration time used for the spectral measurement was 1 s and the laser power measured at the sample surface was ~20 mW. One can see that the spectra are characterized by four very intense Raman peaks located at 601 cm^{-1} (C═O deformation N─CH_3 stretching, and ring vibrations), 680 cm^{-1} (C─NH_2 and C═O stretching and ring vibrations), 846 cm^{-1} (C─NH_2 deformation and ring vibrations) and 908 cm^{-1} (C─C─N stretching), respectively. These Raman peaks are following those reported in the literature [140, 141].

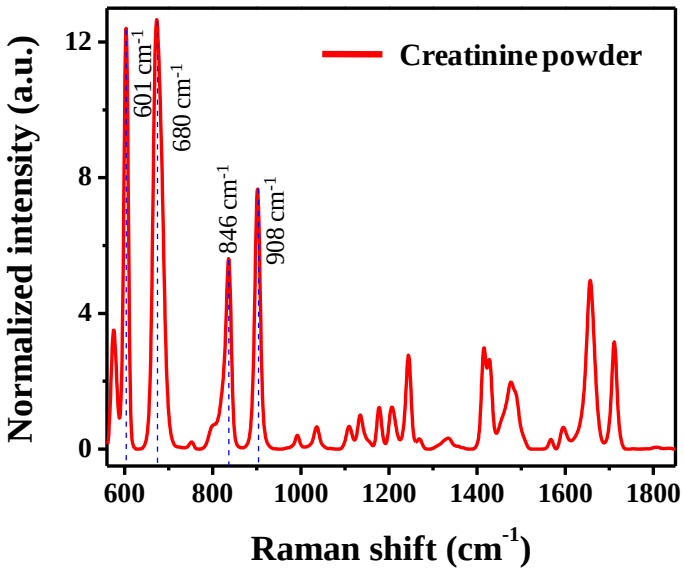

Figure 3.1: *Raman spectrum of creatinine powder with an integration time of 1 s with the laser power of 20 mW*

Following the Raman measurements of pure creatinine powder, aqueous solutions of creatinine were prepared at different concentrations of creatinine including the concentration (~100 mg/dl) at which it is likely to be present in urine under physiological conditions [90]. **Figure 3.2a** displays the measured Raman spectra from the aqueous solutions of three different

concentrations of creatinine. The Raman spectrum of deionized water is also shown in the same figure as reference. For the spectral measurement, the integration time used was 60 s and the laser power at the quartz cuvette containing the aqueous solution was 20 mW. The combination of the laser power and acquisition time was selected such that the full dynamic range of the detector could be utilized for the measurement of the raw Raman spectrum.

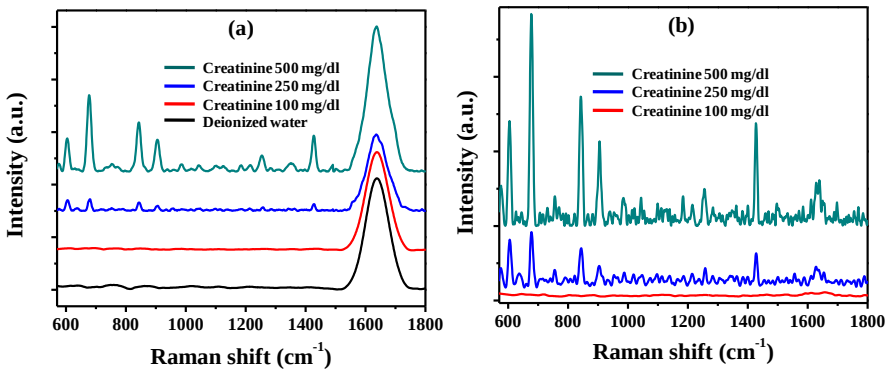

Figure 3.2: ***(a)*** *Conventional Raman spectra of aqueous solutions of creatinine with different concentrations and the spectrum of only deionized water.* ***(b)*** *Water Raman background subtracted conventional Raman spectra of the aqueous solutions of creatinine with different concentrations*

The measured raw spectra were processed for background signal correction of quartz cuvette followed by baseline correction using the background subtraction algorithm [184]. The relatively broader water Raman peak was then subtracted from each of the baselines corrected Raman spectra to retrieve the Raman peaks specific to only creatinine. **Figure 3.2b** represents the water Raman subtracted spectra corresponding to the aqueous solutions of three different concentrations of creatinine. One can see that none of the characteristic Raman peaks of creatinine are visible in the spectra measured from its aqueous solution at the physiological concentration (100 mg/dl).

It is important to mention here that the characteristic creatinine Raman peaks remained undetectable from its aqueous solution at the physiological concentration of ~100 mg/dl even when the laser power was increased from 20 to 50 mW and acquisition time was adjusted accordingly to utilize the full dynamic range of the detector. It was found that the minimum concentration of

creatinine for which at least one of its characteristic Raman peaks could be detected was 250 mg/dl. The integration time used for this measurement was 60 s and the laser power at the sample was 20 mW. From the figure (**Figure 3.2b**) one can see that even at this high concentration (250 mg/dl), the spectrum is not of good quality which is evident from the very poor value (<50) of the estimated signal-to-noise (SNR) ratio.

In order to determine the creatinine concentration required to obtain good quality Raman spectra with reasonable SNR (>100), Raman spectra were recorded from a series of its aqueous solutions containing varying concentrations of creatinine. It was found that the minimum concentration of creatinine required for achieving an SNR of ~100 was 500 mg/dl. The baseline corrected as well as the water Raman subtracted spectra corresponding to the aqueous solution of creatinine of this concentration (500 mg/dl) are displayed in **Figures 3.2(a)** and **3.2(b)**, respectively. Understandably, this concentration is much above the lower limit of the known physiological reference ranges for creatinine i.e. 28 – 259 mg/dl [140]. These results thus clearly indicate limited applicability of the conventional Raman spectroscopy for the detection of physiological concentrations of the urinary creatinine.

The immediate requirement for being able to accomplish sensitive detection of physiological concentration of urinary creatinine with the use of Raman spectroscopic method is to considerably enhance the level of Raman signal so that the measured Raman spectra are of the good signal-to-noise ratio. As a step towards fulfilling that requirement, the performance of DCDRS was investigated. The method requires drying up a microliter volume drop of an aqueous solution of an analyte and then, detecting the Raman signal from the dried-up pattern of the solute which this drop forms on a substrate. The manifold enhancement of the Raman signal in DCDRS is because of increased availability of the analyte under the Raman focal volume owing to the "coffee ring effect" in the evaporating drop [222].

Since the deposition of the solute on a substrate following the complete drying up of the liquid drop is expected to depend on the nature of the substrate, it was required first to systematically investigate the effect of the chosen substrate on the dried up patterns of the creatinine deposit. For that, various materials like glass cover slip, a quartz substrate, silicon wafer, and aluminum foil, which are commonly used for DCDRS measurement, were selected as substrates. A 4 µl liquid drop of creatinine was put on each one of these different substrates, left for air-drying at room temperature, and then imaged (after complete drying up) with a camera (CMOS) under white light illumination. **Figure 3.3** shows the measured images of the liquid drops and the corresponding dried up drops of the creatinine solutions on different substrates. The solid particles of creatinine are seen to be mostly settled at the peripheral region of the circular zone leaving the central region empty. This is because creatinine has a lesser solubility in water at room temperature [224] and it is known that a less soluble component in a solution tends to precipitate earlier [210, 225].

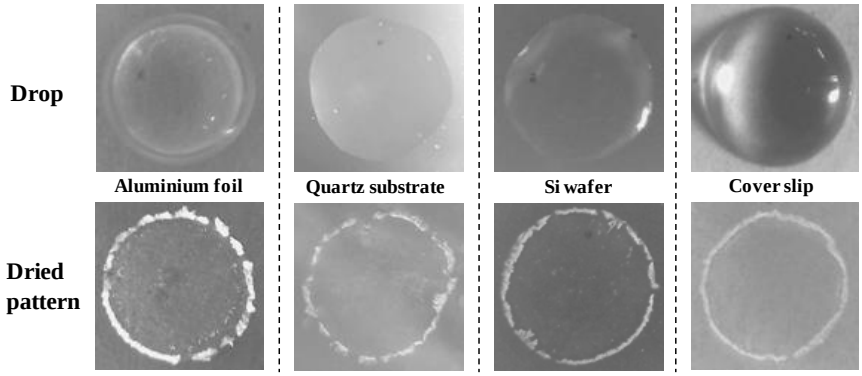

Figure 3.3: *Images of the liquid drops and the corresponding dried up drops of creatinine solution (100 mg/dl) on different substrates*

In addition to the requirement of coffee ring formation, the pattern of the measured Raman spectra from these substrates in the absence of creatinine is also an important factor for the selection of a substrate. The preferred substrate should not introduce spurious spectral features in the acquired signal that can interfere with the Raman signatures of an analyte appearing in its fingerprint region. **Figures 3.4(a)** and **3.4(b)** show the measured raw Raman

spectra and the background-corrected (i.e. zero-baseline) Raman spectra of each substrate without creatinine.

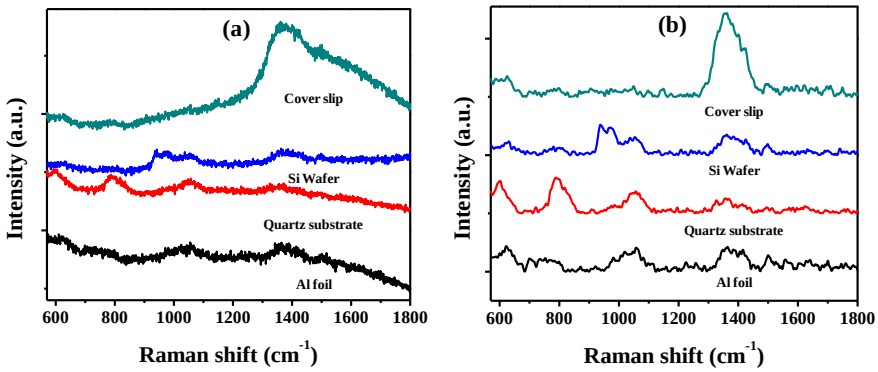

Figure 3.4: ***(a)*** *Measured raw and* ***(b)*** *zero baseline Raman spectra of different DCDR substrates*

A careful examination of these figures reveals that, of all the substrates used, aluminum has the minimum spectral artifacts in the region of interest (i.e. where the creatinine Raman peaks are expected). Further, the spectral artifacts were found to be quite broad in comparison with the Raman peaks of creatinine and could be subtracted using the standard background subtraction procedure [184]. Further, aluminium foil also has low optical absorbance and high optical reflectance which are the two important requirements for qualifying as a DCDRS substrate [226]. Therefore, in the present study on DCDRS of creatinine, the aluminum foil was used as the substrate.

Figure 3.5 shows the DCDRS spectrum measured from the dried up (on aluminium foil) liquid drop of creatinine at average physiological concentration. An integration time of 1 s and a laser power of 20 mW (at the sample) were used for spectral measurements. For comparison's sake, the Raman spectra of creatinine powder (measured with the same integration time and the laser power), as well as an aqueous solution (500 mg/dl) of creatinine (with an integration time of 60 s), are also shown in the same figure. It is apparent from the figure that all the characteristic Raman peaks of creatinine, which were buried in noise in the Raman spectrum of the aqueous solution of creatinine, are now clearly visible in its DCDRS spectrum. Further, it is also

seen that all the Raman peaks are significantly enhanced in intensity in the DCDRS spectra as compared to their aqueous phase counterpart.

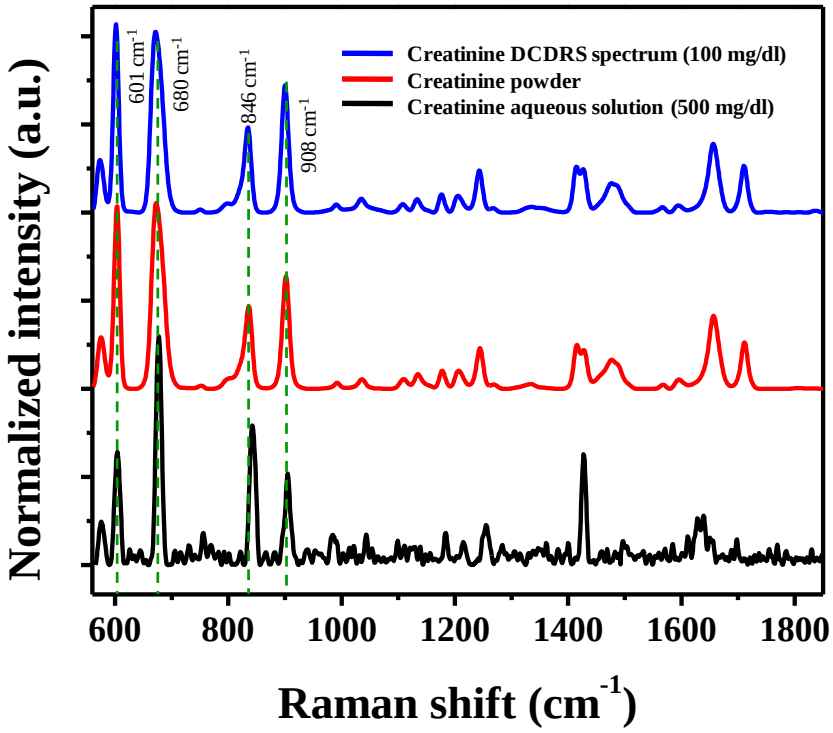

Figure 3.5: *The DCDRS spectrum measured from the dried-up liquid drop of creatinine at the average physiological concentration (100 mg/dl), the conventional Raman spectrum of creatinine powder and the conventional Raman spectrum of the aqueous solution of creatinine (500 mg/dl)*

A comparison of the estimated SNRs of the DCDRS spectra with the corresponding spectra of the aqueous solution of creatinine at its average physiological concentration also showed significant enhancements. Further, the characteristic Raman peaks appearing in the DCDRS spectra are seen to exactly correlate with those found in the conventional Raman spectrum of the creatinine powder. This strongly suggests that creatinine neither undergoes any chemical interaction with the aluminium foil nor does it gets transformed into the glass phase on being dried up.

Since surface-enhanced Raman spectroscopy (SERS) is also known to manifold enhance the Raman signal [227-230], the SERS signal was measured from the aqueous solution of creatinine with a concentration of ~100 mg/dl

(i.e. average physiological concentration). The Raman spectra were measured from a 4 μl aqueous solution of creatinine dropped on dried up sliver nanoparticles on an aluminium foil. **Figure 3.6** shows the measured SERS spectrum of the sample for 1 s integration time with 20 mW laser power at the sample. The spectrum is the average of 15 measurements from 3 different drops of samples. The grey lines represent ± 1 standard deviation of 15 Raman measurements at each wavenumber. The measured SERS spectra have line-shapes comparable with that reported in literatures [231, 232]. Inset of **Figure 3.6** shows the absorption peak of the synthesized silver nanoparticles. The absorption peak at ~ 430 nm is the evidence that the synthesized nanoparticles are spherical and the size is ~ 60 nm [144]. For comparison's sake, the conventional Raman spectrum of 500 mg/dl aqueous solution of creatinine (measured with 60 s integration time) is also shown in the same figure. It is evident from the figure that, even for 1 s integration time, the intensity of the SERS spectrum of creatinine is orders of magnitude higher than that of the conventional Raman spectrum (of its aqueous solution) which was measured from a much higher (around 5 times) concentration and with a much larger (60 times) integration time.

An important parameter in the assessment of the performance of a spectroscopic technique is the reproducibility of spectral measurements carried out using the technique. The standard deviation of a series of spectra measured from samples corresponding to the same concentration of an analyte but prepared independently at different points in time gives the measure of reproducibility. The large standard deviation shown as a grey background in **Figure 3.6** qualitatively indicates poor reproducibility of spectral measurements carried out using the SERS technique. The reproducibility was quantified by calculating the relative standard deviations (RSD) of the intensities of the characteristic Raman peaks appearing in the SERS spectra of creatinine at the average physiological concentration (i.e. 100 mg/dl). The RSD value was found to be in the range of ~ 25 – 30 % confirming poor reproducibility of the SERS measurements. This is the major drawback of

SERS [233, 234] which limits its practical usability for the quantitative determination of urinary creatinine.

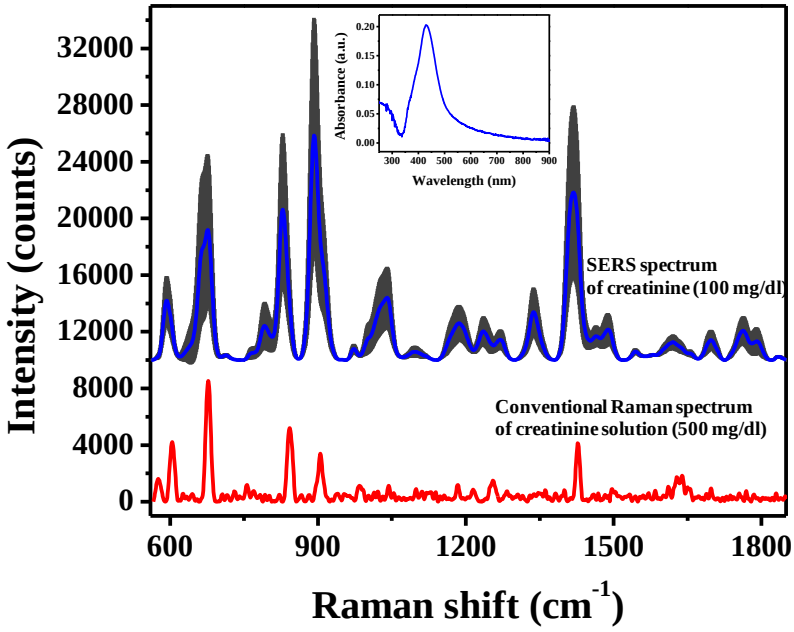

Figure 3.6: *SERS spectrum of the aqueous solution of creatinine with a concentration of ~100 mg/dl (i.e. average physiological concentration). The spectrum is the average of 15 measurements from 3 different drops of samples. The grey lines represent ± 1 standard deviation of 15 Raman measurements at each wavenumber. The conventional Raman spectrum of 500 mg/dl aqueous solution of creatinine is also shown*

In order to assess the reproducibility in size of the dried up drops of creatinine, ten different drops (each of 4 µl volume and 100 mg/dl concentration) of the aqueous solutions of creatinine were made to dry on an aluminum foil at room temperature and the diameter and width of the dried-up coffee ring patterns thus formed were measured. It was found that the diameter and width of the rings were 2.9 mm ± 0.1 mm and 80 µm ± 10 µm. For assessing the reproducibility of the DCDRS measurements of creatinine, the Raman spectra were measured from multiple dried up drops of the aqueous solution of creatinine of the same concentration (100 mg/dl) keeping all other experimental parameters unchanged. **Figure 3.7** shows the measured DCDRS spectra from three different dried-up drops of the aqueous solution of creatinine. The cross signs in each image represent the spatial locations from

where the spectra were measured. The solid red line in each of the figures [**Figures 3.7(a), 3.7(b)**, and **3.7(c)**] shows the mean DCDRS spectrum corresponding to the image in that figure and the grey background represents the corresponding standard deviation. The solid blue line in **Figure 3.7(d)** presents the DCDRS spectrum averaged over the DCDRS spectra of all the three dried-up spots. The grey background shows the ± 1 standard deviation. The RSD of the intensities of the characteristic Raman peaks appearing in the DCDRS spectra was found to be ≤ 8 % indicating excellent reproducibility of DCDRS suggesting that this method can be successfully used for the quantification of urinary creatinine.

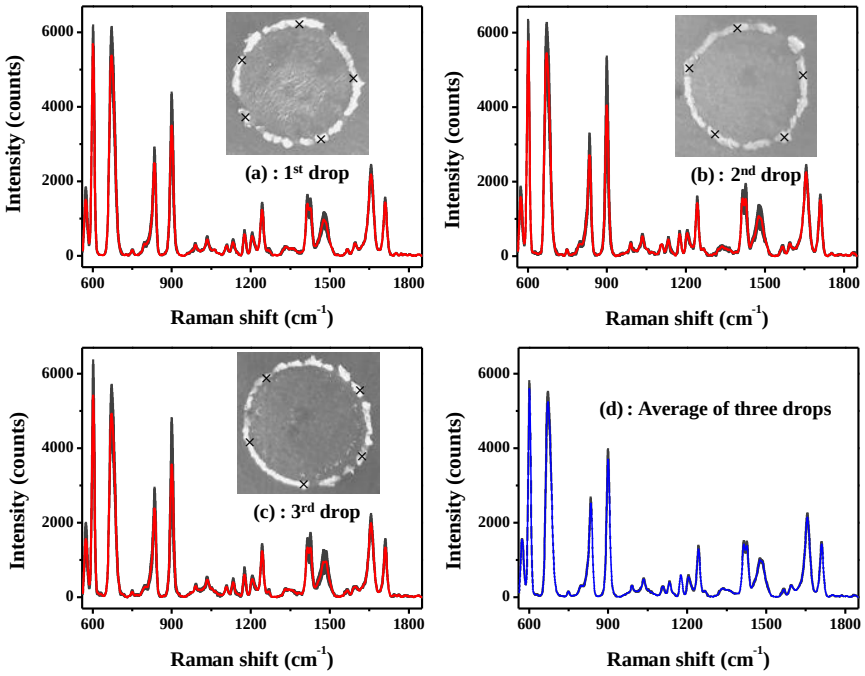

Figure 3.7: ***(a)***, ***(b)*** *and* ***(c)*** *DCDRS spectra measured from three dried up drops of the aqueous solutions of creatinine (100 mg/dl). Each of the spectra is the average of 5 measurements from each sample. The ±1 standard deviations are shown as grey background.* ***(d)*** *Mean DCDRS spectrum. The spectrum is the average over the DCDRS spectra measured from the three different dried up drops of the aqueous solutions of creatinine (100 mg/dl). The ±1 standard deviations are shown as grey background*

The ultimate objective of the present study was to evaluate the feasibility of using DCDRS for the quantitative determination of creatinine as required for the diagnosis of diseases through urinalysis. Since the

concentrations of this analyte are known to vary over a wide range in urine samples of subjects with various diseases [131, 140, 141], it is imperative to assess, in the first step, the ability of DCDRS in quantitative determination of the analyte from its aqueous solutions at a wide range of concentrations encompassing the normal physiological as well clinically relevant range. In order for that, a detailed concentration dependent DCDRS study was carried out. Creatinine aqueous solutions of varying concentrations ranging from 10 mg/dl to 250 mg/dl were prepared and DCDRS measurements from their dried-up drops were carried out. With the observed images of the patterns of the deposits in the dried-up drops of the analyte as a guideline, the DCDRS spectra were recorded from the edge of the drop. Further, the PLS based algorithm was applied on the measured DCDRS spectra for the quantitative determination of creatinine [187]. The measured DCDRS spectra of different concentrations of creatinine were used as the input in the algorithm. For evaluating the performance of the algorithm in quantitatively predicting the concentrations, the leave-one-spectrum-out cross validation method was used. In this method, one spectrum was held out at a time from the full set of spectral data of a particular analyte and the PLS model was built using the remaining spectra of the analyte. The regressions coefficients of the calibrated algorithm were then used to predict the concentration from the left out of the spectrum. This was repeated *m* times, where *m* being the number of spectra, each time excluding a different spectrum for validation and recalibrating the algorithm using the rest of the spectra. The efficiency of the statistical analysis for the quantification of analytes' concentrations was estimated by measuring the root mean square error (RMSE). RMSE measures the average difference between predicted and reference concentrations [189].

Figure 3.8(a) shows the plot of predicted versus reference (known) concentrations for the DCDRS spectral data sets corresponding to creatinine. The error bars represent the ± 1 standard deviation in predictions over the different measurements for a given concentration value. There is a good correlation observed between the predicted and the reference concentrations of

creatinine and the corresponding R^2 value is 0.96. The resulted RMSE error to predict the concentrations of creatinine from their measured DCDRS spectra was 16. The percentage absolute error (PAE), another statistical parameter, was calculated. PAE is described the predictive ability of PLS at each of the concentrations of the analytes [235]. **Figure 3.8(b)** represents the calculated PAE for the analyte. It is apparent from the figure that the PAE values are less than 10 % for the concentrations in the physiological reference range.

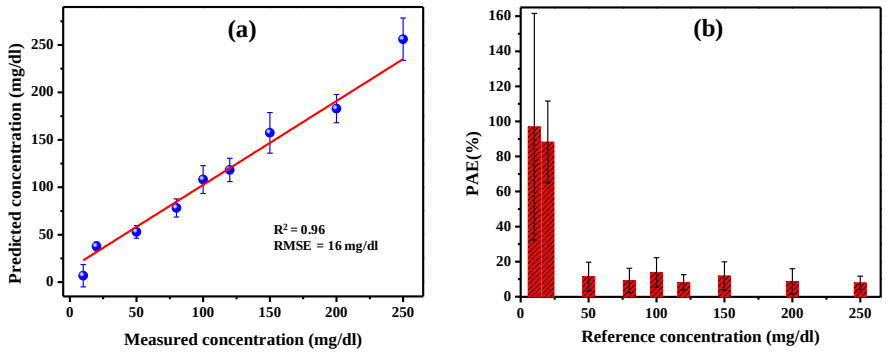

Figure 3.8: ***(a)*** *The predicted versus reference (known) concentrations of creatinine obtained from the PLS analyses of the DCDRS spectral data of the dried-up drops of the aqueous solutions of creatinine. The corresponding R^2 values and root mean square errors (RMSE) are also shown in the same figure.* ***(b)*** *Percentage absolute error (PAE) of creatinine at each of their concentrations. The error bars represent the ± 1 standard deviation in predictions over the different measurements for a given concentration value.*

After having assessed the feasibility of using DCDRS for the quantitative determination of creatinine from its aqueous solutions, in the next step, the ability of the approach in the quantitative determination of the analyte from the DCDRS spectra of a multi-component complex system like urine was investigated. For doing this, samples of artificial urine containing three major constituents of urine like urea, creatinine and uric acid at various concentrations including normal physiological and clinically relevant ones were prepared and the DCDRS spectra were recorded from the dried-up drops of these urine samples of varied analytes concentrations. The sets of spectra were recorded from the ring edge of the dried-up drops for estimating the concentration of creatinine. As before, each of these sets of DCDRS spectra

corresponding to the artificial urine samples comprising different concentrations of the analytes were used as input to the PLS based chemometric algorithm. The performance of the algorithm in quantitatively predicting the analyte concentrations was evaluated following leave-one-spectrum-out cross validation method. The correlation between the reference (known) and the predicted concentrations of creatinine present in artificial urine samples is shown in **Figure 3.9(a)**. The error bars represent the ± 1 standard deviation in predictions over the different measurements for a given concentration value. The result shows that there is good correlation between the predicted and the reference concentrations (R^2 value of 0.94). The corresponding RMSE value in predicting the creatinine concentrations in the artificial urine samples was 21.

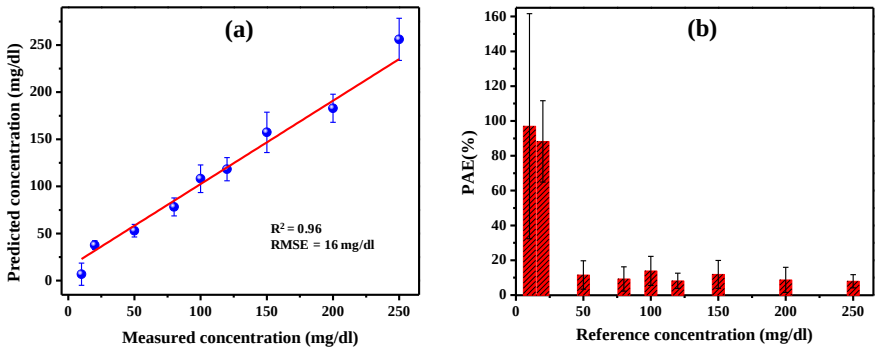

Figure 3.9: ***(a)*** *The predicted versus reference (known) concentrations of creatinine obtained from the PLS analyses of the DCDRS spectral data of the dried-up drops of the artificial urine samples.* ***(b)*** *Percentage absolute error (PAE) of creatinine at each of their concentrations. The error bars represent the ± 1 standard deviation in predictions over the different measurements for a given concentration value.*

These results are consistent with the results observed earlier from the PLS analyses of the DCDRS spectra measured from the dried-up drops of the aqueous creatinine solutions. However, it is pertinent to note that the RMSE value obtained for this constituent analyte in the artificial urine was higher as compared to its corresponding value obtained from the PLS analysis of the DCDRS spectra of the individual analyte. Increased spatial heterogeneity of the dried drop resulting from the simultaneous deposition of the analytes during the process of drying up of the multi-component liquid urine phantom

could be a plausible reason for an increased RMSE. **Figure 3.9(b)** displays the PAE values of creatinine present in artificial urine. It is apparent from the figure that the average PAE for creatinine is found to be ~ 8 – 10 % within the physiological reference concentration range (50 to 300 mg/dl). However, at very low concentrations (<50 mg/dl) these values are seemed to be higher, which is may be due to the poor SNR values of the spectra at low concentration levels.

Since the SNRs of the DCDRS spectra were found to be significantly higher than that of the conventional Raman spectra of the artificial urine samples (liquid), the limit of detection (LOD) of DCDRS (a measure of the sensitivity of the technique) is also expected to be improved. The LOD was defined as the minimum concentration for which the maximum allowed PAE value remained ≤10%. The estimated LOD value for creatinine was found to be 50 mg/dl with the correlation coefficient of ≥ 0.94. Although a direct comparison is not possible it is pertinent to note here that this value is much lower than the LOD value of 150 mg/dl, reported earlier [236] for creatinine using conventional near-infrared Raman spectroscopy.

Following the investigation of the ability of DCDRS in detecting creatinine in artificial urine samples, the next task was to evaluate its ability in detecting the analytes in actual human urine samples. **Figure 3.10(a)** shows the DCDRS spectra measured from the dried-up drops of the human urine samples. For comparison's sake, the conventional Raman spectra measured from the same set of urine samples (liquid) are also shown in the same figure. Each of the Raman spectra is the average over the spectra of urine samples obtained from six volunteers. It is evident from the figure that similar to the case of artificial urine samples; here also significant enhancement is observed in the intensities of almost all the Raman peaks (characteristic of the analytes) in the DCDRS spectrum as compared to the conventional Raman spectrum of actual urine samples. One can see that in the mean Raman spectrum of liquid urine samples, only the most intense Raman peak of urea at ~1006 cm^{-1} is

visible [(**Figure 3.10(a)**]. In contrast, in the DCDRS spectrum, multiple Raman peaks characteristic of not only urea (530, 1006, 1162 and 1465 cm^{-1}) [131, 140, 235] but also creatinine (680, 846 and 908 cm^{-1}) are visible [140]. However, for uric acid, it's characteristic Raman peaks at ~1040 cm^{-1} and 1640 cm^{-1} [237, 238] are only visible with the other peaks remaining undistinguishable. Further, the estimated SNR corresponding to the highest Raman peak was found to be enhanced by around 5 – 8 times in the DCDRS spectra as compared to spectra measured from liquid urine.

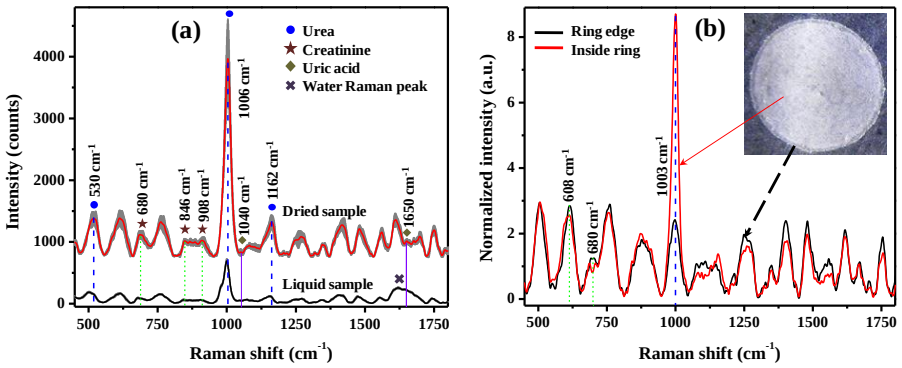

Figure 3.10: ***(a)*** *Raman spectra of human urine sample in dried and liquid forms. The spectra shown are the mean and the corresponding ±1 standard deviation (grey background) of 25 measurements.* ***(b)*** *Raman spectra of urine sample measured from ring edge and inside the ring. The inset of* ***figure (b)*** *shows the microscopic image of a human urine sample under white light illumination*

To visualize the pattern of deposits of urea, creatinine and uric acid, a dried-up drop of a urine sample was imaged under white light illumination. Inset of **Figure 3.10(b)** shows the acquired image of the dried-up drop. Like in the case of artificial urine, here also the solid particles of urea and creatinine are seen to be settled in the peripheral region. **Figure 3.10(b)** shows the Raman spectra of the urine sample measured from the ring edge and inside of the ring edge (near but away from it towards the centre). Like in the case of artificial urine one can see that the intensities of the Raman peaks characteristic of creatine are the maximum in the spectrum from the ring edge. When the spectrum measured from the inside of ring edge the intensities of the Raman peaks of urea are maximum.

In medical practice, it is challenging to predict creatinine in urine samples without sample preprocessing. This study is a step towards this challenge and investigates the feasibility of DCDRS for the same purpose. DCDRS technique has several advantages over currently available techniques for urinalysis. This exploits the fingerprint Raman signatures of creatinine for identification. Hence, it does not need any sample preprocessing and use of chemical reagents. Further, the technique allows the determination of a single analyte like creatinine present in a multi-component sample like urine. So, this could be reducing the time and cost of analysis. These advantages combined with a considerably low limit of detection and excellent reproducibility make DCDRS a promising tool for the quantitative detection of urinary creatinine.

3.3. Summary:

To conclude, evaluated the applicability of DCDRS in detecting Raman signal, not otherwise detectable using conventional Raman spectroscopy, from physiological concentrations of creatinine for urinalysis. A comparison of conventional Raman and DCDRS spectra measured from aqueous solutions of creatinine, artificial urine phantoms as well as real urine samples from human volunteers showed significant improvement in Raman intensity for DCDRS. Further, the results of the study show a high reproducibility (≥ 92 %) of DCDRS as compared to the SERS measurements suggesting the suitability of the approach for quantitative urinalysis. A chemometric technique based on PLS was applied to the DCDRS spectra measured from artificial urine phantoms. The PLS based algorithm was able to predict the concentration of the analyte in good agreement with the true value (accuracy of prediction >94 %). The lower detection limit obtained with DCDRS is also found to be sufficient to determine the presence of the analyte levels lower than the physiological reference range. Overall, the results of this work indicate that DCDRS combined with chemometrics could be a promising tool in the reliable diagnosis of disease using urine samples because of its ability in detecting

physiological concentrations of disease-specific analytes present in urine with excellent sensitivity and reproducibility.

Chapter 4

Nano-Trap Enhanced Raman Spectroscopy (NTERS) for Trace Detection and Quantitative Determination of Bioanalytes[†]

Reliable diagnosis of disease using body fluids requires sensitive and accurate detection of disease-specific analytes present in the fluid. In this chapter a new Raman signal enhancement technique called nano-trap enhanced Raman spectroscopy (NTERS) is proposed, first time, for the sensitive detection of analytes present in body fluids with high reproducibility. Further, the applicability of this analytical technique is investigated for the quantitative determination of metabolites present in body fluids.

4.1 Introduction:

Recent research has demonstrated immense potential of Raman spectroscopy as a tool for disease diagnosis through specific detection of analytes present in body fluids [120, 129]. However, detection of rather weak Raman signals, particularly from biological samples, poses a major challenge for clinical applications of conventional Raman spectroscopy. Surface enhanced Raman spectroscopy (SERS) [172, 175, 239-240], a technique where the Raman signal gets considerably enhanced owing to the electromagnetic

[†]*This chapter is largely taken from the paper:* ***S. B. Dutta et al,*** *"Nano-trap Enhanced Raman Spectroscopy: An Efficient Technique for Trace Detection of Bioanalytes", Analytical Chemistry, (2019), 91, 5, 3555-3560.*

field enhancement due to localized surface plasmon resonances, was proposed to overcome this limitation. A vast body of literature has shown that SERS can lead to significant improvement in the prospects of Raman spectroscopy for detecting molecular signatures in trace amounts of analytes [241-243]. Despite the promising potential of the approach, the clinical applications of SERS are limited by the lack of reproducibility along with large spatial variability in the measured Raman intensities due to differential (and often random) distribution of surface 'hotspots' [234, 244]. Consequently, there have been concerted research efforts in tweaking the procedures leading to signal enhancement in SERS.

For example, one such approach is focused on developing various fabrication techniques for structural optimization of SERS substrates that can optimize the signal enhancement factor [245-248]. However, it still remains challenging to develop a cost effective and time saving method that can offer high sensitivity and reproducibility. The other recent approach is to shorten the gap between the pointed structures either by plasmonic trapping of spherical nanoparticles in combination with lithographic patterns [249-253] or by evaporation on a slippery surface resulting in the formation of 3D aggregates of nanoparticle and analytes [254]. Although these approaches have resulted in good signal enhancement and also largely addressed the problem of lack of reproducibility of SERS, a major common disadvantage is that they all require fabrication of specialized structures or surfaces which is tedious, time consuming and often expensive, and hence, limit the applicability of SERS in clinical situation.

Here, in this chapter, we propose, a novel Raman signal enhancement technique, nano-trap enhanced Raman spectroscopy (NTERS), for efficient detection of trace number of analytes. The technique relies on forming "hotspots" by drying up of a micro volume drop of the liquid containing an aqueous mixture of nanoparticles and analytes in the presence of a focused Raman excitation laser beam, and then, detecting the Raman signal from these "hotspots". During the process of drying, both the analytes and the

nanoparticles move towards the laser focus at the edge of the drop whereby the analyte molecules are trapped in the aggregates of nanoparticle leading to the formation of “hotspots”. The measurement of Raman spectra from these spots results in significantly higher Raman signal. Further, since the laser mediated drying of the sample drop results in more uniform aggregation, it leads to high reproducibility of the measured NTERS signal. The results of our studies showed that as compared to the conventional SERS, NTERS yielded significantly better (around two orders of magnitude) signal enhancement as well as reproducibility. The other significant advantage is that the technique is simple and cost effective as it does not require, unlike SERS, preparation of any specialized substrate.

4.2 Results and Discussions:

For evaluating the performance of NTERS, experiments were carried out using aqueous solutions of Rhodamine 6G (R6G) as samples. The concentrations of R6G in these solutions ranged from 50 nM to 2.5 µM. For evaluating the performance on a biologically relevant molecule, an aqueous solution of urea of 4 mM concentration, which is equivalent to its physiological concentration in human blood, was used. All these samples were prepared by mixing 5 µl of 2.5 nM spherical gold nanoparticles (AuNPs) with 5 µl of aqueous solutions containing varied concentrations of the analyte molecules to be probed. The synthesis of AuNPs was done using citrate reduction method [255].

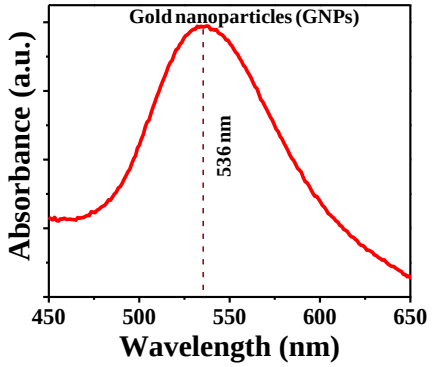

Figure 4.1: *UV-Vis absorbance spectrum of the synthesized AuNPs*

The mean diameter of the synthesized AuNPs was estimated to be 26 ± 4 nm based on the image acquired from a transmission electron microscope (TEM) operating at 200 KV (Philips CM-200). The characteristic plasmon resonance absorption peak of AuNPs was observed at 536 nm using an UV-Visible spectrophotometer (GBC Cintra). **Figure 4.1** shows the absorption maxima of the synthesized AuNPs. AuNPs concentration was measured using Beer's Lambert law [256]. The TEM image along-with the distribution curve is shown in **Figure 4.2**.

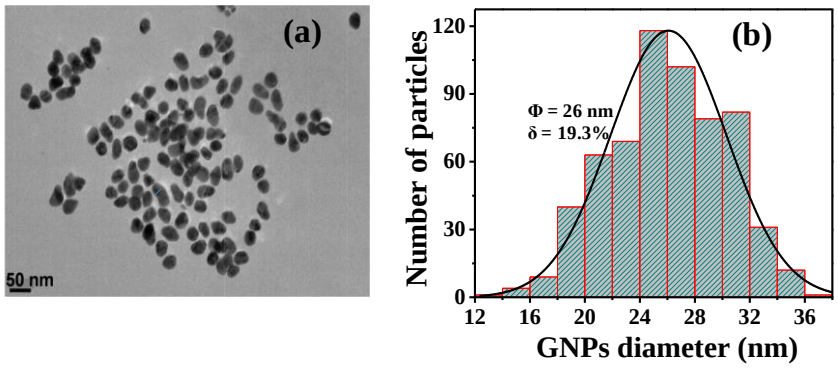

Figure 4.2: (a) *Transmission Electron Microscopy (TEM) image of gold nanoparticles (AuNPs).* ***(b)*** *Histogram of size distribution of AuNPs with a mean size (Φ) of 26 nm. δ represents the percentage distribution of mean size gold nanoparticles. (c) UV-Vis absorbance spectrum of the synthesized AuNPs*

For carrying out the NTERS measurements, a drop of a liquid sample (which is an aqueous mixture of AuNPs and an analyte of a particular concentration) put on a piece of aluminum foil was dried under illumination from the Raman probe beam (i.e. the laser beam of 785 nm wavelength) focused at a point lying in the peripheral region of the drop. As soon as the drop dries up and the 3D clusters of AuNPs embedding the analyte molecules are formed, the Raman spectra were measured. A temporal observation of this process was made to identify the optimum point in time of attaining the maximum Raman signal. It was found that the maximum signal could be obtained only after the complete drying up of the liquid drop. This has been illustrated in **Figure 4.3** which shows the NTERS spectra for R6G at 150 nM

concentration at three different time points; t = 0, 7 and 15 min. The schematic illustration of the NTERS effect and the microscopic image of the drop are also shown in the same figure. One can see, that initially, at t = 0 there is no detectable Raman signal. The enhancement in the signal initiates at t = 7 min and continues up to t = 15 min, when the drop dries up completely. The black spot seen in the microscopic image of the dried drop is the spot of aggregated GNPs after 15 min of drying up under the laser illumination.

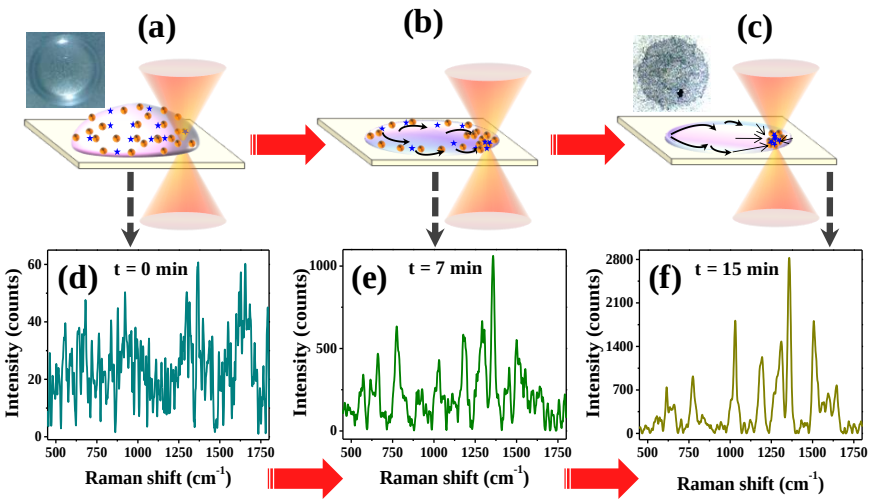

Figure 4.3: ***(a-c)*** *Schematic illustration of the mechanism of nano-trap enhanced Raman spectroscopy (NTERS) of 150 nM R6G with time, showing the process of formation of the AuNPs aggregates. The microscopic images of the drop of R6G and AuNPs are at t=0* ***(a)*** *and t=15 min* ***(c)****. The respective NTERS spectra of R6G at t=0* ***(d)****, t= 7min* ***(e)*** *and t= 15 min* ***(f)*** *are also shown*

It is pertinent to mention here that NTERS effect is observed only if the measurements are made from the peripheral regions of the dried pattern. **Figure 4.4** shows the Raman spectra measured from the dried drop of the aqueous mixture of AuNPs and 2.5 µM of R6G when the laser is not focused in the peripheral region. For comparison's sake, the NTERS spectrum of the same solution drop and the Raman spectrum measured from directly dried drop (i.e. not under laser illumination) of the same sample mixture are also shown in the same figure.

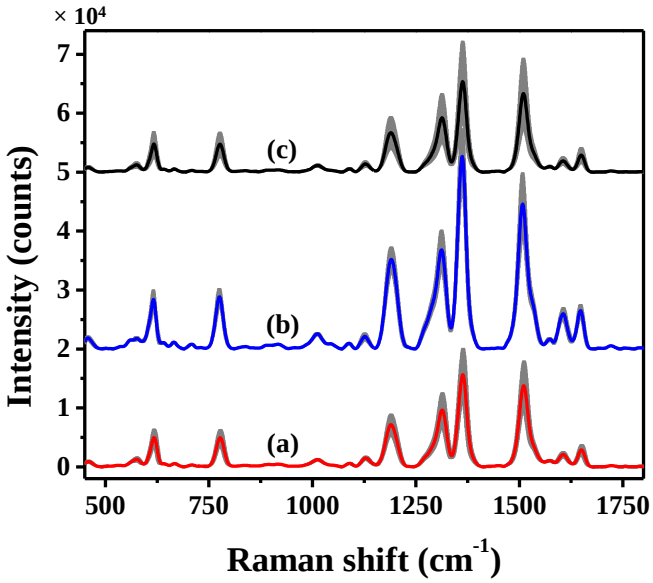

Figure 4.4: *Raman spectra measured from the dried drop of the aqueous mixture of nanoparticles and 2.5 μM Rhodamine 6G* ***(a)*** *when the laser beam is not focused in the peripheral region and* ***(b)*** *the laser beam is focused in the peripheral region (i.e., the NTERS spectrum).* ***(c)*** *The Raman spectrum measured from the peripheral region of the directly dried drop (i.e., not under laser illumination) of the same sample mixture. The spectra shown are the mean spectra averaged over 35 different measurements. The ± 1 standard deviation are shown as gray background*

One can see significantly more intense Rhodamine 6G Raman signal in the NTERS spectrum (i.e. when the laser beam is focused at the peripheral region) as compared to that in both the other spectra. This is because NTERS exploits the synergy of two phenomenon happening simultaneously: (i) the maximum deposition of the solute at the peripheral region due to the "coffee ring effect" [222, 257] during drying up of the solution drop, and (ii) the formation of nanoparticles clusters at the laser beam focus due to optical trapping of the nanoparticles [180]. Thus, in NTERS, when the laser beam is focused at the peripheral region, it leads to the formation of AuNPs aggregates at the region of the maximum deposition of the solute thereby causing maximum enhancement of the backscattered Raman signal. On focusing the laser beam at the non-peripheral region, though AuNPs aggregates are still formed at that spot of laser beam focus, the availability of the solute particles in this region is not sufficient (as compared to that in the peripheral region) for

producing the desired signal enhancement like in NTERS. Similarly, in the directly dried up solution drop of the sample mixture, even though maximum deposition of the solute particles can occur at the peripheral region, the concentration of nanoparticles in this region is considerably less (as compared to the congregation of nanoparticles in NTERS) to lead to further enhancement of Raman signal.

Figure 4.5 shows the NTERS spectrum measured from the dried drop of the aqueous mixture of AuNPs and 2.5 μM of R6G. The SERS spectra and the conventional Raman spectra from the aqueous solutions containing the same concentration of R6G are also shown in **Figure 4.5**. For the conventional Raman measurements, the aqueous solution of the analyte did not contain any AuNPs, whereas for the SERS measurements the sample solution contained AuNPs. One can see in the figure that while the characteristic Raman peaks of R6G are feeble and not distinguishable in the conventional Raman spectrum, they are prominent and significantly enhanced in intensity in the NTERS as well as the SERS spectra. It is pertinent to mention here that the observed peaks of R6G are mainly due to three different modes of vibrations *i.e.* C-C-C ring in- plane bending at 613 cm^{-1}, out of plane bending at 769 cm^{-1}, and ring breathing and aromatic C-C stretching at 1188, 1312, 1362, 1508 and 1648 cm^{-1} [258].

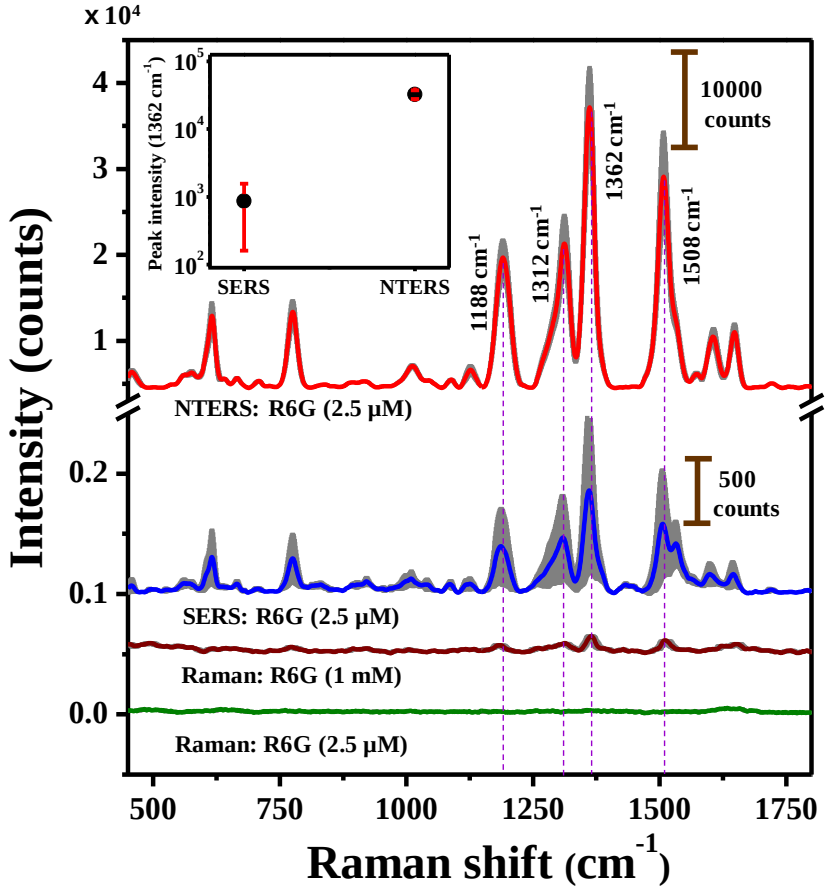

Figure 4.5: *NTERS (red line), SERS (blue line) and conventional Raman (green line) spectra of an aqueous solution of 2.5 µM of R6G. The spectra shown are the mean spectra averaged over 35 different measurements. The ± 1 standard deviation are shown as grey background. The Raman spectrum of 1 mM of R6G is shown in wine colored line. It was used to calculate the SERS analytical enhancement factor. The inset compares the integrated Raman peak intensities of 1362 cm^{-1} for NTERS and SERS measurements. Error bars (red) indicate the corresponding reproducibility*

In order to calculate the SERS analytical enhancement factor, conventional Raman spectrum was measured from an aqueous solution of R6G wherein the concentration of R6G was just sufficient to have its characteristic Raman peaks conspicuous in the measured Raman spectrum. In the present case this concentration was found to be 1 mM. The SERS enhancement factor with respect to the conventional Raman spectrum of 1 mM aqueous solution of R6G (shown as a wine line in **Figure 4.5**) was estimated to be ~10^6 which was found to be in good agreement with that reported in the literature [259-261]. It is important to note here that the NTERS enhancement factor with respect to

the conventional Raman spectrum of 1 mM aqueous solution of R6G was estimated to be ~10^8 , which is two orders of magnitude larger than SERS.

Another important parameter in the assessment of the performance of a given spectroscopic technique is the reproducibility of spectral measurements carried out using the technique. The standard deviation of a series of spectra measured from samples corresponding to the same concentration of an analyte, but prepared independently in different points in time, gives the measure of reproducibility. One can see in **Figure 4.5** that the standard deviation over 35 measurements (shown as grey background in the figure) of the SERS spectra from the aqueous mixtures (of AuNPs and R6G) of 2.5 μM of R6G is significantly larger as compared to that of the NTERS spectra measured from the laser mediated aggregates of the same samples indicating significantly better reproducibility of NTERS as compared to SERS. This is further corroborated by the fact that the intensity variation in the most intense Raman peak at 1362 cm^{-1} (inset of the **Figure 4.5**) is much smaller in the case of NTERS as compared to that of SERS.

Since the enhancement of Raman signal in NTERS measurements is found to be considerably larger than that in SERS, it is expected that the limit of detection (LOD) using NTERS would also be improved. The LOD was defined as the minimum concentration for which the SNR of the most intense Raman peak (1362 cm^{-1}) remained larger than 50. **Figure 4.6(a)** shows the NTERS spectra of decreasing concentrations of R6G, from 500 nM to 50 nM. The LOD of R6G using NTERS was found to be 50 nM (figure 5b) with a value of SNR of ~75. In contrast, the LOD of R6G using SERS was 2.5μM with a value of SNR of ~ 100. **Figure 4.6(b)** shows the plot of integrated intensities of the Raman band at 1362 cm^{-1} in the NTERS spectra measured from the R6G samples of various concentrations. It is clearly seen that there is a linear relationship (R^2 = 0.93) between the integrated intensity of the Raman band at 1362 cm^{-1} for NTERS measurements and the R6G concentration. This suggests that unlike SERS, where lack of linearity (resulting from random distribution of surface 'hotspots') is a major concern, NTERS provides a linear

relation between the spectral intensity and concentration showing significant promise for quantitative estimation of an analyte.

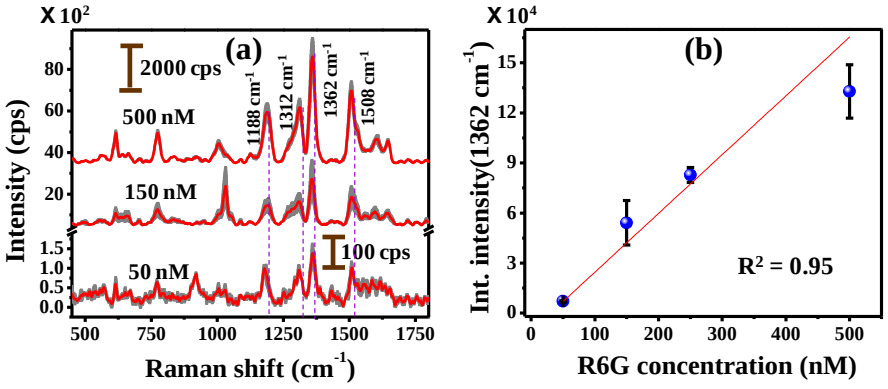

Figure 4.6: ***(a)*** *NTERS spectra of 500 nM, 150 nM and 50 nM R6G, depicting the concentration dependence of the peaks.* ***(b)*** *Integrated Raman peak intensity of the Raman band at 1362 cm^{-1} in the NTERS spectra measured from different concentrations of R6G*

Following evaluation of the performance of NTERS using R6G, its performance was assessed using urea, a biologically relevant molecule. Urea is the principal nitrogenous waste product of protein metabolism in the body and its physiological concentration in blood is generally found to be ~4 mM [262]. A comparison of conventional Raman, SERS and NTERS spectra corresponding to 4 mM concentration of urea is shown in **Figure 4.7**. One can see that while the characteristic (and most intense) Raman peak of urea at 1001 cm^{-1}, attributed to symmetric N-C-N stretching [235] , is seen only with NTERS measurement (the estimated SNR value was ~500 for 1s integration time), the peak is not at all identifiable in the case of conventional as well SERS measurements. This clearly suggests that NTERS holds considerable promise in sensitive detection of trace amount of a bio-analyte, often time required for diagnosis of a disease based on body fluids.

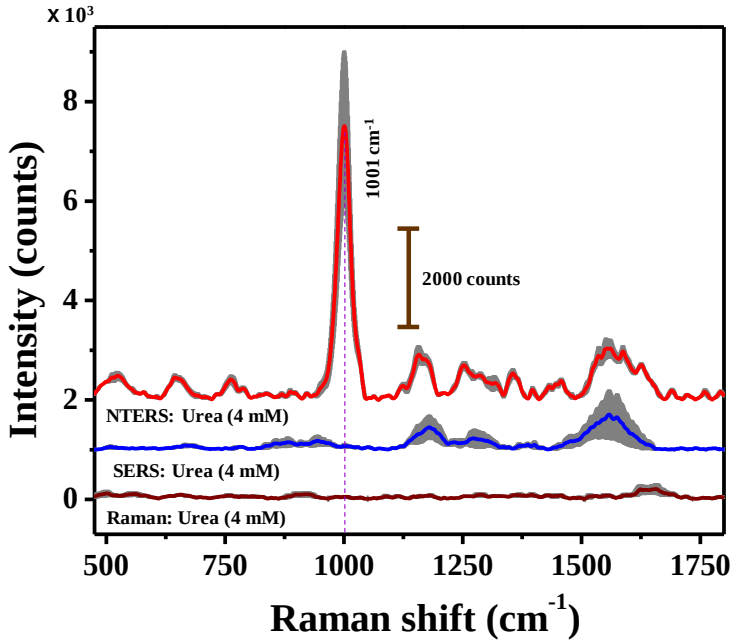

Figure 4.7: *NTERS (red line), SERS (blue line) and conventional Raman (wine line) spectra of 4 mM aqueous solution of urea. The spectra shown are the mean spectra averaged over 35 different measurements. The ± 1 standard deviation are shown as grey background*

The following discussion will help better understand the underlying reasons for signal enhancement and reproducibility of the technique of NTERS. As has been shown, for NTERS measurements, one needs to prepare "hotspots" by drying up a micro volume drop of a liquid, containing an aqueous mixture of nanoparticles and analytes in the presence of a focused laser beam and then, detect the Raman signal from these spots containing the analytes localized within the nanoparticle aggregates. A focused laser beam on a nanoparticle creates two forces; gradient and scattering [180]. While the gradient force pushes the particle towards the focus of the beam, the scattering force is proportional to the particle's absorption and scattering cross sections and pushes it along the direction of beam propagation. If the wavelength of the laser is chosen away from the absorption band of the nanoparticle, the gradient force dominates over the scattering force and the particle is pushed towards the focus of the beam i.e. it is trapped [180]. Due to trapping, nanoparticles form clusters around the focus of the laser beam. In NTERS, this process is

simultaneous with the evaporation of the liquid which results in the capillary outward flow of the solvent in the drop, induced by faster solvent evaporation near the contact line with the surface. This phenomenon results in concentration gradient of the analyte, lower to higher, from the center to the periphery of the drop. It is important to note that the movements of nanoparticles and the solute particles are independent of each other in the whole process. The movement of nanoparticles is dictated by the position of the laser beam focus which in other words means that the nanoparticle clusters can be formed at any region of the circular spot depending on where one focuses the laser beam. On the contrary, the movement of the analyte (i.e. solute) particles has nothing to do with the position of the laser beam focus. These will always tend to move towards the peripheral region, upon drying up of the solution drop, due to the coffee ring effect. NTERS requires the laser beam to be always focused at the peripheral region, because then only it can lead to the formation of nanoparticle aggregates at the region of the maximum deposition of the solute (i.e. "hotspots") thereby causing maximum enhancement of the backscattered Raman signal from the analytes. The stability of laser power allows for maintaining the constant gradient force required for trapping of the nanoparticles. The high reproducibility in the laser mediated formation of the nanoparticle aggregates combined with simultaneous drying up of the aqueous drop leading to efficient embedding of the analyte molecules in the 3D aggregates (of nanoparticles) results in a very high reproducibility in the measured NTERS signal.

The ultimate objective of the present study was to evaluate the feasibility of using optical spectroscopy for accurate and sensitive detection and quantitative determination of the analytes present in body fluids including urine as required for diagnosis of diseases. Since the concentrations of these analytes are known to vary over a wide range in body fluids samples of subjects with various diseases. It is imperative to assess, in the first step, the ability of NTERS in quantitative determination of the analytes at a wide range

of concentrations encompassing the normal physiological as well clinically relevant range.

In order for that a detailed concentration dependent NTERS study of uric acid was carried out. Uric acid is the final product of nucleic acids produced by purine metabolism in human [263, 264]. It acts as a clinically important biomarker to identify different metabolic disorders such as renal failure, gout and cardiovascular disease etc. [265-274]. The normal concentration range of uric acid in blood and urine are 2.6 – 7.2 mg/dl (155 – 428 µM) and 16 – 100 mg/dl (0.9 – 5.9 mM) respectively [132, 275]. The production and excretion rate of uric acid balanced the physiological level of it in body fluids. The increased production, decreased excretion or a combination of both maintain the level of uric acid in blood and the increased elevated level of it referred as the hyperuricemia [276, 277]. The elevated level of this is an indication of gout, renal disorders and Lysch-Nyhan syndrome etc [278, 279]. This elevated level is also related to the signs and symptoms of obesity, diabetes, kidney stones, high cholesterol and heart diseases [280-282]. Therefore, it is a need of urge for the quantitative determination of uric acid present in urine and blood serum efficiently.

Different solutions of uric acid with varying concentrations ranging from 25 – 500 µM were prepared. To dissolve the uric acid in water completely 2 ml of 1M NaOH was added with the 98 ml of each sample solutions. Before, the NTERS measurements, we measured the Raman spectra of pure uric acid powders as shown in **Figure 4.8(a).**The Raman peaks obtained for uric acid were similar to those reported in previous studies.In the Raman spectrum of uric acid (**Figure 8a**), the four prominent Raman peaks observed at 630 cm^{-1}, 1040 cm^{-1}, 1405 cm^{-1} and 1650 cm^{-1} are attributed to the ring breathing mode, C─N stretching, N─C─C stretching and C═O stretching respectively [132, 231, 237]. After that the NTERS measurements were carried out from the prepared aqueous solutions of uric acid. **Figure 4.8(b)** shows the measured NTERS spectra of uric acid at three different concentrations values

(25 µM, 200 µM, and 500 µM respectively). The spectra shown are the mean spectra averaged over 25 different measurements.

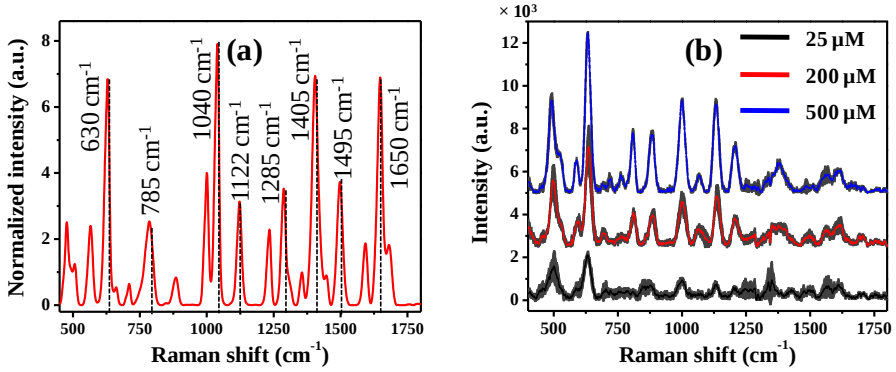

Figure 4.8: ***(a)*** *Raman spectra of uric acid measured from their corresponding powder form.* ***(b)*** *NTERS spectra of uric acid at three different concentrations values. The spectra shown are the mean spectra averaged over 25 different measurements. The ± 1 standard deviations are shown as grey background*

A chemometric algorithm, developed using the partial least square (PLS) model, and employed in the respective set of NTERS spectra to quantitatively predict the concentrations of uric acid. The measured NTERS spectra corresponding to different concentrations of each analyte were used as input to the PLS algorithm. For evaluating the performance of the algorithm in quantitatively predicting the concentrations, leave-one-spectrum-out cross validation method was used. In this method, one spectrum was held out at a time from the full set of spectral data of a particular analyte and PLS model was built (i.e. its calibration was performed) using the remaining spectra of the analyte. The regressions coefficients of the calibrated algorithm were then used to predict the concentration from the left-out spectrum. This was repeated *m* times, *m* being the number of spectra, each time excluding a different spectrum for the purpose of validation and recalibrating the algorithm using the rest of the spectra. The efficiency of the PLS algorithm to quantify the analyte concentrations was assessed by evaluating the root mean square error (RMSE). It measures the average difference between predicted and reference concentrations.

Figure 4.9(a) shows the plots of predicted versus reference (known) concentrations for the NTERS spectral datasets corresponding to uric acid. The error bars represent ± 1 standard deviations of the predictions over the different measurements for a given concentration value. The plot shows a clear correlation between the predicted and the reference concentrations, and the corresponding R^2 value is of 0.96. The resulted RMSE error calculated by the PLS algorithm in predicting the concentrations of uric acid from their NTERS spectra was 28. The percentage absolute error (PAE), another statistical parameter, was calculated as the figure of merit. It describes the predictive ability of PLS at each of the concentrations of the analyte. **Figure 4.9(b)** represents the calculated PAE for uric acid. It is apparent from the figure that, the PAE values are less than 10 % for the concentrations in the physiological reference range. However, at very low concentrations (< 100 µM) the values are seen to be much higher, which indicates that there is high relative uncertainty in prediction at the concentration level lower than the physiological level. The relatively poor SNR values at lower concentrations range is the explanation for this high PAE.

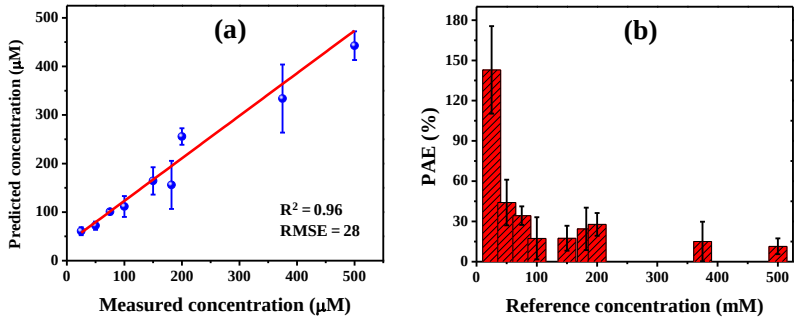

Figure 4.9: ***(a)*** *The predicted versus reference (known) concentrations of uric acid obtained from the PLS analyses of the NTERS spectral data of the samples. The corresponding R^2 values and root mean square errors (RMSE) are also shown in the same figure.* ***(b)*** *The percentage absolute error (PAE) of uric acid at each of their concentrations. The error bars represent ± 1 standard deviation of the predictions over the different measurements for a given concentration value*

This exploratory study is a step towards the investigation of the feasibility of NTERS technique for the quantitative measurement of the analytes present in body fluids. There are various advantages of NTERS over

currently available techniques for body fluids analysis. First, this identifies the chemical structures of uric acid in the form of Raman peaks. Hence, it does not need any sample preprocessing steps in which chemical reagents are require. Secondly, in this technique a much smaller volume of sample is needed for the spectral measurement than the other standard techniques. All these advantages combined with considerably low limit of detection and excellent reproducibility make NTERS a promising tool for the quantitative detection of analytes present in body fluids.

4.3 Summary:

To conclude, we propose a novel Raman spectroscopic technique, nano-trap enhanced Raman spectroscopy (NTERS), in detecting Raman signal from trace quantities of an analyte which otherwise is not detectable using conventional Raman spectroscopy. The technique relies on preparing "hotspots" by drying up a micro volume drop of the liquid, containing the aqueous mixture of nanoparticles and analytes in the focal volume of the Raman excitation laser, and then detecting the Raman signal from these spots containing the analytes localized within the nanoparticle aggregates. The performance of the technique was evaluated in detecting trace quantities of two Raman active analytes, Rhodamine 6G (R6G) and urea. It was found that R6G and urea could be detected down to a concentration of 50 nM with SNR value of ~75 and 4 mM with SNR value of ~500, respectively. A comparison with SERS revealed that NTERS not only had significantly larger (around two orders of magnitude) signal enhancement but also had considerably higher reproducibility because of its intrinsic ability to form nanoparticle aggregates with high repetitiveness. Another advantage of NTERS is its simplicity and cost effectiveness as it does not require any specialized substrate. All these put together suggest that NTERS could be a better candidate as compared to SERS for reliable diagnosis of disease using body fluids because of its intrinsic ability in detecting trace quantities of disease-specific analytes present in body fluids with considerably higher sensitivity and reproducibility.

Chapter 5

Fluorescence Photobleaching of Urine and its Applicability in Oral Cancer Diagnosis[‡]

Recently, optical spectroscopy-based urine analysis has got considerable interest for monitoring the health status of human beings. In this view, fluorescence and Raman spectroscopy are preferable than others due to their ability of detecting the specific biochemical changes at molecular level. While studying the two techniques for urine analysis a phenomenon, commonly known as photobleaching is often overlooked. The role of fluorescence photobleaching for both fluorescence and Raman spectroscopic measurements of human urine samples are described in this chapter.

5.1 Introduction:

In recent, optical spectroscopy, in particular fluorescence and Raman spectroscopy have been emerged as alternate analytical techniques for urine analysis [91, 113, 202, 283, 284]. The vast body of literature provides enough evidence that the optical spectroscopy based urine analysis could be used as a potential tool for disease diagnosis including cancer [285-289].In fluorescence spectroscopy, the emission of various intrinsic fluorophores like urinary albumin, reduced nicotinamide adenine dinucleotide (NADH), collagen, elastin, flavin adenine dinucleotide (FAD), porphyrins, and aromatic amino

[‡] *This chapter is largely taken from the paper:* ***S. B. Dutta et al.*** *"Fluorescence Photo-bleaching of Urine and Its Applicability in Oral Cancer Diagnosis", Photodiagnosis and Photodynamic Therapy, (2019), 28, 18-24*

acids like tryptophan, tyrosine and phenylalanine are used as the diagnostic parameters [110, 290-292]. This spectroscopic technique has been successfully used for identifying many diseases such as Microalbuminuria (MAU) [293, 294], cancer spreading in different human organs like oral [295-297], bladder [298-300], cervix [91, 301] and ovary [302, 303] etc., by quantitatively predicting the concentrations of fluorophores present in human urine. The differences in spectral intensity distribution as well as intensities across the spectral bands of various fluorophores (believed to be present in urine) were then used for discriminating the urine samples of healthy and cancerous individuals. On the other hand, in Raman spectroscopy, inelastically scattered light from the Raman active analytes (like urea, creatinine, uric acid etc.,) of human urine is observed. Raman spectroscopy of urine also has been shown the potentiality for diagnosis of various cancers including oral cancer [285, 304-307].

However, in all these studies, one common concern is that the phenomenon of photo-bleaching of urine has not been taken into account while recording its fluorescence a well as Raman. This is important because the onset of fluorescence photo-bleaching of urine is almost immediate (i.e. it starts as soon as one puts on the excitation light) and by the time the spectra measurement from a urine sample is complete, the sample is expected to have undergone considerable photo-bleaching. Now, since the temporal characteristics of photo-bleaching are not expected to be the same for all the fluorescent biomolecules comprising urine, the emission spectra measured from the same urine sample with varying integration times or at different points in time under continuous illumination could have line-shapes very different from each other. Consequently, the observed differences in the spectra of the urine samples of cancer patients and healthy individuals would completely depend on the length of time (or time delay between the start of the spectral measurement and switching of the fluorescence excitation light) one sets for recording fluorescence from each of these samples and might not remain the same even for the same set of urine samples of cancer patients and

healthy individuals. As a result, the outcome of a particular discrimination model with the measured (inter-category) spectral differences [295, 303, 308, 309]as its input might not be unique for a given set of urine samples belonging to cancer patients and healthy individuals. A detailed study on fluorescence photo-bleaching of human urine samples, not carried out thus far to the best of our knowledge, is therefore necessary.

We report here the results of a comprehensive study on fluorescence photo-bleaching of human urine samples. We also present the results of a preliminary investigation on evaluation of the applicability of photo-bleaching characteristics of urine for discriminating patients with oral cancer from healthy volunteers.

5.2 Results and Discussions:

It was observed that the fluorescence background has decreased surprisingly with time during the Raman spectroscopic measurements of urine samples using a 785 nm diode laser. To proceed further, the samples were continuously illuminated using the same diode laser (λ = 785 nm) with a total time of 500 s and the Raman spectra were measured continuously with an integration time of 1s. **Figure 5.1(a)** displays the measured raw Raman spectra at t = 1, 10, 50 and 500 s respectively for a given urine sample. In the figure, there are two noteworthy observations. One is the background usually known as fluorescence background is decreasing with time. The other one is that the Raman signal intensity of the highest Raman peak at ~1003 cm^{-1} (due to symmetric N-C-N stretching in a urea molecule [310] seems to be get enhanced, although this requires a more careful attention. The first observation is verified from the **figure 5.1(b)**, which plots the integrated intensities of the fluorescence background in the raw Raman spectra with respect to the illumination time. The corresponding fluorescence decay fit is also shown in the same figure and results a decay constant of ~ 40 s.

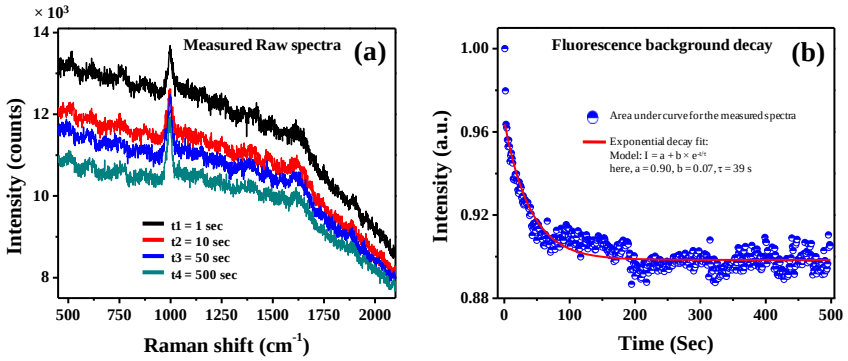

Figure 5.1: ***(a)*** *Typical raw Raman spectra of a urine sample measured at different time under continuous laser exposure ($\lambda_{excitation}$ = 785 nm),* ***(b)*** *the corresponding decay curve generated from the background intensity loss with respect to the illumination time*

To clarify the second observation, the measured Raman spectra were further processed i.e., noise smoothened, and background subtracted. The processed Raman spectra are shown in **Figure 5.2(a)**. This figure makes clear that the intensity of the Raman peak centered at 1003 cm^{-1} (i.e. I_{1003}) improves with time. Hence, we have plotted the average peak intensity of this Raman peak (1003 cm^{-1}) as a function of time for all urine samples of healthy volunteers (n = 18) as shown in **Figure 5.2(b)**. The error bars shown in grey background represent ±1 standard deviation.

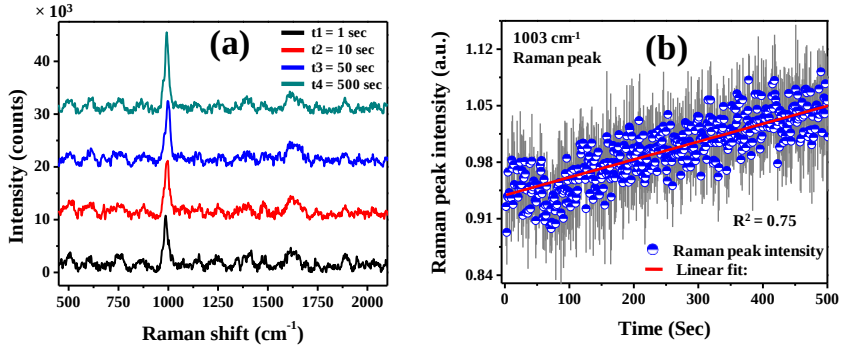

Figure 5.2: ***(a)*** *Noise smoothened and fluorescence background corrected Raman spectra of a urine sample.* ***(b)*** *Average peak intensity of the Raman peak (1003 cm^{-1}) as a function of time of urine samples of healthy volunteers (n = 18) at different times ranging from 1 s to 500 s*

A linear relationship is achieved (R^2 = 0.75) between the peak intensity and time which suggests that the fluorescence photo-bleaching could be boon

in Raman analysis of human urine samples. This is further verified by calculating the signal to noise and signal to background ratios (SNR and SBR) for the measured Raman spectra of urine samples. The calculated SNR and SBR values at different time points are present in **Table 5.1.** It shows that both the SNR and SBR values are increased significantly at decay constant time (at $t = \tau$) with respect to the initial time (at $t = 0$).

Urine Samples				
	At t = 0 s	At t = τ, i.e., Decay constant	At t > τ (~200 s)	At t >> τ (~500 s)
Signal to noise ratio (SNR)	87 ± 23	122 ± 14	138 ± 18	145 ± 12
Signal to background ratio (SBR)	0.066 ± 0.01	0.084 ± 0.02	0.091 ± 0.02	0.097 ± 0.02

Table 5.1: *The calculated SNR and SBR values for the measured Raman spectra of urine samples at different time points*

It is pertinent to mention here that, the above observations pointed out that the urine samples are going through the photo-bleaching process even when the samples were excited by 785 nm laser. However, it was very curious to us that why this is happening and is this phenomenon has any significance if we excite the same sample by ultraviolet or visible (UV-Vis) light. As these are the wavelength regions, in which the maximum number of native fluorophores present in urine samples are getting excited. Therefore, in the remaining part of this thesis work, the fluorescence photo-bleaching dynamics of urine samples (using a 405 nm diode laser) are studied. Further, the applicability of the photo-bleaching dynamics was investigated to differentiate the oral cancer patients form healthy volunteers using urine sample.

Figure 5.3(a) shows the typical fluorescence emission spectrum of a urine sample of a healthy volunteer measured with 405 nm excitation. The

observed emission maxima are seen to be consistent with the characteristic fluorescence emission bands reported in literature [91, 116]. For example, the spectrum is characterized by a major emission maximum centered at 515 nm and a shoulder around ~ 475 nm, and two minor wavelength bands peaking around ~ 620 nm and ~ 680 nm, respectively. The fluorophores responsible for the 515 nm band and the 475 nm shoulder are believed to be the co-enzymes FAD and NADH/ NADPH respectively, and that for the ~620 nm and ~680 nm bands are the porphyrin.

Figure 5.3(b) shows the fluorescence emission spectra of the urine samples of cancer patients and healthy individuals. Each spectrum is the average of the fluorescence spectra corresponding to urine samples of the oral cancer patients and healthy volunteers and the error bars (at the peak positions) represent ±1 standard deviation. The relative standard deviation (RSD) for the major emission band was observed to be in the range of ~19 – 68 % over the respective number of urine samples investigated. The spectra are similar to those reported in the fluorescence spectroscopic studies of urine by others [91, 116, 311, 312].

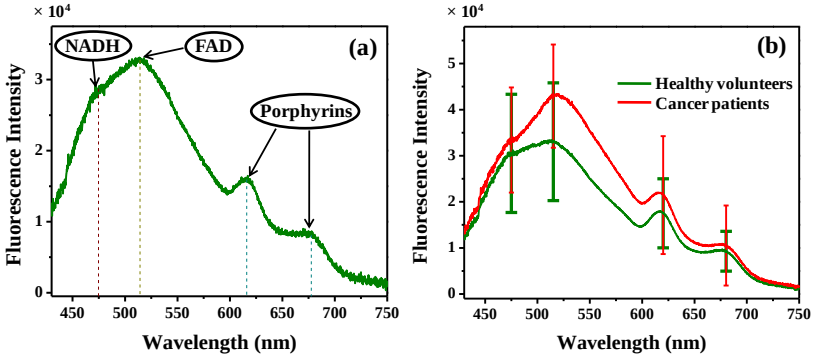

Figure 5.3: (a) *Fluorescence spectrum of the urine sample of a healthy volunteer. The healthy volunteer was chosen randomly out of 22 healthy volunteers.* ***(b)*** *Mean fluorescence spectra of urine samples corresponding to patients with oral cancer and healthy volunteers. Each spectrum is the average of the spectra over urine samples of 22healthy volunteers and 18 oral cancer patients*

It is apparent from the figure that the fluorescence intensities are much higher for urine samples of patients with oral cancer as compared to that for healthy volunteers. The difference spectrum obtained by subtracting the mean

spectrum of urine samples of healthy volunteers from cancer patients is plotted in **Figure 5.4** along with 95% confidence interval at each wavelength and shown in grey band. The differences outside the grey band represent the region of statistically significant spectral differences. From the figure, it is evident that the peak around 515 nm corresponding to FAD is statistically pronounced ($p < 0.05$) in the urine spectra of cancerous patients as compared to the healthy volunteers implying a considerably larger FAD concentration in the urine of cancer patients. It is important to mention here that this is consistent with the findings reported in literature [116].

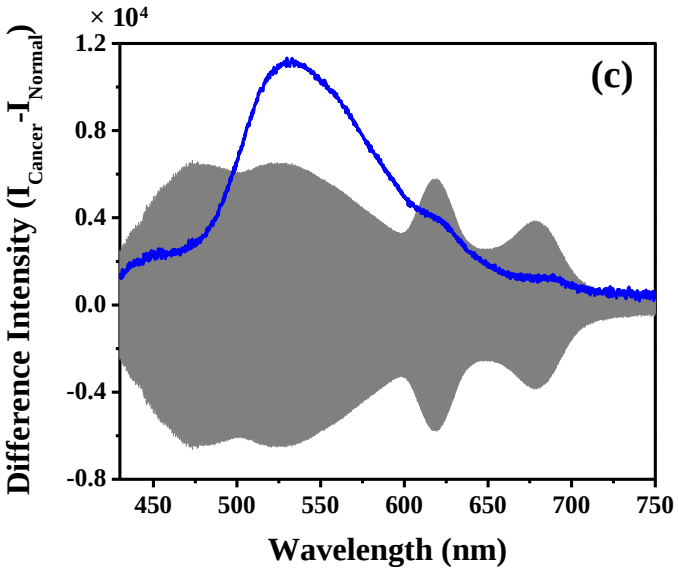

Figure 5.4: *Mean difference spectra showing statistical differences between fluorescence spectra of cancer patients and healthy volunteers. Grey bands indicate 95% confidence intervals of the difference determined by standard error confidence intervals. The spectrum from each of the patients and healthy volunteers was measured immediately following putting on of the illumination laser.*

Figures 5.5(a) and **5.5(b)** show the emission spectra measured from the urine samples of a healthy volunteer and a patient at eight different points in time (t1= 0 s, t2 = 50 s, t3 = 100 s, t4 = 200 s, t5 = 300 s, t6 = 400 s, t7 = 500 s and t8 = 600 s) under continuous illumination (from the 405 nm diode laser). While significant differences are observed in the spectra of cancerous patients and healthy volunteers, these differences are found to be varying with time till

the intensities of the observed fluorescence spectra corresponding to the two categories of urine samples become stable. **Figure 5.5(c)** shows the difference spectra derived from the set of spectra measured at different points in time from the urine samples of the same oral cancer patient and healthy volunteer. From the figure it is apparent that the inter-category spectral differences are varying significantly till t = 200 s beyond which it is found to remain almost constant.

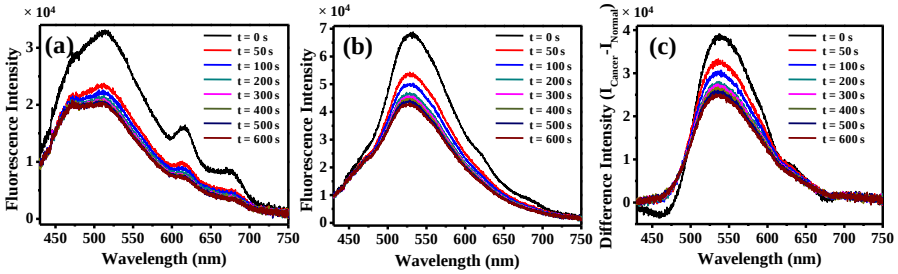

Figure 5.5: *Fluorescence spectra measured from the urine samples of **(a)** a healthy volunteer, **(b)** a patient at eight different points in time following putting on of the illumination light.**(c)**The difference spectra between the urine samples of the same patient and the healthy volunteer corresponding to those time points.*

In order to see whether this observed variation in the inter-category spectral differences has any effect on the efficacy in separating the urine samples of cancerous patients from those of healthy volunteers, spectrally integrated intensities (ΣI) were estimated from the full set of fluorescence spectra of urine samples of patients and healthy subjects acquired at different time-points of measurements, and used as input to a classification algorithm developed based on nearest mean classifier (NMC) [313, 314]. A nearest mean-classifier is based on the least Euclidean distance of the test data from the means of the prototype data of the corresponding classes in the training set [313-315]. The algorithm was applied on the ΣI value in leave-one-subject-out-cross validation mode. In this method, training of the algorithm is performed using data of urine samples of N-1 subjects (N being the total number of subjects) and test is carried out only on the data of the urine sample of the excluded subject. **Table 5.2** lists the sensitivities and specificities yielded by the NMC based classification algorithm. One can see that the sensitivity and

specificity values are decreasing with time and are also different for the different sets of spectra acquired till t = 200 s. Since the primary basis of discrimination between the urine samples is the observed differences in the urine spectra of patients and healthy volunteers, the varying spectral differences resulted at different time points of measurements (under continuous illumination) have led to varying results of discrimination even for the same set of urine samples of cancer patients and healthy subjects. However, the sensitivity and specificity values are found to remain the same for the remaining sets of spectra acquired at t > 200 s since no appreciable variation in the spectral differences is observed for these sets of spectra measured at t > 200 s.

Acquisition time (sec)	Sensitivity	Specificity	Overall accuracy
At t = 0	72%	73%	72%
At t = 50	67%	73%	70%
At t = 100	61%	73%	68%
At t = 200	61%	68%	65%
At t = 300	61%	68%	65%
At t = 400	61%	68%	65%
At t = 500	61%	68%	65%
At t = 600	61%	68%	65%

Table 5.2: *The classification results yielded by the nearest mean classifier based classification algorithm in discriminating urine samples of the oral cancer patients (n = 18) from that of the healthy volunteers (n = 22) using spectrally integrated intensities estimated from the fluorescence spectra measured at different points in time following putting on of the illumination light as input. The classification results are based on leave-one-subject-out cross validation*

In order to understand the temporal characteristics of reduction in the intensities of the urine fluorescence, ΣI value estimated from the fluorescence spectra (shown in **Figure 5.5**) of urine samples of the healthy volunteer and the oral cancer patient were plotted against the different time-points of spectral measurements. **Figure 5.6** shows the plot of ΣI as a function of time-points of measurements. It is apparent from the figure that the urine sample from the healthy subject has faster rate of fluorescence photo-bleaching as compared to the urine sample of the patient with oral cancer. For quantifying this inter-category difference in the temporal characteristics of the reduction in fluorescence (i.e. fluorescence photo-bleaching), the ΣI versus time-point of

spectral measurements curves were fitted with a double-exponential decay function given by:

$$\sum I(t) = A + B\ exp^{-\frac{1}{\tau_1}} + C\ exp^{-\frac{1}{\tau_2}} \quad \ldots\ldots\ldots\ldots\ldots\ldots (1)$$

where *A*, *B* and *C* are constants, τ_1 and τ_2 are the time constants for the fast and slow phases of photo-bleaching, *t* is the time and ΣI (*t*) is the spectrally integrated intensity as a function of time.

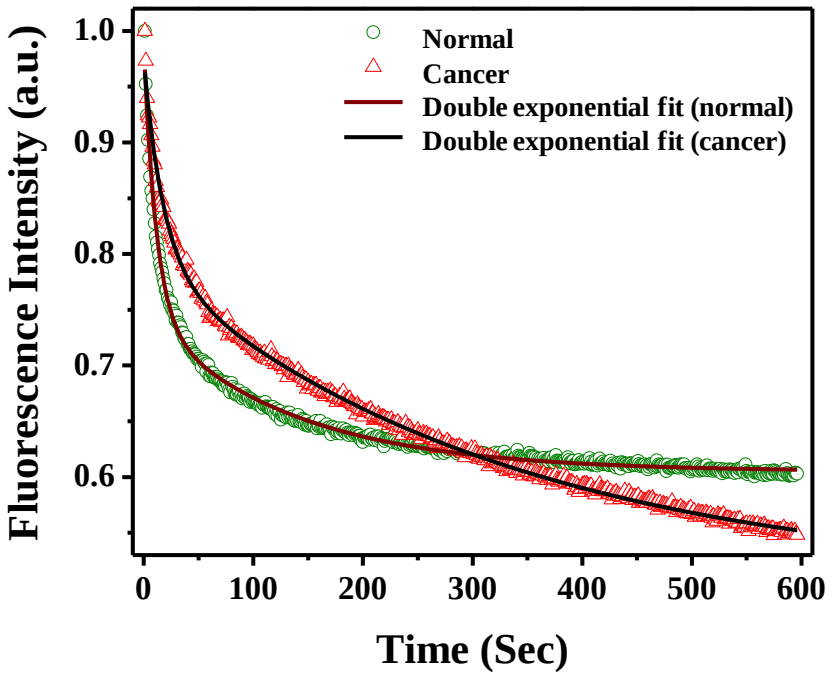

Figure 5.6: *Plot of integrated fluorescence intensities as a function of time-points of measurements for the urine samples belonging to a healthy volunteer and a cancer patient. The solid line represents the double-exponential fit to the measured data.*

Figure 5.6 shows the double-exponential fits to the ΣI versus time-point of spectral measurements curves for the urine samples of the healthy subject and the oral cancer patient. The fits were found to result in a R^2 value of ~0.99. The double exponential behavior can be attributed to the Gaussian profile of the excitation laser beam which leads to inhomogeneous power distribution along the transverse plane [316]. The constant of the faster photo-bleaching represents the molecules exposed by the high intensity region near

the axis, whereas the slower photo-bleaching constant is due to the outermost low intensity region of the laser [316, 317].

Health state	τ_1 (sec)	τ_2 (sec)
Normal	7.6 ± 3.6	107.9 ± 44.3
Cancer	16.0 ± 3.8	216.7 ± 67.5

Table 5.3: *The fast (τ_1) and slow (τ_2) photo-bleaching time constants corresponding to the urine samples of cancer patients and healthy individuals*

Table 5.3 shows the mean ± standard deviation (σ) of the photo-bleaching time-constants, $\tau_1$and τ_2, estimated from the ΣI versus time-point of spectral measurements curves of the urine samples belonging to all the healthy subjects and the patients with oral cancer. It can be seen that both the fast (τ_1) and slow (τ_2) time-constants are considerably smaller in urine samples obtained from the healthy volunteers as compared to that from patients with oral cancer. A Student's t-test confirmed that the differences in the mean values of these time constants between the two categories (cancer and normal) were indeed statistically significant ($p < 0.001$).

Figure 5.7 shows a graphical presentation of the fast (τ_1) versus slow (τ_2) time constants for the urine samples corresponding to patients with oral cancer and healthy subjects. The graph is plotted along with a probability ellipsoid around each of the urine sample categories. The probability ellipsoid [318] around a category (of data) defines the region that contains 90% of data belonging to that category assuming Gaussian distribution. Thus, from the probability ellipsoids shown in figure 5 it is apparent that there is significant separation between the urine samples belonging to patients with oral cancer and healthy subjects.

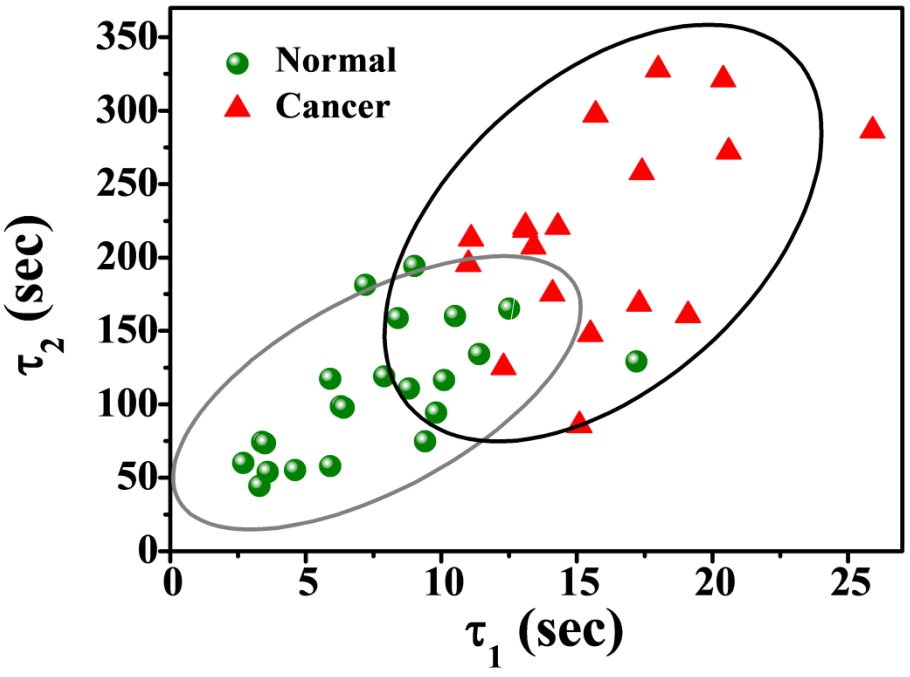

Figure 5.7: *A graphical presentation of the fast (τ_1) versus slow (τ_2) photo-bleaching time constants for the urine samples corresponding to patients with oral cancer and healthy subjects. The graph is plotted along with a 90%probability ellipsoid around each of the urine sample categories.*

In order to further quantify the potential of the photo-bleaching time-constants in discriminating the two categories of urine samples, the NMC based algorithm [313-315] was employed in leave-one-sample-out cross validation mode where the values of the time constants were used as input. **Table 5.4** lists the sensitivity and specificity values yielded by the algorithm in discriminating the urine samples belonging to patients with oral cancer and healthy subjects. The sensitivity and specificity were found to be 78% and 86%, respectively. One can see that by considering the temporal characteristics of photo-bleaching of urine samples, the overall classification accuracy was improved to 82% as compared to the maximum of 72% obtained when the integrated fluorescence intensity was considered for classification (**Table 5.2**).

Pathology diagnosis	Sensitivity	Specificity	Overall accuracy
Normal (n = 22) vs. Cancer (n = 18)	78%	86%	82%

Table 5.4: *The classification results yielded by the nearest mean classifier-based classification algorithm in discriminating urine samples of the oral cancer patients from that of the healthy volunteers using fast (τ_1) and slow (τ_2) photo-bleaching time constants estimated from the curve-fitting analyses. The classification results are based on leave-one-subject-out cross validation.*

After establishing the applicability of the photo-bleaching time constants in discriminating urine samples of the oral cancer patients from that of the healthy subjects, the next important task was to find out the underlying reason for the differences in the temporal patterns of photo-bleaching for the two categories of urine samples. In order for that fluorescence emission spectra measured from all the urine samples belonging to the two categories (i.e. patients with oral cancer and healthy subjects) at different points in time under continuous illumination were spectrally decomposed into a set of three basis spectra corresponding to the emission spectra of NADH, FAD, and porphyrins respectively. The choice of these basis set spectra was guided by the fact that the human urine samples are known to contain three major fluorophores, NADH, FAD and Protoporphyrin IX that could be excited by light of 405 nm wavelength [91, 116, 319]. The first step towards carrying out the spectral decomposition is generation of the basis set spectra. For that, the fluorescence emission spectra of the authentic NADH, FAD and Protoporphyrin IX were recorded using 405 nm excitation in the same experimental set up used to measure the spectra of urine samples. The spectra were then peak-normalized and linearly combined to fit the measured time-lapse fluorescence emission of the different urine samples belonging to the two different categories. The linear fit is justified in this case because urine, having very little or almost no turbidity, can be considered as a solution very close to a dilute solution. **Figure**

5.8 shows the peak-normalized fluorescence emission spectra of NADH, FAD and porphyrins. It is apparent from the figure that while the fluorescence spectra of NADH and FAD are characterized by single emission bands, the porphyrin fluorescence spectrum shows two emission bands.

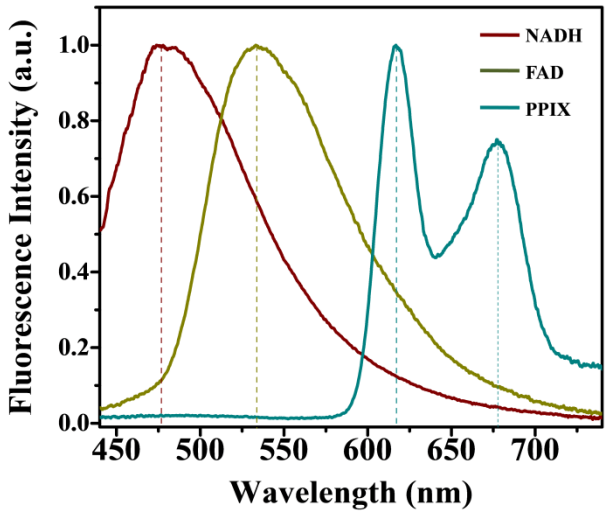

Figure 5.8: *The peak normalized fluorescence emission spectra of reduced Nicotinamide Adenine Dinucleotide (NADH), Flavin Adenine Dinucleotide (FAD) and Protoporphyrin IX (PPIX).*

The results of the spectral fitting analyses are graphically demonstrated in **Figure 5.9**. The spectral fitting is shown for a set of two urine samples, one corresponding to a healthy subject and the other corresponding to a patient with oral cancer. One can clearly see that the relative contribution of the spectral band, characteristics of FAD, is more in urine samples of the cancer patients than that of the healthy subject. It is pertinent to note that a similar increase was obtained by Al-Salhi, Mohammad, et al. [320] for the urine samples of cancer patients with 400 nm excitation and attributed to an increase in FAD concentration [321].

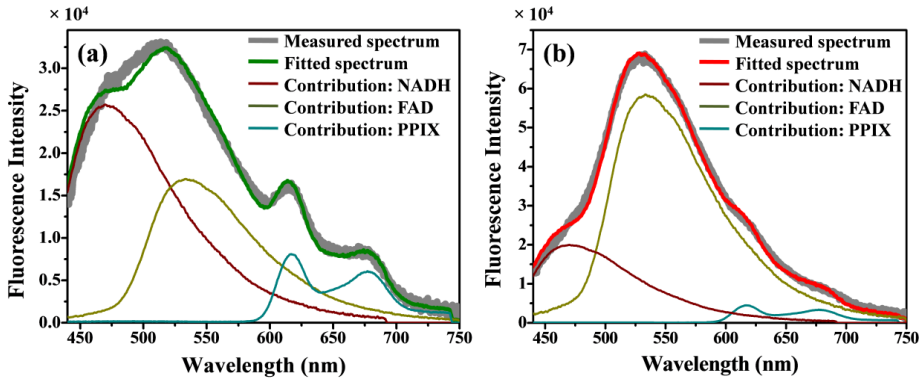

Figure 5.9: *Fluorescence spectra measured immediately following putting on of the illumination laser from urine samples corresponding to* ***(a)*** *a healthy volunteer and* ***(b)*** *a patient with oral cancer. Each spectrum was fitted with peak-normalized emission spectra of NADH (solid blue line), FAD (solid purple line) and Protoporphyrin IX (solid magenta line).*

However, it is apparent from the figure that there is no significant difference in the relative contribution of NADH or porphyrins between the two categories of urine samples. This is supported by the difference spectrum shown in **Figure 5.4(c)** where it is observed that their absolute contributions in the spectra of urine samples of the cancer patient and the healthy subject are within the limit of inter-subject variation.

Table 5.5 lists the fast (τ_1) and slow (τ_2) photo-bleaching time constants corresponding to NADH, FAD and porphyrins, respectively, obtained from the spectral fitting of the measured time-lapse fluorescence emission spectra of the full set of urine samples belonging to patients with oral cancer and healthy subjects.

Fluorophores	Health state	τ_1 (sec)	τ_2 (sec)
NADH	**Normal**	5.6 ± 3.7	84.7 ± 63.9
	Cancer	6.3 ± 3.2	109.2 ± 90.1
FAD	**Normal**	12.5 ± 3.5	167.5 ± 31.6
	Cancer	19.5 ± 2.7	231.7 ± 52.3
PpIX	**Normal**	13.3 ± 3.7	145.45 ± 17.4
	Cancer	12.2 ± 5.1	155.6 ± 59.4

Table 5.5: *The fast (τ_1) and slow (τ_2) photo-bleaching time constants corresponding to NADH, FAD and porphyrins, respectively, obtained from the spectral fitting of the measured time-lapse fluorescence emission spectra of the full set of urine samples belonging to patients with oral cancer and healthy subjects.*

A perusal of the table shows: (i) both τ_1 and τ_2 corresponding to NADH are significantly smaller ($p < 0.05$) as compared to FAD in the urine samples of both the cancer patients and healthy subjects implying faster photo-bleaching rate of NADH in comparison with FAD (ii) τ_2 of FAD is much larger for the urine of the cancer patients than the urine of the healthy subjects suggesting slower photo-bleaching of urine in the cancer patients, and (iii) no statistically significant differences in τ_1 and τ_2 corresponding to NADH and porphyrins are observed between the urine samples of the cancer patients and that of the healthy subjects suggesting that these fluorophores seem to have no or little contribution in the observed differences in the temporal patterns of photo-bleaching of urine belonging to the two categories. These observations are in qualitative agreement with the photo-bleaching time constants of the urine samples of the cancer patients and healthy subjects tabulated in **Table 5.2**. In particular it is important to note here that the observed photo-bleaching

time-constants of the urine of the cancer patients are found to be close in value to the time-constants estimated for FAD. This is plausibly due to the fact that the urine of cancer patients is reported to contain significantly larger FAD [91, 116, 320, 321]. The photo-bleaching rates also depend upon the chemical environment in which the fluorophores are present [322-324]. This might also be the reason for variations in the time constants of the same fluorophore in urine of cancer patients and healthy subjects.

The primary objective of the present study was to understand the fluorescence photo-bleaching characteristics of human urine samples and show how the use of urine fluorescence which was still undergoing photo-bleaching could lead to discrimination results very different from what was obtained when it was used after becoming stable following the completion of photo-bleaching. The other important objective was to assess the discrimination ability of the photo-bleaching time constants in separating the urine samples of cancer patients and healthy individuals. For performing both these tasks, a supervised classifier which is simple enough in its mathematical formulation and does not require optimization of any of its design parameters, while being trained, was sufficient. NMC being a geometric classifier and its performance solely being dependent on the linear separation of spectral data at disposal, unlike a statistical classifier whose performance also depends on the optimization of algorithm parameters for each of the classification tasks, was therefore deemed appropriate for the present job.

However, it should be noted here that in the next phase of our study (already in progress) where the objective is to establish a model of oral cancer diagnosis based on fluorescence photo-bleaching data of large population of patients, we will be employing a probability based statistical classification algorithm [325], which was developed earlier based on the mathematical formulation of sparse multinomial logistic regression [326] and used in several of our earlier studies [327-329]. The algorithm was found to provide best classification accuracy of 92% (leave-one-out cross validation mode) as compared to that of 82% using NMC. However, when the algorithm was

applied in “no cross-validation mode” (i.e. same set of data used for both training and validation), the classification accuracy was 100%.

5.3 Summary:

To conclude, we have studied the effect of photo-bleaching on fluorescence and Raman spectral measurements of human urine samples. Photo-stability of urine is important for the optical spectroscopy-based diagnosis of any disease where urine is used as a sample of choice. Urine Raman spectra should be recorded well after the decay constant time. Further, a detailed study on fluorescence photo-bleaching of human urine samples was carried out. The time lapse fluorescence spectra were recorded from the urine samples obtained from patients with oral cancer as well as from healthy volunteers under continuous illumination of 405 nm radiation from a diode laser. It was found that while significant differences existed in the spectra of cancerous patients and healthy volunteers, these differences were varying with time till the intensities of the observed fluorescence spectra corresponding to the two categories of urine samples became stable. In order to quantify the spectral differences, integrated fluorescence intensity (ΣI) was calculated for each spectrum and a classification algorithm developed based on NMC was applied in leave-one-subject-out cross-validation mode on ΣI values for each of the sets of spectra measured from the two categories of the urine samples at different points in time. The sensitivity and specificity values yielded by the algorithm were found to decrease till t = 200 s beyond which they were found to remain almost unchanged. A decay curve was generated by plotting ΣI vs. time and fitted with a double-exponential decay function. The photo-bleaching constants, obtained from curve-fitting, were found to have statistically significant differences corresponding to the urine samples of cancerous patients and healthy volunteers. The NMC based classification algorithm applied on the photo-bleaching constants in leave-one-subject-out cross-validation mode was found to provide a sensitivity and specificity of up to 86%

in discriminating the two categories of urine samples. Overall, the results of the studies showed that the temporal characteristic of photo-bleaching had promising potential to be used as an alternate tool for oral cancer diagnosis.

Chapter 6

Conclusion and Future Perspectives

This chapter presents the summary of this thesis work and the future prospects of this research.

6.1 Conclusion:

Optical spectroscopy along with nanotechnology is pioneering the advancements of biophotonics in clinical practice. The present thesis investigates the applications of Raman and fluorescence spectroscopy-based urine analysis for rapid and reliable disease diagnosis. In particular, the presented research addresses the limitations of the current optical spectroscopy-based techniques for urine analysis. The results shown in this thesis suggest that the quantitative determination of trace amount of analytes present in urine is possible with the help of nanotechnology and improved signal detection strategies. Thus, these techniques could be used in clinical settings to differentiate the normal and disease conditions more efficiently.

In the first part of this study, an experimental arrangement was developed for drop coating deposition Raman spectroscopic (DCDRS) measurement and used it for the quantitative detection of urinary creatinine. It is pertinent to mention here that although the DCDRS technique was applied previously for the analysis of different body fluids (blood, tears, etc.), the applicability of the same was unexplored for urine analysis. A multi-variate partial least square regression analysis was applied on the DCDRS spectra measured from artificial urine samples and the quantity of creatinine present in the artificial urine was predicted with an accuracy of >94%. The lower detection limit of the analytes present in artificial urine suggests that the sensitive detection of the analytes is possible using DCDRS when the analytes'

concentration range is lower than the physiological concentration range found in urine. Hence, DCDRS combined with chemometrics could be a promising tool for reliable disease diagnosis using urine samples. Further, a novel Raman signal enhancement technique for liquid samples, nano-trap enhanced Raman spectroscopy (NTERS), is introduced, first time. In this technique the nanoaggregates are formed at the focal spot of the incident laser. The analytes present in the sample get trapped within these nanoaggregates and the Raman signal of the analytes or molecules are measured from these aggregates. Hence, the Raman signal of the analytes is enhanced significantly and at the same time constant experimental parameters provide high repeatability. The results also suggest that the NTERS quantitatively predicts the uric acid concentration with an accuracy of ~96%. This technique could be used for the quantitative determination of trace amount of analytes present in body fluids with high reproducibility. These results suggest that the two variants of Raman spectroscopy used in this thesis work, namely DCDRS and NTERS, could be used for rapid and accurate analysis of urine samples as well as other body fluids. Apart from the development and use of the two Raman spectroscopic based techniques, the temporal characteristic of fluorescence photo-bleaching of urine samples was also studied and used for oral cancer diagnosis. The photobleaching decay constants estimated for urine samples of healthy volunteers and oral cancer patients were found to be significantly different ($p < 0.001$). Further, the classification accuracy for the two categories of samples was improved (~82%) when these decay constants were involved in the algorithm as compared to the case without involving the decay constants. The overall findings of this thesis suggest that optical spectroscopy-based urine analysis has great prospects and can be used as a potential alternative tool for accurate and rapid diagnosis of various diseases including cancer.

6.2 Future Perspectives:

The results of this thesis show that both the DCDRS and NTERS techniques have immense potential for the quantitative determination of analytes or metabolites present in urine. Therefore, in future, the capabilities of these techniques will be assessed for the analysis of other body fluids and will be used in clinical practice for rapid and accurate disease diagnosis.

Results of the present thesis work also show that the temporal characteristic of fluorescence photobleaching of urine plays crucial role in the improvement of the classification accuracy during oral cancer diagnosis when urine is used as a sample of choice. Thus, the other important future task will be the development of a simple, cost effective, and portable fluorescence spectroscopy based system with specific light source and detector for the rapid screening of oral cancer in a larger scale, as it is one of the profoundly occurred cancers in India. Such development will helpful in increasing the patient survival rate as the diagnosis could be done in the early stages of the disease. Another important future task will be to evaluate the performance of the developed system for on-field preclinical and clinical applications for early stage disease diagnosis in the rural parts of the country.

Additionally, it would also be very interesting to develop a combined Raman, fluorescence spectroscopy, and white light imaging-based system. Such combined system could differentiate the depositing patterns of body fluids in different pathological conditions. Then the morphology and molecular properties of the clinical specimens could be examined more precisely, which would increase the diagnosis accuracy significantly. There also remains a possibility that such system can be not only used for the disease diagnosis, but also for on spot forensic applications.

References

1. Wians F. H. (2009), Clinical Laboratory Tests: Which, Why, and What Do The Results Mean?, Laboratory Medicine, 40, 105-113 (10.1309/LM4O4L0HHUTWWUDD)
2. Jiang F., Jiang Y., Zhi H., Dong Y., Li H., Ma S., Wang Y., Dong Q., Shen H.Wang Y. (2017), Artificial intelligence in healthcare: past, present and future, Stroke and Vascular Neurology, 2, 230 (10.1136/svn-2017-000101)
3. Ndao M. (2009), Diagnosis of Parasitic Diseases: Old and New Approaches, Interdisciplinary Perspectives on Infectious Diseases, 2009, 15 (10.1155/2009/278246)
4. Lee S., Huang H.Zelen M. (2004), Early detection of disease and scheduling of screening examinations, Statistical Methods in Medical Research, 13, 443-456 (10.1191/0962280204sm377ra)
5. Croft P., Altman D. G., Deeks J. J., Dunn K. M., Hay A. D., Hemingway H., LeResche L., Peat G., Perel P., Petersen S. E., Riley R. D., Roberts I., Sharpe M., Stevens R. J., Van Der Windt D. A., Von Korff M.Timmis A. (2015), The science of clinical practice: disease diagnosis or patient prognosis? Evidence about “what is likely to happen” should shape clinical practice, BMC Medicine, 13, 20 (10.1186/s12916-014-0265-4)
6. Morabia A.Zhang F. F. (2004), History of medical screening: from concepts to action, Postgraduate Medical Journal, 80, 463 (10.1136/pgmj.2003.018226)
7. Doria A., Zen M., Canova M., Bettio S., Bassi N., Nalotto L., Rampudda M., Ghirardello A.Iaccarino L. (2010), SLE diagnosis and treatment: When early is early, Autoimmunity Reviews, 10, 55-60 (https://doi.org/10.1016/j.autrev.2010.08.014)
8. Smith R. A.Wender R. C. (2004), Cancer screening and the periodic health examination, Cancer, 100, 1553-1557 (10.1002/cncr.20170)
9. Er O., Yumusak N.Temurtas F. (2010), Chest diseases diagnosis using artificial neural networks, Expert Systems with Applications, 37, 7648-7655 (https://doi.org/10.1016/j.eswa.2010.04.078)
10. Mroz T. A., Picone G., Sloan F.Yashkin A. P. (2016), Screening for a chronic disease: a multiple stage duration model with partial observability, International Economic Review, 57, 915-934 (10.1111/iere.12180)

11. Jammeh E., Zhao P., Carroll C., Pearson S.Ifeachor E. (2016), Identification of blood biomarkers for use in point of care diagnosis tool for Alzheimer's disease, 2016 38th Annual International Conference of the IEEE Engineering in Medicine and Biology Society (EMBC), 2415-2418 (10.1109/EMBC.2016.7591217)
12. Saghir Z., Dirksen A., Ashraf H., Bach K. S., Brodersen J., Clementsen P. F., Døssing M., Hansen H., Kofoed K. F., Larsen K. R., Mortensen J., Rasmussen J. F., Seersholm N., Skov B. G., Thorsen H., Tønnesen P.Pedersen J. H. (2012), CT screening for lung cancer brings forward early disease. The randomised Danish Lung Cancer Screening Trial: status after five annual screening rounds with low-dose CT, Thorax, 67, 296 (10.1136/thoraxjnl-2011-200736)
13. Vandeborne L., van Overbeeke E., Dooms M., De Beleyr B.Huys I. (2019), Information needs of physicians regarding the diagnosis of rare diseases: a questionnaire-based study in Belgium, Orphanet Journal of Rare Diseases, 14, 99 (10.1186/s13023-019-1075-8)
14. Fiehn C., Hajjar Y., Mueller K., Waldherr R., Ho A. D.Andrassy K. (2003), Improved clinical outcome of lupus nephritis during the past decade: importance of early diagnosis and treatment, Annals of the Rheumatic Diseases, 62, 435 (10.1136/ard.62.5.435)
15. Hankinson J. L.Wagner G. R. (1993), Medical screening using periodic spirometry for detection of chronic lung disease, Occupational medicine (Philadelphia, Pa.), 8, 353-361
16. Yager P., Edwards T., Fu E., Helton K., Nelson K., Tam M. R.Weigl B. H. (2006), Microfluidic diagnostic technologies for global public health, Nature, 442, 412-418 (10.1038/nature05064)
17. Cottin V.Richeldi L. (2014), Neglected evidence in idiopathic pulmonary fibrosis and the importance of early diagnosis and treatment, European Respiratory Review, 23, 106 (10.1183/09059180.00008613)
18. Vaught J. B.Henderson M. K. (2011), Biological sample collection, processing, storage and information management, IARC Sci Publ, 163, 23-42
19. McEwen C. N., McKay R. G.Larsen B. S. (2005), Analysis of solids, liquids, and biological tissues using solids probe introduction at atmospheric pressure on commercial LC/MS instruments, Analytical Chemistry, 77, 7826-7831
20. Su S.-B., Poon T. C. W.Thongboonkerd V. (2013), Human Body Fluid, BioMed Research International, 2013, 2 (10.1155/2013/918793)

21. Hu S., Loo J. A.Wong D. T. (2006), Human body fluid proteome analysis, PROTEOMICS, 6, 6326-6353 (10.1002/pmic.200600284)
22. Pettitt J., Higgs E., Fallah M., Nason M., Stavale E., Marchand J., Reilly C., Jensen K., Dighero-Kemp B., Tuznik K., Logue J., Bolay F.Hensley L. (2016), Assessment and Optimization of the GeneXpert Diagnostic Platform for Detection of Ebola Virus RNA in Seminal Fluid, The Journal of Infectious Diseases, 215, 547-553 (10.1093/infdis/jiw599)
23. Rabinowitz J. C.Snell E. E. (1949), Vitamin B6 Group. XV. Urinary Excretion of Pyridoxal, Pyridoxamine, Pyridoxine, and 4-Pyridoxic Acid in Human Subjects, Proceedings of the Society for Experimental Biology and Medicine, 70, 235-240
24. Risley E. H. (1911), The treatment of cancer with body fluids and cancerous ascitic fluid, jama, lvi, 1383-1389 (10.1001/jama.1911.02560190011007)
25. Sauter E. R. (2017), Reliable biomarkers to identify new and recurrent cancer, European Journal of Breast Health, 13, 162
26. Yang Z., Xu G., Reboud J., Ali S. A., Kaur G., McGiven J., Boby N., Gupta P. K., Chaudhuri P.Cooper J. M. (2018), Rapid Veterinary Diagnosis of Bovine Reproductive Infectious Diseases from Semen Using Paper-Origami DNA Microfluidics, ACS Sensors, 3, 403-409 (10.1021/acssensors.7b00825)
27. Jimenez-Luna C., Torres C., Ortiz R., Dieguez C., Martinez-Galan J., Melguizo C., Prados J. C.Caba O. (2018), Proteomic biomarkers in body fluids associated with pancreatic cancer, Oncotarget, 9, 16573
28. Murphy W. M.Ng A. B. P. (1972), Determination of Primary Site by Examination of Cancer Cells in Body Fluids, American Journal of Clinical Pathology, 58, 479-488 (10.1093/ajcp/58.5.479)
29. Badiee P. (2013), Evaluation of Human Body Fluids for the Diagnosis of Fungal Infections, BioMed Research International, 2013, 8 (10.1155/2013/698325)
30. Pastore A. L., Palleschi G., Silvestri L., Moschese D., Ricci S., Petrozza V., Carbone A.Di Carlo A. (2015), Serum and Urine Biomarkers for Human Renal Cell Carcinoma, Disease Markers, 2015, 9 (10.1155/2015/251403)
31. Fenocchio E., Colombi F., Calella M. G., Filippi R., Depetris I., Chilà G., Lombardi P., Marino D., Cagnazzo C., Ferraris R., Vaira M., Aglietta M.Leone F. (2019), Improvement of Metastatic Colorectal Cancer Patient Survival: Single Institution Experience, Cancers, 11, 369 (10.3390/cancers11030369)

32. Garza A. G., Gratton M. C., Salomone J. A., Lindholm D., McElroy J.Archer R. (2009), Improved Patient Survival Using a Modified Resuscitation Protocol for Out-of-Hospital Cardiac Arrest, Circulation, 119, 2597-2605 (doi:10.1161/CIRCULATIONAHA.108.815621)
33. T F. W. (1898), The Blood; how to examine and diagnose its Diseases, Nature, 58, 269-269 (10.1038/058269a0)
34. Sun H., Yin C.-Q., Liu Q., Wang F.Yuan C.-H. (2017), Clinical Significance of Routine Blood Test-Associated Inflammatory Index in Breast Cancer Patients, Medical science monitor : international medical journal of experimental and clinical research, 23, 5090-5095 (10.12659/msm.906709)
35. Lima D. P., Diniz D. G., Moimaz S. A. S., Sumida D. H.Okamoto A. C. (2010), Saliva: reflection of the body, International Journal of Infectious Diseases, 14, e184-e188 (https://doi.org/10.1016/j.ijid.2009.04.022)
36. Shah S. (2018), Salivaomics: The current scenario, Journal of oral and maxillofacial pathology: JOMFP, 22, 375
37. Walker A. B. (1895), THE IMPORTANCE OF URINALYSIS IN DIAGNOSIS, JAMA, XXIV, 122-123 (10.1001/jama.1895.02430040016002d)
38. Piech T. L.Wycislo K. L. (2019), Importance of Urinalysis, Veterinary Clinics of North America: Small Animal Practice, 49, 233-245 (https://doi.org/10.1016/j.cvsm.2018.10.005)
39. Leboulleux S., Rubino C., Baudin E., Caillou B., Hartl D. M., Bidart J.-M., Travagli J.-P.Schlumberger M. (2005), Prognostic Factors for Persistent or Recurrent Disease of Papillary Thyroid Carcinoma with Neck Lymph Node Metastases and/or Tumor Extension beyond the Thyroid Capsule at Initial Diagnosis, The Journal of Clinical Endocrinology & Metabolism, 90, 5723-5729 (10.1210/jc.2005-0285)
40. Rockson S. G. (2008), Diagnosis and Management of Lymphatic Vascular Disease, Journal of the American College of Cardiology, 52, 799 (10.1016/j.jacc.2008.06.005)
41. Blennow K., Hampel H., Weiner M.Zetterberg H. (2010), Cerebrospinal fluid and plasma biomarkers in Alzheimer disease, Nature Reviews Neurology, 6, 131-144 (10.1038/nrneurol.2010.4)
42. Brannan S. R.Jerrard D. A. (2006), Synovial fluid analysis, The Journal of emergency medicine, 30, 331-339
43. Shmerling R. H. (1994), Synovial fluid analysis. A critical reappraisal, Rheumatic diseases clinics of North America, 20, 503-512

44. Tadeu B. T. M.Geelhoed D. (2016), “This thing of testing our blood is really very important”: a qualitative study of primary care laboratory services in Tete Province, Mozambique, International Journal for Equity in Health, 15, 133 (10.1186/s12939-016-0418-5)
45. Basu D.Kulkarni R. (2014), Overview of blood components and their preparation, Indian journal of anaesthesia, 58, 529-537 (10.4103/0019-5049.144647)
46. Malamud D. (2011), Saliva as a Diagnostic Fluid, Dental Clinics of North America, 55, 159-178 (https://doi.org/10.1016/j.cden.2010.08.004)
47. Giannobile W. V., Beikler T., Kinney J. S., Ramseier C. A., Morelli T.Wong D. T. (2009), Saliva as a diagnostic tool for periodontal disease: current state and future directions, Periodontology 2000, 50, 52-64 (10.1111/j.1600-0757.2008.00288.x)
48. Zhang C.-Z., Cheng X.-Q., Li J.-Y., Zhang P., Yi P., Xu X.Zhou X.-D. (2016), Saliva in the diagnosis of diseases, International Journal of Oral Science, 8, 133-137 (10.1038/ijos.2016.38)
49. Zhang A., Sun H.Wang X. (2012), Saliva metabolomics opens door to biomarker discovery, disease diagnosis, and treatment, Applied biochemistry and biotechnology, 168, 1718-1727
50. Liu J.Duan Y. (2012), Saliva: A potential media for disease diagnostics and monitoring, Oral Oncology, 48, 569-577 (https://doi.org/10.1016/j.oraloncology.2012.01.021)
51. Malamud D.Niedbala R. S. (2007), Oral-based diagnostics,
52. Grus F. H., Boehm N., Berneiser S., Lamparter J., Wiegand M., Wiegel N.Pfeiffer N. (2009), Analysis of Tear Protein Profiles in Dry-Eye Patients by Mass Spectrometry, Investigative Ophthalmology & Visual Science, 50, 2546-2546
53. Zhou L.Beuerman R. W. (2017), The power of tears: how tear proteomics research could revolutionize the clinic, Expert Review of Proteomics, 14, 189-191 (10.1080/14789450.2017.1285703)
54. Jung J. H., Ji Y. W., Hwang H. S., Oh J. W., Kim H. C., Lee H. K.Kim K. P. (2017), Proteomic analysis of human lacrimal and tear fluid in dry eye disease, Scientific Reports, 7, 13363 (10.1038/s41598-017-13817-y)
55. Zhou L.Beuerman R. W. (2012), Tear analysis in ocular surface diseases, Progress in Retinal and Eye Research, 31, 527-550 (https://doi.org/10.1016/j.preteyeres.2012.06.002)
56. Soria J., Acera A., Merayo-Lloves J., Durán J. A., González N., Rodriguez S., Bistolas N., Schumacher S., Bier F. F., Peter H.,

Stöcklein W.Suárez T. (2017), Tear proteome analysis in ocular surface diseases using label-free LC-MS/MS and multiplexed-microarray biomarker validation, Scientific Reports, 7, 17478 (10.1038/s41598-017-17536-2)

57. Pettersson Bergstrand M., Beck O.Helander A. (2018), Urine analysis of 28 designer benzodiazepines by liquid chromatography–high-resolution mass spectrometry, Clinical Mass Spectrometry, 10, 25-32 (https://doi.org/10.1016/j.clinms.2018.08.004)
58. Penders J., Fiers T.Delanghe J. R. (2002), Quantitative Evaluation of Urinalysis Test Strips, Clinical Chemistry, 48, 2236
59. Khristenko N.Domon B. (2015), Quantification of proteins in urine samples using targeted mass spectrometry methods, Clinical Proteomics, 207-220
60. Delanghe J.Speeckaert M. (2014), Preanalytical requirements of urinalysis, Biochemia medica, 24, 89-104 (10.11613/BM.2014.011)
61. Swan A., Amer H.Dieppe P. (2002), The value of synovial fluid assays in the diagnosis of joint disease: a literature survey, Annals of the Rheumatic Diseases, 61, 493 (10.1136/ard.61.6.493)
62. Denton J. (2012), Synovial fluid analysis in the diagnosis of joint disease, Diagnostic Histopathology, 18, 159-168 (10.1016/j.mpdhp.2012.03.001)
63. Shi M., Bradner J., Hancock A. M., Chung K. A., Quinn J. F., Peskind E. R., Galasko D., Jankovic J., Zabetian C. P., Kim H. M., Leverenz J. B., Montine T. J., Ginghina C., Kang U. J., Cain K. C., Wang Y., Aasly J., Goldstein D.Zhang J. (2011), Cerebrospinal fluid biomarkers for Parkinson disease diagnosis and progression, Annals of Neurology, 69, 570-580 (10.1002/ana.22311)
64. Stoeck K., Sanchez-Juan P., Gawinecka J., Green A., Ladogana A., Pocchiari M., Sanchez-Valle R., Mitrova E., Sklaviadis T., Kulczycki J., Slivarichova D., Saiz A., Calero M., Knight R., Aguzzi A., Laplanche J.-L., Peoc'h K., Schelzke G., Karch A., van Duijn C. M.Zerr I. (2012), Cerebrospinal fluid biomarker supported diagnosis of Creutzfeldt–Jakob disease and rapid dementias: a longitudinal multicentre study over 10 years, Brain, 135, 3051-3061 (10.1093/brain/aws238)
65. Rockson S. G. (2008), Diagnosis and Management of Lymphatic Vascular Disease, Journal of the American College of Cardiology, 52, 799-806 (https://doi.org/10.1016/j.jacc.2008.06.005)

66. Summers G. D.McNicol M. W. (1980), Tuberculosis of superficial lymph nodes, British Journal of Diseases of the Chest, 74, 369-373 (https://doi.org/10.1016/0007-0971(80)90071-6)
67. Bouatra S., Aziat F., Mandal R., Guo A. C., Wilson M. R., Knox C., Bjorndahl T. C., Krishnamurthy R., Saleem F., Liu P., Dame Z. T., Poelzer J., Huynh J., Yallou F. S., Psychogios N., Dong E., Bogumil R., Roehring C.Wishart D. S. (2013), The human urine metabolome, PloS one, 8, e73076-e73076 (10.1371/journal.pone.0073076)
68. Goligorsky M. S., Addabbo F.Riordan E. (2007), Diagnostic Potential of Urine Proteome: A Broken Mirror of Renal Diseases, Journal of the American Society of Nephrology, 18, 2233 (10.1681/ASN.2006121399)
69. Armstrong J. A. (2007), Urinalysis in Western culture: A brief history, Kidney International, 71, 384-387 (https://doi.org/10.1038/sj.ki.5002057)
70. Tuuminen T. (2012), Urine as a Specimen to Diagnose Infections in Twenty-First Century: Focus on Analytical Accuracy, Frontiers in Immunology, 3, 45
71. Rosenhek J. (2005), History of medicine: liquid gold, Doctor's Rev: Med Move, 23,
72. Connor H. (2001), Medieval uroscopy and its representation on misericords–part 1: uroscopy, Clinical Medicine, 1, 507-509
73. Simerville J. A., Maxted W. C.Pahira J. J. (2005), Urinalysis: a comprehensive review, American family physician, 71,
74. Gowda S., Desai P. B., Kulkarni S. S., Hull V. V., Math A. A. K.Vernekar S. N. (2010), Markers of renal function tests, North American journal of medical sciences, 2, 170-173
75. Rosner M. H.Bolton W. K. (2006), Renal Function Testing, American Journal of Kidney Diseases, 47, 174-183 (10.1053/j.ajkd.2005.08.038)
76. Vassalotti J. A., Stevens L. A.Levey A. S. (2007), Testing for Chronic Kidney Disease: A Position Statement From the National Kidney Foundation, American Journal of Kidney Diseases, 50, 169-180 (10.1053/j.ajkd.2007.06.013)
77. Limdi J.Hyde G. (2003), Evaluation of abnormal liver function tests, Postgraduate medical journal, 79, 307-312
78. Gross J. L., De Azevedo M. J., Silveiro S. P., Canani L. H., Caramori M. L.Zelmanovitz T. (2005), Diabetic nephropathy: diagnosis, prevention, and treatment, Diabetes care, 28, 164-176

79. Wilson M. L.Gaido L. (2004), Laboratory Diagnosis of Urinary Tract Infections in Adult Patients, Clinical Infectious Diseases, 38, 1150-1158 (10.1086/383029)
80. Mozolowski W. (1948), Chemical composition of normal urine, The Lancet, 251, 423
81. Putnam D. F. (1971), Composition and concentrative properties of human urine,
82. Khamis M. M., Adamko D. J.El-Aneed A. (2017), Mass spectrometric based approaches in urine metabolomics and biomarker discovery, Mass Spectrometry Reviews, 36, 115-134 (10.1002/mas.21455)
83. Bar-Or D., Rael L. T., Bar-Or R., Craun M. L., Statz J.Garrett R. E. (2007), Mass spectrometry analysis of urine and catheter of a patient with purple urinary bag syndrome, Clinica Chimica Acta, 378, 216-218 (https://doi.org/10.1016/j.cca.2006.11.015)
84. Kumps A., Duez P., Genin J.Mardens Y. (1999), Gas Chromatography–Mass Spectrometry Analysis of Organic Acids: Altered Quantitative Response for Aqueous Calibrators and Dilute Urine Specimens, Clinical Chemistry, 45, 1297
85. Madrid-Gambin F., Brunius C., Garcia-Aloy M., Estruel-Amades S., Landberg R.Andres-Lacueva C. (2018), Untargeted 1H NMR-Based Metabolomics Analysis of Urine and Serum Profiles after Consumption of Lentils, Chickpeas, and Beans: An Extended Meal Study To Discover Dietary Biomarkers of Pulses, Journal of Agricultural and Food Chemistry, 66, 6997-7005 (10.1021/acs.jafc.8b00047)
86. Reo N. V. (2002), NMR-based metabolomics, Drug and Chemical Toxicology, 25, 375-382 (10.1081/DCT-120014789)
87. Klapkova E., Fortova M., Prusa R., Moravcova L.Kotaska K. (2016), Determination of Urine Albumin by New Simple High-Performance Liquid Chromatography Method, Journal of Clinical Laboratory Analysis, 30, 1226-1231 (10.1002/jcla.22007)
88. Kemperman R. F. J., Horvatovich P. L., Hoekman B., Reijmers T. H., Muskiet F. A. J.Bischoff R. (2007), Comparative Urine Analysis by Liquid Chromatography−Mass Spectrometry and Multivariate Statistics: Method Development, Evaluation, and Application to Proteinuria, Journal of Proteome Research, 6, 194-206 (10.1021/pr060362r)
89. Embade N., Cannet C., Diercks T., Gil-Redondo R., Bruzzone C., Ansó S., Echevarría L. R., Ayucar M. M. M., Collazos L., Lodoso B., Guerra E., Elorriaga I. A., Kortajarena M. Á., Legorburu A. P., Fang F., Astigarraga I., Schäfer H., Spraul M.Millet O. (2019), NMR-based

newborn urine screening for optimized detection of inherited errors of metabolism, Scientific Reports, 9, 13067 (10.1038/s41598-019-49685-x)
90. Premasiri W. R., Clarke R. H.Womble M. E. (2001), Urine analysis by laser Raman spectroscopy, Lasers in Surgery and Medicine, 28, 330-334 (10.1002/lsm.1058)
91. Masilamani V., AlSalhi M. S., Vijmasi T., Govindarajan K., Rai R. R., Atif M., Prasad S.Aldwayyan A. (2012), Fluorescence spectra of blood and urine for cervical cancer detection, Journal of biomedical optics, 17, 098001
92. Kiviat N. B.Critchlow C. W. (2002), Novel Approaches to Identification of Biomarkers for Detection of Early Stage Cancer, Disease Markers, 18, (10.1155/2002/589075)
93. Noguchi T.Berthomieu C. (2005), Molecular analysis by vibrational spectroscopy, Photosystem II, 367-387
94. Huang Q. (1971), Basic principles of spectroscopy,
95. Chattaraj P.Maiti B. (2001), Electronic structure principles and atomic shell structure, Journal of Chemical Education, 78, 811
96. Tykodi R. (1987), The ground state electronic structure for atoms and monoatomic ions, Journal of Chemical Education, 64, 943
97. Lakowicz J. R. (2013), Principles of fluorescence spectroscopy,
98. HORIBA Scientific. 2020. Fluorescence Spectroscopy - Applications and Principles. AZoM, viewed 24 June 2020, https://www.azom.com/article.aspx?ArticleID=16086
99. Degiorgio V. (1983), Physical principles of light scattering, The Application of Laser Light Scattering to the Study of Biological Motion, 9-30
100. Øgendal L. (2013), Light Scattering,
101. Raman C. V.Krishnan K. S. (1928), A New Type of Secondary Radiation, Nature, 121, 501-502 (10.1038/121501c0)
102. Bumbrah G. S.Sharma R. M. (2016), Raman spectroscopy – Basic principle, instrumentation and selected applications for the characterization of drugs of abuse, Egyptian Journal of Forensic Sciences, 6, 209-215 (https://doi.org/10.1016/j.ejfs.2015.06.001)
103. Weisstein E. W. (2004), Taylor series,
104. Hashimoto K., Badarla V. R., Kawai A.Ideguchi T. (2019), Complementary vibrational spectroscopy, Nature Communications, 10, 4411 (10.1038/s41467-019-12442-9)
105. Laserna J. (2014), An introduction to Raman spectroscopy: introduction and basic principles, Raman/Infrared Spectroscopy,

106. Graves P.Gardiner D. (1989), Practical raman spectroscopy, Springer,
107. Vo-Dinh T.Cullum B. M. (2014), Fluorescence spectroscopy for biomedical diagnostics, Biomedical photonics handbook, 508-565
108. Marcu L. (2012), Fluorescence lifetime techniques in medical applications, Annals of biomedical engineering, 40, 304-331 (10.1007/s10439-011-0495-y)
109. Leiner M. J. P., Hubmann M. R.Wolfbeis O. S. (1987), The total fluorescence of human urine, Analytica Chimica Acta, 198, 13-23 (https://doi.org/10.1016/S0003-2670(00)85002-3)
110. Kušnír J., Dubayova K., Lešková L.Lajtar M. (2005), Concentration matrices—solutions for fluorescence definition of urine, Analytical letters, 38, 1559-1567
111. Anwer A. G., Sandeep P. M., Goldys E. M.Vemulpad S. (2009), Distinctive autofluorescence of urine samples from individuals with bacteriuria compared with normals, Clinica Chimica Acta, 401, 73-75 (https://doi.org/10.1016/j.cca.2008.11.021)
112. Perinchery S. M., Kuzhiumparambil U., Vemulpad S.Goldys E. M. (2010), The potential of autofluorescence spectroscopy to detect human urinary tract infection, Talanta, 82, 912-917 (https://doi.org/10.1016/j.talanta.2010.05.049)
113. Wan Y.-Q., Tang L.-J.Tan T. (2010), Simultaneous determination of xanthopterin and isoxanthopterin in human urine by synchronous fluorescence spectroscopy, Journal of fluorescence, 20, 1191-1198
114. Rajasekaran R., Aruna P. R., Koteeswaran D., Padmanabhan L., Muthuvelu K., Rai R. R., Thamilkumar P., Murali Krishna C.Ganesan S. (2013), Characterization and Diagnosis of Cancer by Native Fluorescence Spectroscopy of Human Urine, Photochemistry and Photobiology, 89, 483-491 (10.1111/j.1751-1097.2012.01239.x)
115. Lang A., Heckl C., Vogeser M., Stauch T., Homann C., Hennig G., Sroka R.Stepp H. (2018), Rapid spectrophotometric quantification of urinary porphyrins and porphobilinogen as screening tool for attacks of acute porphyria, Journal of biomedical optics, 23, 055006
116. Masilamani V., Trinka V., Al Salhi M., Govindaraj K., Raghavan A. P. V.Antonisamy B. (2010), Cancer detection by native fluorescence of urine, Journal of biomedical optics, 15, 057003
117. Movasaghi Z., Rehman S.Rehman I. U. (2007), Raman Spectroscopy of Biological Tissues, Applied Spectroscopy Reviews, 42, 493-541 (10.1080/05704920701551530)
118. Eikje N. S., Aizawa K.Ozaki Y. (2005), Vibrational spectroscopy for molecular characterisation and diagnosis of benign, premalignant and

malignant skin tumours, Biotechnology Annual Review, 11, 191-225 (https://doi.org/10.1016/S1387-2656(05)11006-0)

119. Bispo J. A. M., Vieira E. E. d. S., Jr. L. S.Fernandes A. B. (2013), Correlating the amount of urea, creatinine, and glucose in urine from patients with diabetes mellitus and hypertension with the risk of developing renal lesions by means of Raman spectroscopy and principal component analysis, Journal of Biomedical Optics, 18, 1-8, 8
120. Kong K., Kendall C., Stone N.Notingher I. (2015), Raman spectroscopy for medical diagnostics—From in-vitro biofluid assays to in-vivo cancer detection, Advanced drug delivery reviews, 89, 121-134
121. Ramírez-Elías M. G.González F. J. (2018), Raman Spectroscopy for In Vivo Medical Diagnosis, Raman Spectroscopy, 293
122. McMurdy J. W.Berger A. J. (2003), Raman Spectroscopy-Based Creatinine Measurement in Urine Samples from a Multipatient Population, Applied Spectroscopy, 57, 522-525 (10.1366/000370203321666533)
123. Shapiro A., Gofrit O. N., Pizov G., Cohen J. K.Maier J. (2011), Raman Molecular Imaging: A Novel Spectroscopic Technique for Diagnosis of Bladder Cancer in Urine Specimens, European Urology, 59, 106-112 (https://doi.org/10.1016/j.eururo.2010.10.027)
124. Premasiri W., Chen Y., Williamson P., Bandarage D., Pyles C.Ziegler L. (2017), Rapid urinary tract infection diagnostics by surface-enhanced Raman spectroscopy (SERS): identification and antibiotic susceptibilities, Analytical and bioanalytical chemistry, 409, 3043-3054
125. Canetta E., Mazilu M., De Luca A. C., Carruthers A. E., Dholakia K., Neilson S., Sargeant H., Briscoe T., Herrington C. S.Riches A. C. (2011), Modulated Raman spectroscopy for enhanced identification of bladder tumor cells in urine samples, Journal of biomedical optics, 16, 037002
126. Goodacre R., Burton R., Kaderbhai N., Woodward A. M., Kell D. B.Rooney P. J. (1998), Rapid identification of urinary tract infection bacteria using hyperspectral whole-organism fingerprinting and artificial neural networks, Microbiology, 144, 1157-1170
127. Kloß S., Kampe B., Sachse S., Rösch P., Straube E., Pfister W., Kiehntopf M.Popp J. (2013), Culture Independent Raman Spectroscopic Identification of Urinary Tract Infection Pathogens: A Proof of Principle Study, Analytical Chemistry, 85, 9610-9616 (10.1021/ac401806f)
128. Park C., Kim K., Choi J.Park K. (2007), Classification of glucose concentration in diluted urine using the low-resolution Raman

spectroscopy and kernel optimization methods, Physiological Measurement, 28, 583-593 (10.1088/0967-3334/28/5/011)
129. Qi D.Berger A. J. (2007), Chemical concentration measurement in blood serum and urine samples using liquid-core optical fiber Raman spectroscopy, Applied optics, 46, 1726-1734
130. Wang T.-L., Chiang H. K., Lu H.-H.Peng F.-Y. (2005), Semi-quantitative surface enhanced Raman scattering spectroscopic creatinine measurement in human urine samples, Optical and quantum electronics, 37, 1415-1422
131. Bispo J. A. M., de Sousa Vieira E. E., Silveira L.Fernandes A. B. (2013), Correlating the amount of urea, creatinine, and glucose in urine from patients with diabetes mellitus and hypertension with the risk of developing renal lesions by means of Raman spectroscopy and principal component analysis, Journal of biomedical optics, 18, 087004
132. Westley C., Xu Y., Thilaganathan B., Carnell A. J., Turner N. J.Goodacre R. (2017), Absolute quantification of uric acid in human urine using surface enhanced Raman scattering with the standard addition method, Analytical chemistry, 89, 2472-2477
133. Goodall B. L., Robinson A. M.Brosseau C. L. (2013), Electrochemical-surface enhanced Raman spectroscopy (E-SERS) of uric acid: a potential rapid diagnostic method for early preeclampsia detection, Physical Chemistry Chemical Physics, 15, 1382-1388 (10.1039/C2CP42596C)
134. Huang R., Han S.Li X. S. (2013), Detection of tobacco-related biomarkers in urine samples by surface-enhanced Raman spectroscopy coupled with thin-layer chromatography, Analytical and bioanalytical chemistry, 405, 6815-6822
135. Moreira L. P., Silveira L., Pacheco M. T. T., da Silva A. G.Rocco D. D. F. M. (2018), Detecting urine metabolites related to training performance in swimming athletes by means of Raman spectroscopy and principal component analysis, Journal of Photochemistry and Photobiology B: Biology, 185, 223-234 (https://doi.org/10.1016/j.jphotobiol.2018.06.013)
136. Zou Y., Huang M., Wang K., Song B., Wang Y., Chen J., Liu X., Li X., Lin L.Huang G. (2016), Urine surface-enhanced Raman spectroscopy for non-invasive diabetic detection based on a portable Raman spectrometer, Laser Physics Letters, 13, 065604 (10.1088/1612-2011/13/6/065604)
137. Kastanos E., Kyriakides A., Hadjigeorgiou K., Pitris C. E. D. G. I. P. J.Svanberg K. (2009), UTI Diagnosis and Antibiogram Using Raman

Spectroscopy, Clinical and Biomedical Spectroscopy, 7368, 7368_0U (10.1364/ECBO.2009.7368_0U)
138. Leordean C., Canpean V.Astilean S. (2012), Surface-Enhanced Raman Scattering (SERS) Analysis of Urea Trace in Urine, Fingerprint, and Tear Samples, Spectroscopy Letters, 45, 550-555 (10.1080/00387010.2011.649439)
139. Parachalil D. R., Bruno C., Bonnier F., Blasco H., Chourpa I., Baker M. J., McIntyre J.Byrne H. J. (2019), Analysis of bodily fluids using vibrational spectroscopy: a direct comparison of Raman scattering and infrared absorption techniques for the case of glucose in blood serum, Analyst, 144, 3334-3346 (10.1039/C9AN00125E)
140. Saatkamp C. J., Almeida M. L. d., Bispo J. A. M., Pinheiro A. L. B., Fernandes A. B.Jr. L. S. (2016), Quantifying creatinine and urea in human urine through Raman spectroscopy aiming at diagnosis of kidney disease, Journal of Biomedical Optics, 21, 1-7, 7
141. Yu K.-H., Luo S.-F., Tsai W.-P.Huang Y.-Y. (2004), Intermittent elevation of serum urate and 24-hour urinary uric acid excretion, Rheumatology, 43, 1541-1545
142. Enustun B. V.Turkevich J. (1963), Coagulation of Colloidal Gold, Journal of the American Chemical Society, 85, 3317-3328 (10.1021/ja00904a001)
143. Kumar S., Gandhi K. S.Kumar R. (2007), Modeling of Formation of Gold Nanoparticles by Citrate Method, Industrial & Engineering Chemistry Research, 46, 3128-3136 (10.1021/ie060672j)
144. Agnihotri S., Mukherji S.Mukherji S. (2014), Size-controlled silver nanoparticles synthesized over the range 5–100 nm using the same protocol and their antibacterial efficacy, RSC Advances, 4, 3974-3983 (10.1039/C3RA44507K)
145. Swinehart D. F. (1962), The Beer-Lambert Law, Journal of Chemical Education, 39, 333 (10.1021/ed039p333)
146. Egerton, R. F. (2005). Physical principles of electron microscopy (Vol. 56). New York: Springer.
147. Paxton W. F. (2013), Thermionic Electron Emission Properties of Nitrogen-incorporated Polycrystalline Diamond Films
148. Campbell F. W.Gubisch R. W. (1966), Optical quality of the human eye, The Journal of physiology, 186, 558-578 (10.1113/jphysiol.1966.sp008056)
149. Artal P., Benito A.Tabernero J. (2006), The human eye is an example of robust optical design, Journal of Vision, 6, 1-1

150. Weisenburger S.Sandoghdar V. (2015), Light microscopy: an ongoing contemporary revolution, Contemporary Physics, 56, 123-143 (10.1080/00107514.2015.1026557)
151. Agocs E.Attota R. K. (2018), Enhancing optical microscopy illumination to enable quantitative imaging, Scientific Reports, 8, 4782 (10.1038/s41598-018-22561-w)
152. Heintzmann R.Ficz G. (2006), Breaking the resolution limit in light microscopy, Briefings in Functional Genomics, 5, 289-301 (10.1093/bfgp/ell036)
153. Pospíšil J., Fliegel K., Švihlík J.Klíma M. (2018), Comparison of resolution estimation methods in optical microscopy, SPIE Optical Engineering + Applications, 10752,
154. Chen X., Zheng B.Liu H. (2011), Optical and digital microscopic imaging techniques and applications in pathology, Analytical cellular pathology (Amsterdam), 34, 5-18 (10.3233/ACP-2011-0006)
155. Meilan P. F.Garavaglia M. (1997), Rayleigh resolution criterion for light sources of different spectral composition, Brazilian Journal of Physics, 27, 638-643
156. Ram S., Ward E. S.Ober R. J. (2006), Beyond Rayleigh's criterion: A resolution measure with application to single-molecule microscopy, Proceedings of the National Academy of Sciences of the United States of America, 103, 4457 (10.1073/pnas.0508047103)
157. Latychevskaia T. (2019), Lateral and axial resolution criteria in incoherent and coherent optics and holography, near-and far-field regimes, Applied optics, 58, 3597-3603
158. Henshaw D. (1958), Atomic distribution in liquid and solid neon and solid argon by neutron diffraction, Physical Review, 111, 1470
159. Padmavathi D. A. (2011), Potential energy curves & material properties, Materials Sciences and Applications, 2, 97
160. Logiurato F. (2012), Relativistic derivations of de Broglie and Planck-Einstein equations, arXiv preprint arXiv:1208.0119,
161. Kastner R. E. (2013), De Broglie waves as the “bridge of becoming” between quantum theory and relativity, Foundations of science, 18, 1-9
162. Deegan R. D., Bakajin O., Dupont T. F., Huber G., Nagel S. R.Witten T. A. (1997), Capillary flow as the cause of ring stains from dried liquid drops, Nature, 389, 827-829 (10.1038/39827)
163. Tarasevich Y. Y. (2005), Simple analytical model of capillary flow in an evaporating sessile drop, Physical Review E, 71, 027301

164. Bouchenna C., Aitsaada M., Chikh S.Tadrist L. (2017), Fluid flow inside and outside an evaporating sessile drop, Journal of Physics: Conference Series, 925, 012006
165. Malinowski R., Volpe G., Parkin I. P.Volpe G. (2018), Dynamic control of particle deposition in evaporating droplets by an external point source of vapor, The journal of physical chemistry letters, 9, 659-664
166. Mampallil D. (2014), Some physics inside drying droplets, Resonance, 19, 123-134
167. Brutin D.Starov V. (2018), Recent advances in droplet wetting and evaporation, Chemical Society Reviews, 47, 558-585
168. Tadmor R. (2009), Marangoni flow revisited, Journal of Colloid and Interface Science, 332, 451-454 (https://doi.org/10.1016/j.jcis.2008.12.047)
169. Kitahata H.Yoshinaga N. (2018), Effective diffusion coefficient including the Marangoni effect, The Journal of Chemical Physics, 148, 134906 (10.1063/1.5021502)
170. Suciu D. G., Smigelschi O.Ruckenstein E. (1967), Some experiments on the Marangoni effect, AIChE Journal, 13, 1120-1124 (10.1002/aic.690130616)
171. Washburn E. W. (1921), The Dynamics of Capillary Flow, Physical Review, 17, 273-283 (10.1103/PhysRev.17.273)
172. Stiles, P. L., Dieringer, J. A., Shah, N. C., & Van Duyne, R. P. (2008). Surface-enhanced Raman spectroscopy. Annu. Rev. Anal. Chem., 1, 601-626.
173. Zong, C., Xu, M., Xu, L. J., Wei, T., Ma, X., Zheng, X. S., ... & Ren, B. (2018). Surface-enhanced Raman spectroscopy for bioanalysis: reliability and challenges. Chemical reviews, 118(10), 4946-4980.
174. Liu, Y., Zhou, H., Hu, Z., Yu, G., Yang, D., & Zhao, J. (2017). Label and label-free based surface-enhanced Raman scattering for pathogen bacteria detection: A review. Biosensors and Bioelectronics, 94, 131-140.
175. Willets, K. A., & Van Duyne, R. P. (2007). Localized surface plasmon resonance spectroscopy and sensing. Annu. Rev. Phys. Chem., 58, 267-297.
176. Ashkin A. (1992), Forces of a single-beam gradient laser trap on a dielectric sphere in the ray optics regime, Biophysical journal, 61, 569-582

177. Ashkin A., Dziedzic J. M., Bjorkholm J.Chu S. (1986), Observation of a single-beam gradient force optical trap for dielectric particles, Optics letters, 11, 288-290
178. Ashkin A. (1997), Forces of a single-beam gradient laser trap on a dielectric sphere in the ray optics regime, Methods in cell biology, 55, 1-27
179. Ashkin A. (1970), Acceleration and trapping of particles by radiation pressure, Physical review letters, 24, 156
180. Svoboda K.Block S. M. (1994), Optical trapping of metallic Rayleigh particles, Optics letters, 19, 930-932
181. Lehmuskero A., Johansson P., Rubinsztein-Dunlop H., Tong L.Käll M. (2015), Laser Trapping of Colloidal Metal Nanoparticles, ACS Nano, 9, 3453-3469 (10.1021/acsnano.5b00286)
182. Saija R., Denti P., Borghese F., Marago O. M.Iati M. A. (2009), Optical trapping calculations for metal nanoparticles. Comparison with experimental data for Au and Ag spheres, Optics express, 17, 10231-10241
183. Savitzky A.Golay M. J. (1964), Smoothing and differentiation of data by simplified least squares procedures, Analytical chemistry, 36, 1627-1639
184. Krishna H., Majumder S. K.Gupta P. K. (2012), Range-independent background subtraction algorithm for recovery of Raman spectra of biological tissue, Journal of Raman Spectroscopy, 43, 1884-1894
185. Tobias R. D. (1995), An introduction to partial least squares regression, Proceedings of the twentieth annual SAS users group international conference, 1250-1257
186. Ng K. S. (2013), A simple explanation of partial least squares, The Australian National University, Canberra,
187. Geladi P.Kowalski B. R. (1986), Partial least-squares regression: a tutorial, Analytica chimica acta, 185, 1-17
188. Barker M.Rayens W. (2003), Partial least squares for discrimination, Journal of Chemometrics: A Journal of the Chemometrics Society, 17, 166-173
189. Chai T.Draxler R. R. (2014), Root mean square error (RMSE) or mean absolute error (MAE)?–Arguments against avoiding RMSE in the literature, Geoscientific model development, 7, 1247-1250
190. De Myttenaere A., Golden B., Le Grand B.Rossi F. (2016), Mean absolute percentage error for regression models, Neurocomputing, 192, 38-48

191. Hosmer D. W.Lemeshow S. (1992), Confidence interval estimation of interaction, Epidemiology (Cambridge, Mass.), 3, 452-456
192. Brookmeyer R.Crowley J. (1982), A confidence interval for the median survival time, Biometrics, 29-41
193. Shi H., Ma Y.Ma Y. (1995), A simple and fast method to determine and quantify urinary creatinine, Analytica Chimica Acta, 312, 79-83 (https://doi.org/10.1016/0003-2670(95)00208-H)
194. Heise H. M., Voigt G., Lampen P., Küpper L., Rudloff S.Werner G. (2001), Multivariate Calibration for the Determination of Analytes in Urine Using Mid-Infrared Attenuated Total Reflection Spectroscopy, Applied Spectroscopy, 55, 434-443
195. Delanghe J. R.Speeckaert M. M. (2011), Creatinine determination according to Jaffe—what does it stand for?, Nephrology Dialysis Transplantation Plus, 4, 83-86
196. Kalantari K.Bolton W. K. (2013), A good reason to measure 24-hour urine creatinine excretion, but not to assess kidney function, Clinical journal of the American Society of Nephrology : CJASN, 8, 1847-1849 (10.2215/CJN.09770913)
197. Carter C. E., Katz R., Kramer H., de Boer I. H., Kestenbaum B. R., Peralta C. A., Siscovick D., Sarnak M. J., Levey A. S., Inker L. A. S., Allison M. A., Criqui M. H., Shlipak M. G.Ix J. H. (2013), Influence of urine creatinine concentrations on the relation of albumin-creatinine ratio with cardiovascular disease events: the Multi-Ethnic Study of Atherosclerosis (MESA), American journal of kidney diseases : the official journal of the National Kidney Foundation, 62, 722-729 (10.1053/j.ajkd.2013.05.010)
198. Miller T. R., Anderson R. J., LINAS S. L., Henrich W. L., BERNS A. S., GABOW P. A.SCHRIER R. W. (1978), Urinary diagnostic indices in acute renal failure: a prospective study, Annals of internal medicine, 89, 47-50
199. Han W., Waikar S., Johnson A., Betensky R., Dent C., Devarajan P.Bonventre J. (2008), Urinary biomarkers in the early diagnosis of acute kidney injury, Kidney international, 73, 863-869
200. Schrier R. W., Wang W., Poole B.Mitra A. (2004), Acute renal failure: definitions, diagnosis, pathogenesis, and therapy, The Journal of clinical investigation, 114, 5-14
201. Heron E., Chatellier G., Billaud E., Foos E.Plouin P.-F. (1996), The urinary metanephrine-to-creatinine ratio for the diagnosis of pheochromocytoma, Annals of internal medicine, 125, 300-303

202. McMurdy III J. W.Berger A. J. (2003), Raman spectroscopy-based creatinine measurement in urine samples from a multipatient population, Applied spectroscopy, 57, 522-525
203. Gangopadhyay D., Sharma P., Nandi R., Das M., Ghosh S.Singh R. K. (2016), In vitro concentration dependent detection of creatinine: a surface enhanced Raman scattering and fluorescence study, RSC Advances, 6, 112562-112567 (10.1039/C6RA22886K)
204. Naglic P. (2012), Raman spectroscopy for medical diagnostics, University of Ljubljana,
205. Pence I.Mahadevan-Jansen A. (2016), Clinical instrumentation and applications of Raman spectroscopy, Chemical Society Reviews, 45, 1958-1979
206. Krafft C.Popp J. (2015), The many facets of Raman spectroscopy for biomedical analysis, Analytical and bioanalytical chemistry, 407, 699-717
207. Li M., Du Y., Zhao F., Zeng J., Mohan C.Shih W.-C. (2015), Reagent- and separation-free measurements of urine creatinine concentration using stamping surface enhanced Raman scattering (S-SERS), Biomedical optics express, 6, 849-858
208. Wang H., Malvadkar N., Koytek S., Bylander J., Reeves W. B.Demirel M. C. (2010), Quantitative analysis of creatinine in urine by metalized nanostructured parylene, Journal of biomedical optics, 15, 027004
209. Wang T. L., Chiang H.-h. K.Lu H.-h. (2005), SERS quantitative urine creatinine measurement of human subject, Plasmonics in Biology and Medicine II, 5703, 17-24
210. Zhang D., Xie Y., Mrozek M. F., Ortiz C., Davisson V. J.Ben-Amotz D. (2003), Raman detection of proteomic analytes, Analytical chemistry, 75, 5703-5709
211. Pazderka T.Kopecký Jr V. (2017), Drop coating deposition Raman spectroscopy of proteinogenic amino acids compared with their solution and crystalline state, Spectrochimica Acta Part A: Molecular and Biomolecular Spectroscopy, 185, 207-216
212. Barman I., Dingari N. C., Kang J. W., Horowitz G. L., Dasari R. R.Feld M. S. (2012), Raman spectroscopy-based sensitive and specific detection of glycated hemoglobin, Analytical chemistry, 84, 2474-2482
213. Kočišová E., Antalík A.Procházka M. (2013), Drop coating deposition Raman spectroscopy of liposomes: role of cholesterol, Chemistry and physics of lipids, 172, 1-5
214. Filik J.Stone N. (2009), Investigation into the protein composition of human tear fluid using centrifugal filters and drop coating deposition

Raman spectroscopy, Journal of Raman Spectroscopy: An International Journal for Original Work in all Aspects of Raman Spectroscopy, Including Higher Order Processes, and also Brillouin and Rayleigh Scattering, 40, 218-224

215. Ortiz C., Zhang D., Xie Y., Davisson V. J.Ben-Amotz D. (2004), Identification of insulin variants using Raman spectroscopy, Analytical biochemistry, 332, 245-252
216. Hu P., Zheng X. S., Zong C., Li M. H., Zhang L. Y., Li W.Ren B. (2014), Drop-coating deposition and surface-enhanced Raman spectroscopies (DCDRS and SERS) provide complementary information of whole human tears, Journal of Raman spectroscopy, 45, 565-573
217. Huang Z., Wang J., Lin J., Chen X., Sun Y., Cao G., Lin J., Lei J., Lin H.Chen R. (2014), Drop coating deposition Raman spectroscopy as a potential tool for identification and determination of fructose in seminal plasma, Journal of Raman Spectroscopy, 45, 879-883
218. Ryzhikova E., Kazakov O., Halamkova L., Celmins D., Malone P., Molho E., Zimmerman E. A.Lednev I. K. (2015), Raman spectroscopy of blood serum for Alzheimer's disease diagnostics: specificity relative to other types of dementia, Journal of biophotonics, 8, 584-596
219. Esmonde-White K. A., Mandair G. S., Raaii F., Jacobson J. A., Miller B. S., Urquhart A. G., Roessler B. J.Morris M. D. (2009), Raman spectroscopy of synovial fluid as a tool for diagnosing osteoarthritis, Journal of biomedical optics, 14, 034013
220. Klener J., Hofbauerová K., Bartoš A., Říčný J., Řípová D.Kopecký V. (2014), Instability of cerebrospinal fluid after delayed storage and repeated freezing: a holistic study by drop coating deposition Raman spectroscopy, Clinical chemistry and laboratory medicine, 52, 657-664
221. Weon B. M.Je J. H. (2010), Capillary force repels coffee-ring effect, Physical Review E, 82, 015305
222. Deegan R. D., Bakajin O., Dupont T. F., Huber G., Nagel S. R.Witten T. A. (1997), Capillary flow as the cause of ring stains from dried liquid drops, Nature, 389, 827
223. Shaw M., Bella A.Ryadnov M. G. (2017), CREIM: Coffee ring effect imaging model for monitoring protein self-assembly in situ, The journal of physical chemistry letters, 8, 4846-4851
224. Myers V. C.Fine M. S. (1919), Comparative distribution of urea, creatinine, uric acid, and sugar in the blood and spinal fluid, Journal of Biological Chemistry, 37, 239-244

225. Zhang D., Mrozek M. F., Xie Y.Ben-Amotz D. (2004), Chemical segregation and reduction of Raman background interference using drop coating deposition, Applied spectroscopy, 58, 929-933
226. Cui L., Butler H. J., Martin-Hirsch P. L.Martin F. L. (2016), Aluminium foil as a potential substrate for ATR-FTIR, transflection FTIR or Raman spectrochemical analysis of biological specimens, Analytical methods, 8, 481-487
227. Kneipp K., Kneipp H., Deinum G., Itzkan I., Dasari R. R.Feld M. S. (1998), Single-molecule detection of a cyanine dye in silver colloidal solution using near-infrared surface-enhanced Raman scattering, Applied spectroscopy, 52, 175-178
228. Chen Q., Fu Y., Zhang W., Ye S., Zhang H., Xie F., Gong L., Wei Z., Jin H.Chen J. (2017), Highly sensitive detection of glucose: A quantitative approach employing nanorods assembled plasmonic substrate, Talanta, 165, 516-521
229. Yu B., Cao C., Li P., Mao M., Xie Q.Yang L. (2018), Sensitive and simple determination of zwitterionic morphine in human urine based on liquid-liquid micro-extraction coupled with surface-enhanced Raman spectroscopy, Talanta, 186, 427-432
230. Meng J., Tang X., Zhou B., Xie Q.Yang L. (2017), Designing of ordered two-dimensional gold nanoparticles film for cocaine detection in human urine using surface-enhanced Raman spectroscopy, Talanta, 164, 693-699
231. Lu Y., Wu C., You R., Wu Y., Shen H., Zhu L.Feng S. (2018), Superhydrophobic silver film as a SERS substrate for the detection of uric acid and creatinine, Biomedical optics express, 9, 4988-4997
232. Wang Y., Chen J., Wu Y., Chen Y., Pan J., Lei J., Chen Y., Sun L., Feng S.Chen R. (2012), Surface-enhanced Raman spectroscopy of creatinine in silver colloid, Tenth International Conference on Photonics and Imaging in Biology and Medicine (PIBM 2011), 8329, 83290K
233. Dutta S. B., Shrivastava R., Krishna H., Khan K. M., Gupta S.Majumder S. K. (2019), Nanotrap-Enhanced Raman Spectroscopy: An Efficient Technique for Trace Detection of Bioanalytes, Analytical chemistry, 91, 3555-3560
234. Liu Z., Yang Z., Peng B., Cao C., Zhang C., You H., Xiong Q., Li Z.Fang J. (2014), Highly Sensitive, Uniform, and Reproducible Surface-Enhanced Raman Spectroscopy from Hollow Au-Ag Alloy Nanourchins, Advanced Materials, 26, 2431-2439

235. Khan K. M., Krishna H., Majumder S. K.Gupta P. K. (2015), Detection of urea adulteration in milk using near-infrared Raman spectroscopy, Food analytical methods, 8, 93-102
236. Dou X., Yamaguchi Y., Yamamoto H., Doi S.Ozaki Y. (1996), Quantitative analysis of metabolites in urine using a highly precise, compact near-infrared Raman spectrometer, Vibrational spectroscopy, 13, 83-89
237. Kodati V. R., Tu A. T.Turumin J. L. (1990), Raman spectroscopic identification of uric-acid-type kidney stone, Applied spectroscopy, 44, 1134-1136
238. Curran D. J., Rubin L.Towler M. R. (2015), Raman spectroscopy applied to the noninvasive detection of monosodium urate crystal deposits, Clinical Medicine Insights: Arthritis and Musculoskeletal Disorders, 8, CMAMD. S29061
239. Le Ru E.Etchegoin P. (2008), Principles of Surface-Enhanced Raman Spectroscopy: and related plasmonic effects,
240. Moskovits M. (1985), Surface-enhanced spectroscopy, Reviews of modern physics, 57, 783
241. Premasiri W., Lee J.Ziegler L. (2012), Surface-enhanced Raman scattering of whole human blood, blood plasma, and red blood cells: cellular processes and bioanalytical sensing, The Journal of Physical Chemistry B, 116, 9376-9386
242. Bonifacio A., Cervo S.Sergo V. (2015), Label-free surface-enhanced Raman spectroscopy of biofluids: fundamental aspects and diagnostic applications, Analytical and bioanalytical chemistry, 407, 8265-8277
243. Huh Y. S., Chung A. J.Erickson D. (2009), Surface enhanced Raman spectroscopy and its application to molecular and cellular analysis, Microfluidics and nanofluidics, 6, 285
244. Oh Y. J.Jeong K. H. (2012), Glass Nanopillar Arrays with Nanogap-Rich Silver Nanoislands for Highly Intense Surface Enhanced Raman Scattering, Advanced Materials, 24, 2234-2237
245. Anker J. N., Hall W. P., Lyandres O., Shah N. C., Zhao J.Van Duyne R. P. (2010), Biosensing with plasmonic nanosensors, Nanoscience and Technology: A Collection of Reviews from Nature Journals, 308-319
246. Fu Q., Zhan Z., Dou J., Zheng X., Xu R., Wu M.Lei Y. (2015), Highly reproducible and sensitive SERS substrates with Ag inter-nanoparticle gaps of 5 nm fabricated by ultrathin aluminum mask technique, ACS applied materials & interfaces, 7, 13322-13328

247. Cho W. J., Kim Y.Kim J. K. (2011), Ultrahigh-density array of silver nanoclusters for SERS substrate with high sensitivity and excellent reproducibility, ACS nano, 6, 249-255
248. Strobbia P., Mayer A.Cullum B. M. (2017), Improving Sensitivity and Reproducibility of SERS Sensing in Microenvironments Using Individual, Optically Trapped Surface-Enhanced Raman Spectroscopy (SERS) Probes, Applied spectroscopy, 71, 279-287
249. Hong S., Shim O., Kwon H.Choi Y. (2016), Autoenhanced Raman spectroscopy via plasmonic trapping for molecular sensing, Analytical chemistry, 88, 7633-7638
250. Maragò O. M., Jones P. H., Gucciardi P. G., Volpe G.Ferrari A. C. (2013), Optical trapping and manipulation of nanostructures, Nature nanotechnology, 8, 807
251. Shoji T.Tsuboi Y. (2014), Plasmonic optical tweezers toward molecular manipulation: tailoring plasmonic nanostructure, light source, and resonant trapping, The journal of physical chemistry letters, 5, 2957-2967
252. Kosiorek A., Kandulski W., Chudzinski P., Kempa K.Giersig M. (2004), Shadow nanosphere lithography: simulation and experiment, Nano Letters, 4, 1359-1363
253. Barik A., Chen X.Oh S.-H. (2016), Ultralow-power electronic trapping of nanoparticles with sub-10 nm gold nanogap electrodes, Nano letters, 16, 6317-6324
254. Yang S., Dai X., Stogin B. B.Wong T.-S. (2016), Ultrasensitive surface-enhanced Raman scattering detection in common fluids, Proceedings of the National Academy of Sciences, 113, 268-273
255. Enustun B.Turkevich J. (1963), Coagulation of colloidal gold, Journal of the American chemical society, 85, 3317-3328
256. Swinehart D. (1962), The beer-lambert law, Journal of chemical education, 39, 333
257. Shur V. Y., Bykov D., Mingaliev E., Tyurnina A., Burban G., Kadushnikov R.Mizgulin V. (2015), Coffee ring effect during drying of colloid drop: experiment and computer simulation, Ferroelectrics, 476, 47-53
258. Tian F., Bonnier F., Casey A., Shanahan A. E.Byrne H. J. (2014), Surface enhanced Raman scattering with gold nanoparticles: effect of particle shape, Analytical Methods, 6, 9116-9123
259. Yockell-Lelièvre H., Lussier F.Masson J.-F. (2015), Influence of the particle shape and density of self-assembled gold nanoparticle sensors

on LSPR and SERS, The Journal of Physical Chemistry C, 119, 28577-28585

260. Hong S.Li X. (2013), Optimal size of gold nanoparticles for surface-enhanced Raman spectroscopy under different conditions, Journal of nanomaterials, 2013, 49
261. Ameer F. S., Pittman C. U.Zhang D. (2013), Quantification of Resonance Raman Enhancement Factors for Rhodamine 6G (R6G) in Water and on Gold and Silver Nanoparticles: Implications for Single-Molecule R6G SERS, The Journal of Physical Chemistry C, 117, 27096-27104 (10.1021/jp4105932)
262. Higgins C. (2016), Urea and the clinical value of measuring blood urea concentration,
263. Maiuolo J., Oppedisano F., Gratteri S., Muscoli C.Mollace V. (2016), Regulation of uric acid metabolism and excretion, International journal of cardiology, 213, 8-14
264. Chaudhary K., Malhotra K., Sowers J.Aroor A. (2013), Uric acid-key ingredient in the recipe for cardiorenal metabolic syndrome, Cardiorenal medicine, 3, 208-220
265. Wells H. G. (1916), The accumulation of uric acid in the tissues during suppression of urine, Studies from the Otho SA Sprague Memorial Institute: Collected Reprints, 4, 767
266. Wang Y., Deng X., Xu Y., Ji L.Zhang Z. (2018), Detection of uric acid crystal deposition by ultrasonography and dual-energy computed tomography: A cross-sectional study in patients with clinically diagnosed gout, Medicine, 97, e12834-e12834 (10.1097/MD.0000000000012834)
267. Giordano C., Karasik O., King-Morris K.Asmar A. (2015), Uric acid as a marker of kidney disease: review of the current literature, Disease markers, 2015,
268. Weiner D. E., Tighiouart H., Elsayed E. F., Griffith J. L., Salem D. N.Levey A. S. (2008), Uric acid and incident kidney disease in the community, Journal of the American Society of Nephrology, 19, 1204-1211
269. Chonchol M., Shlipak M. G., Katz R., Sarnak M. J., Newman A. B., Siscovick D. S., Kestenbaum B., Carney J. K.Fried L. F. (2007), Relationship of uric acid with progression of kidney disease, American Journal of Kidney Diseases, 50, 239-247
270. Culleton B. F., Larson M. G., Kannel W. B.Levy D. (1999), Serum Uric Acid and Risk for Cardiovascular Disease and Death: The

Framingham Heart Study, Annals of Internal Medicine, 131, 7-13 (10.7326/0003-4819-131-1-199907060-00003)
271. Qin L., Yang Z., Gu H., Lu S., Shi Q., Xing Y., Li X., Li R., Ning G.Su Q. (2014), Association between serum uric acid levels and cardiovascular disease in middle-aged and elderly Chinese individuals, BMC Cardiovascular Disorders, 14, 26 (10.1186/1471-2261-14-26)
272. Martínez-Quintana E., Tugores A.Rodríguez-González F. (2016), Serum uric acid levels and cardiovascular disease: the Gordian knot, Journal of thoracic disease, 8, E1462-E1466 (10.21037/jtd.2016.11.39)
273. Niskanen L. K., Laaksonen D. E., Nyyssönen K., Alfthan G., Lakka H.-M., Lakka T. A.Salonen J. T. (2004), Uric Acid Level as a Risk Factor for Cardiovascular and All-Cause Mortality in Middle-aged Men: A Prospective Cohort Study, JAMA Internal Medicine, 164, 1546-1551 (10.1001/archinte.164.14.1546)
274. Muiesan M. L., Agabiti-Rosei C., Paini A.Salvetti M. (2016), Uric Acid and Cardiovascular Disease: An Update, European cardiology, 11, 54-59 (10.15420/ecr.2016:4:2)
275. Desideri G., Castaldo G., Lombardi A., Mussap M., Testa A., Pontremoli R., Punzi L.Borghi C. (2014), Is it time to revise the normal range of serum uric acid levels, Eur Rev Med Pharmacol Sci, 18, 1295-306
276. Jin M., Yang F., Yang I., Yin Y., Luo J. J., Wang H.Yang X.-F. (2012), Uric acid, hyperuricemia and vascular diseases, Frontiers in bioscience: a journal and virtual library, 17, 656
277. Becker M. A. (2012), Asymptomatic hyperuricemia, UpToDate Inc [online]. Available at: http://www. uptodate. com/contents/asymptomatichyperuricemia. Accessed October, 1,
278. Torres R. J.Puig J. G. (2007), Hypoxanthine-guanine phosophoribosyltransferase (HPRT) deficiency: Lesch-Nyhan syndrome, Orphanet journal of rare diseases, 2, 48
279. Jinnah H., Ceballos-Picot I., Torres R. J., Visser J. E., Schretlen D. J., Verdu A., Larovere L. E., Chen C.-J., Cossu A.Wu C.-H. (2010), Attenuated variants of Lesch-Nyhan disease, Brain, 133, 671-689
280. Persky V. W., Dyer A. R., Idris-Soven E., Stamler J., Shekelle R., Schoenberger J., Berkson D.Lindberg H. (1979), Uric acid: a risk factor for coronary heart disease?, Circulation, 59, 969-977
281. Reunanen A., Takkunen H., Knekt P.Aromaa A. (1982), Hyperuricemia as a risk factor for cardiovascular mortality, Acta Medica Scandinavica, 212, 49-59

282. Levine W., Dyer A. R., Shekelle R. B., Schoenberger J. A.Stamler J. (1989), Serum uric acid and 11.5-year mortality of middle-aged women: findings of the Chicago Heart Association Detection Project in Industry, Journal of clinical epidemiology, 42, 257-267
283. Olivieri A. C., Arancibia J. A., Muñoz de la Peña A., Duran-Meras I.Espinosa Mansilla A. (2004), Second-Order Advantage Achieved with Four-Way Fluorescence Excitation− Emission− Kinetic Data Processed by Parallel Factor Analysis and Trilinear Least-Squares. Determination of Methotrexate and Leucovorin in Human Urine, Analytical chemistry, 76, 5657-5666
284. Premasiri W. R., Clarke R. H.Womble M. E. (2001), Urine analysis by laser Raman spectroscopy, Lasers in Surgery and Medicine: The Official Journal of the American Society for Laser Medicine and Surgery, 28, 330-334
285. Cui S., Zhang S.Yue S. (2018), Raman spectroscopy and imaging for cancer diagnosis, Journal of healthcare engineering, 2018,
286. Alfano R., Tang G., Pradhan A., Lam W., Choy D.Opher E. (1987), Fluorescence spectra from cancerous and normal human breast and lung tissues, IEEE Journal of Quantum Electronics, 23, 1806-1811
287. Alfano R., Pradhan A., Tang G.Wahl S. (1989), Optical spectroscopic diagnosis of cancer and normal breast tissues, JOSA B, 6, 1015-1023
288. Evers D., Hendriks B., Lucassen G.Ruers T. (2012), Optical spectroscopy: current advances and future applications in cancer diagnostics and therapy, Future oncology, 8, 307-320
289. Liu Q. (2011), Role of optical spectroscopy using endogenous contrasts in clinical cancer diagnosis, World journal of clinical oncology, 2, 50
290. Leiner M. J., Hubmann M. R.Wolfbeis O. S. (1987), The total fluorescence of human urine, Analytica Chimica Acta, 198, 13-23
291. Dubayová K. n., Kušnír J.Podracká L. u. (2003), Diagnostic monitoring of urine by means of synchronous fluorescence spectrum, Journal of biochemical and biophysical methods, 55, 111-119
292. Anwer A. G., Sandeep P. M., Goldys E. M.Vemulpad S. (2009), Distinctive autofluorescence of urine samples from individuals with bacteriuria compared with normals, Clinica chimica acta, 401, 73-75
293. Kessler M. A., Meinitzer A., Petek W.Wolfbeis O. S. (1997), Microalbuminuria and borderline-increased albumin excretion determined with a centrifugal analyzer and the Albumin Blue 580 fluorescence assay, Clinical chemistry, 43, 996-1002
294. Laiwattanapaisal W., Saythanu P., Nubtueboon P., Tencomnao T.Santiyanont R. (2008), A High-throughput Nonimmunological

Method for Determination of Microalbuminuria Based on Utilization of Albumin Blue 580, Laboratory Medicine, 39, 727-729

295. Pachaiappan R., Prakasarao A., Kesavan A.Singaravelu G. (2017), Native fluorescence spectroscopy: An optical tool in delineating oral cancer patients from normal subjects and diabetic patients using urine, 2017 Trends in Industrial Measurement and Automation (TIMA), 1-4
296. Dutta S. B., Krishna H., Gupta S.Majumder S. K. (2019), Fluorescence photo-bleaching of urine and its applicability in oral cancer diagnosis, Photodiagnosis and Photodynamic Therapy, 28, 18-24 (https://doi.org/10.1016/j.pdpdt.2019.08.007)
297. Cheng S., Hwang D. Y., Cuenca R., Malik B., Maitland K. C., Wright J., Cheng Y. L.Jo J. A. (2016), In Vivo Detection of Oral Epithelial Pre-Cancer and Cancer by Endogenous Fluorescence Lifetime Imaging (FLIM) Endoscopy, Cancer Imaging and Therapy, CTh4A. 3
298. Kollarik B., Zvarik M., Bujdak P., Weibl P., Rybar L., Sikurova L.Hunakova L. (2018), Urinary fluorescence analysis in diagnosis of bladder cancer, Neoplasma, 65, 234-241
299. Goodison S., Rosser C. J.Urquidi V. (2013), Bladder cancer detection and monitoring: assessment of urine-and blood-based marker tests, Molecular diagnosis & therapy, 17, 71-84
300. Kollarik B., Zvarik M., Bujdak P., Weibl P., Rybar L., Sikurová L.Hunáková L. (2018), Urinary fluorescence analysis in diagnosis of bladder cancer, Neoplasma, 65, 234-241 (10.4149/neo_2018_170610N420)
301. Masilamani V., Vijmasi T., AlSalhi M., Govindarajan K., VijayaRaghavan A. P.Rai R. R. (2011), Detection of cervical cancer by fluorescence emission and stokes' shift spectra of blood and urine, SPIE BiOS, 7895,
302. Martinicky D., Zvarik M., Sikurova L., Lajdova I.Hunakova L. (2015), Fluorescence analysis of urine and its potential for ovarian cancer screening, Neoplasma, 62, 500-506
303. Zvarik M., Martinicky D., Hunakova L., Lajdova I.Sikurova L. (2013), Fluorescence characteristics of human urine from normal individuals and ovarian cancer patients, Neoplasma, 60, 533-537
304. Elumalai B., Prakasarao A., Ganesan B., Dornadula K.Ganesan S. (2015), Raman spectroscopic characterization of urine of normal and oral cancer subjects, Journal of Raman Spectroscopy, 46, 84-93
305. Yang H., Zhao C., Li R., Shen C., Cai X., Sun L., Luo C.Yin Y. (2018), Noninvasive and prospective diagnosis of coronary heart disease with

urine using surface-enhanced Raman spectroscopy, Analyst, 143, 2235-2242

306. Chisanga M., Muhamadali H., Ellis D. I.Goodacre R. (2019), Enhancing disease diagnosis: biomedical applications of surface-enhanced Raman scattering, Applied Sciences, 9, 1163
307. Saatkamp C. J., de Almeida M. L., Bispo J. A. M., Pinheiro A. L. B., Fernandes A. B.Silveira L. (2016), Quantifying creatinine and urea in human urine through Raman spectroscopy aiming at diagnosis of kidney disease, Journal of biomedical optics, 21, 037001
308. Rajasekaran R., Aruna P. R., Koteeswaran D., Bharanidharan G., Baludavid M.Ganesan S. (2014), Steady-state and time-resolved fluorescence spectroscopic characterization of urine of healthy subjects and cervical cancer patients, Journal of biomedical optics, 19, 037003
309. Atif M., AlSalhi M., Devanesan S., Masilamani V., Farhat K.Rabah D. (2018), A study for the detection of kidney cancer using fluorescence emission spectra and synchronous fluorescence excitation spectra of blood and urine, Photodiagnosis and photodynamic therapy, 23, 40-44
310. Keuleers R., Desseyn H., Rousseau B.Van Alsenoy C. (1999), Vibrational analysis of urea, The Journal of Physical Chemistry A, 103, 4621-4630
311. AlSalhi M., Mehmadi A. A., Abdo A. A., Prasad S.Masilamani V. (2012), Diagnosis of liver cancer and cirrhosis by the fluorescence spectra of blood and urine, Technology in cancer research & treatment, 11, 345-351
312. AlSalhi M. S., Al Mehmadi A. M., Abdoo A.Masilamani V. (2012), Liver cancer diagnosis by fluorescence spectra of blood and urine, Tenth International Conference on Photonics and Imaging in Biology and Medicine (PIBM 2011), 8329, 83290X
313. Datta P.Kibler D. (1997), Symbolic nearest mean classifiers, AAAI/IAAI, 82-87
314. Majumder S. K., Ghosh N.Gupta P. K. (2005), Relevance vector machine for optical diagnosis of cancer, Lasers in Surgery and Medicine: The Official Journal of the American Society for Laser Medicine and Surgery, 36, 323-333
315. Majumder S., Ghosh N.Gupta P. K. (2005), Support vector machine for optical diagnosis of cancer, Journal of Biomedical Optics, 10, 024034
316. Berglund A. (2004), Nonexponential statistics of fluorescence photobleaching, The Journal of chemical physics, 121, 2899-903 (10.1063/1.1773162)

317. Gupta S., Goswami P., Agarwal A.Pradhan A. (2004), Experimental and theoretical investigation of fluorescence photobleaching and recovery in human breast tissue and tissue phantoms, Applied optics, 43, 1044-1052
318. Adkins L. C.Carter Hill R. (1990), An improved confidence ellipsoid for the linear regression model, Journal of statistical computation and simulation, 36, 9-18
319. Inaguma M.Hashimoto K. (1999), Porphyrin-like fluorescence in oral cancer: In vivo fluorescence spectral characterization of lesions by use of a near-ultraviolet excited autofluorescence diagnosis system and separation of fluorescent extracts by capillary electrophoresis, Cancer: Interdisciplinary International Journal of the American Cancer Society, 86, 2201-2211
320. Al-Salhi M., Masilamani V., Vijmasi T., Al-Nachawati H.VijayaRaghavan A. (2011), Lung cancer detection by native fluorescence spectra of body fluids—a preliminary study, Journal of fluorescence, 21, 637-645
321. Rajasekaran R., Aruna P., Koteeswaran D., Baludavid M.Ganesan S. (2014), Synchronous luminescence spectroscopic characterization of urine of normal subjects and cancer patients, Journal of fluorescence, 24, 1199-1205
322. Song L., Hennink E., Young I. T.Tanke H. J. (1995), Photobleaching kinetics of fluorescein in quantitative fluorescence microscopy, Biophysical journal, 68, 2588-2600
323. Benson D. M., Bryan J., Plant A. L., Gotto A. M.Smith L. C. (1985), Digital imaging fluorescence microscopy: spatial heterogeneity of photobleaching rate constants in individual cells, The Journal of cell biology, 100, 1309-1323
324. Wüstner D., Christensen T., Solanko L.Sage D. (2014), Photobleaching kinetics and time-integrated emission of fluorescent probes in cellular membranes, Molecules, 19, 11096-11130
325. Majumder S. K., Gebhart S., Johnson M. D., Thompson R., Lin W.-C.Mahadevan-Jansen A. (2007), A Probability-Based Spectroscopic Diagnostic Algorithm for Simultaneous Discrimination of Brain Tumor and Tumor Margins from Normal Brain Tissue, Applied Spectroscopy, 61, 548-557
326. Krishnapuram B., Carin L., Figueiredo M. A.Hartemink A. J. (2005), Sparse multinomial logistic regression: Fast algorithms and generalization bounds, IEEE transactions on pattern analysis and machine intelligence, 27, 957-968

327. Majumder S. K., Keller M. D., Boulos F. I., Kelley M. C.Mahadevan-Jansen A. (2008), Comparison of autofluorescence, Diffuse Reflectance, and Raman Spectroscopy for Breast Tissue Discrimination, J of Biomed Opt, 13,
328. Krishna H., Majumder S. K., Chaturvedi P., Sidramesh M.Gupta P. K. (2014), In vivo Raman spectroscopy for detection of oral neoplasia: a pilot clinical study, Journal of biophotonics, 7, 690-702
329. Krishna H., Majumder S. K., Chaturvedi P.Gupta P. K. (2013), Anatomical variability of in vivo Raman spectra of normal oral cavity and its effect on oral tissue classification, Biomedical Spectroscopy and Imaging, 2, 199-217